Andreas Wenig BSc.

Development of a post processing and analysis routine for the AE-testing method for rock burst prone rocks

Master's Thesis

Submitted in fulfilment of the requirements for the degree of

Diplom-Ingenieur

Master's programme Civil Engineering, Geotechnics and Hydraulics

at

Graz University of Technology

Supervisor:

O. Univ.-Prof. Dipl.-Ing. Dr. mont. Wulf Schubert

Institute of Rock Mechanics and Tunnelling

Graz University of Technology

Dipl.-Ing. Angelika Klammer

Institute of Rock Mechanics and Tunnelling

Graz University of Technology

Graz, March 2018

EIDESSTATTLICHE ERKLÄRUNG
AFFIDAVIT

Ich erkläre an Eides statt, dass ich die vorliegende Arbeit selbstständig verfasst, andere als die angegebenen Quellen/Hilfsmittel nicht benutzt, und die den benutzten Quellen wörtlich und inhaltlich entnommenen Stellen als solche kenntlich gemacht habe. Das in TUGRAZonline hochgeladene Textdokument ist mit der vorliegenden Masterarbeit identisch.

Ich declare that I have authored this thesis independently, that I have not used other than the declared sources/resources, and that I have explicitly marked all material which has been quoted either literally or by content from the used sources. The text document uploaded to TUGRAZonline is identical to the present master's thesis.

_____   _____
Datum / Date   Unterschrift / Signature

Danksagung

Abstract

The Acoustic Emission Testing (AET) is part of the non-destructive testing methods and is a versatile method for investigating materials in all fields and professions. Due to this acoustic emission analysis, rock instabilities and micro crack propagation can be traced back, which gives an idea, how the rock mass will behave under certain stress conditions. In mining and tunnelling it is used to track and predict rock mass failure like rock burst.

Although there are many codes and standards of how to set up the measurements, there are no sophisticated codes or guidelines of how to post-process and analyse the results. To this date, post-processing and analysis of the results mainly depend on the experience and subjective assessment of the operator. The Rock Mechanics and Tunnelling laboratory at the University of Technology Graz conducts AE-measurements and a practical directive was developed, to post-process and analyse the results.

Four of several previously tested samples, have been processed and analysed for this master thesis. One goal was to be able to distinguish the crack level indicators with the AE-measurements, which could be achieved with a combination of AE-energy and pattern recognition. The results of those analyses were compared with the volumetric strain analysis and could be confirmed.

Another goal was to compare the AE-results from different rock types. It can be said, that the hits- and the energy-comparison are shown to be applicable and correlations between hits/energy and rock parameters can be drawn. On the other side, an event-comparison between different samples was not leading to satisfying results to this point.

With this proposed directive, more samples can be post-processed and additional conclusions can be drawn.

Kurzfassung

Der Akustische-Emissionsmessung gehört zu den zerstörungsfreien Prüfverfahren und ist eine vielseitige Methode, zur Untersuchung von Materialien in allen Bereichen. Durch diese Schallemissionsanalyse können Gesteinsinstabilitäten und Mikrorissausbreitungen beobachtet werden, die Rückschlüsse zulassen, wie sich die Gesteinsmasse unter bestimmten Belastungsbedingungen verhält. Im Berg- und Tunnelbau wird es verwendet, um das Versagen von Gesteinsmassen wie Bergschlag zu überwachen und vorherzusagen.

Obwohl es viele Normen und Richtlinien für den Aufbau der Messungen gibt, ist keine bestehende Nachbearbeitungsroutine zur Analyse der Ergebnisse vorhanden. Bis zum heutigen Zeitpunkt hängt dies hauptsächlich von den Erfahrungen und subjektiven Einschätzungen des Anwenders ab. Das Labor für Felsmechanik und Tunnelbau an der Technischen Universität Graz führt AE-Messungen durch und es wurde eine praktische Empfehlung entwickelt, um die Ergebnisse nachzubearbeiten, zu analysieren und vergleichen zu können.

Vier Versuchs-Ergebnisse, von mehreren vorab getesteten Proben, wurden nachbearbeitet, analysiert und verglichen. Ein Ziel war es, die Bruchzonen mit den AE-Messungen zu unterscheiden, welches mit einer Kombination aus AE-Energie und Mustererkennung erreicht werden konnte. Die Ergebnisse dieser Analyse wurden mit der volumetrischen Dehnungs-Analyse verglichen und konnten bestätigt werden.

Ein weiteres Ziel war der Vergleich der AE-Ergebnisse verschiedener Gesteinstypen. Es kann gesagt werden, dass der Hit- und der Energievergleich dazu geeignet ist und Korrelationen zwischen Hits/Energie- und Gesteinsparametern ersichtlich sind. Bis zum jetzigen Zeitpunkt konnte jedoch keine Korrelation von Events zwischen verschiedenen Proben festgestellt werden.

Mit diesem entwickelten Leitfaden können mehr Proben nachbearbeitet, und dadurch zusätzliche Schlussfolgerungen getroffen werden.

Table of contents

List of figures

List of tables

Abbreviations

AET .... Acoustic Emission Testing

AE .... Acoustic Emission

UCS .... Uniaxial Compressive strength

SDE .... Specific Destruction Energy (MJ/m³)

PR .... Pattern Recognition

EMI .... Electromagnetic Interference

Symbols

d .... diameter [mm]

l .... rock sample length [mm]

ε .... axial strain [-]

σ .... axial stress [MPa]

E .... elastic Modulus [N/mm²]

V .... deformation Modulus [N/mm²]

υ .... Poisson´s ratio [-]

K .... bulk modulus [GPa]

G .... shear modulus [GPa]

ρ .... density [kg/m³]

1 Introduction

The Acoustic Emission Testing (AET) is part of the non-destructive testing methods and is a versatile method for investigating materials in all fields and professions. The foundation of this method was set by J. Kaiser in the 1950s who investigated fracture and deformation of metals. The investigation of fractured rock with the AET was firstly done by Mogi and Scholz in the 1960s [1].

In Civil Engineering, this method is now used to supervise structures and to investigate or predict failure in all kinds of materials (metal, concrete, wood, rock). In Geotechnic particularly, this method is used in tunnelling and mining, to investigate failure prone zones and to predict rock failure, especially rock burst [2]. Rock burst is a sudden and violent failure of the rock mass, which occurs in the excavation areas of underground rock masses. Failure processes of rocks are characterized by crack initiation, propagation and coalescence with associated damage and evolution [3].

Acoustic emission (AE) is a quick release of accumulated elastic energy at a local source in a material in forms of transient elastic waves, which is also known as stress wave emission [4]. It is important to know that AE-waves are neither ultrasonic waves nor acoustic waves. AE-waves are elastic waves in a solid due to dislocation motions [1]. Fracture mechanics deals with those dislocation processes and describes the formation, growth and discrete propagation of an individual crack or cracks [5]. This generates the AE, at different spatial and temporal scales, covering from breaking atomic bonds to seismic faults [6].

In an ideal isotropic material these waves evenly propagate in all directions until they reach the surface. The AE sensor on the surface converts the AE – wave into an electric signal, which is sent to the measurement electronics and signal analysis unit for post processing (Figure 1). Though, rocks are not isotropic and the wave velocity changes during the test, which influences the accuracy of the analysis. With this kind of measurement technique, it is possible to analyse failure of the material e.g. location, failure energy, different failures-types or "predicting" eventual the failure of the sample.
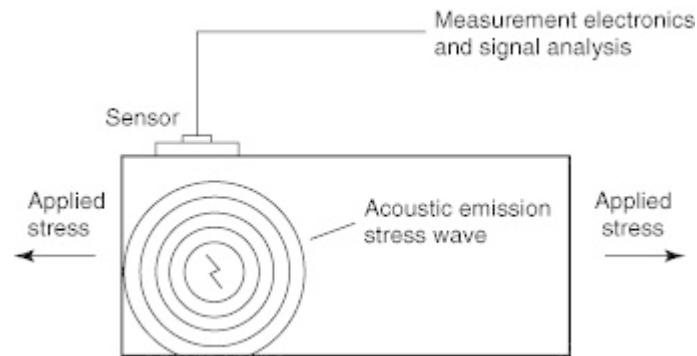
Figure 1: Working principle of the AE method [7]

To be able to locate acoustic emission sources, four or more AE-sensors have to be coupled to the rock sample, and all of them have to receive a signal from the same AE-source. To ensure a proper coupling of the sensors to the rock sample throughout the entire test, special couplants have to be used. These couplants have to meet certain requirements regarding the time depending behaviour and the sound propagation characteristic.

1.1 Objective of this Master-Thesis

The Acoustic Emission measurement and post processing is still not 100% developed. Although there are many codes and standards of how to set up the measurements, there are no sophisticated codes or guidelines of how to post-process and analyse the results. To this date, post-processing and analysis of the results mainly depend on the experience and subjective assessments of the operator.

For this reason, this Master-Thesis should serve as a practical directive for the AET analysis which are conducted at the University of Technology Graz, particularly on the Institute of Rock Mechanics and Tunnelling and should be a guideline for post-processing and analysing the results of the conducted tests.

The main goal is to be able to compare the AET results of different rock types and to conclude how they behave under certain stress conditions. Another part of this Master thesis deals with the automated analysis supported by the NOESIS software. This software is known for its user-friendly FFT (Fast Fourier Transformation) and pattern recognition (unsupervised and supervised).

2 Unconfined Compression Test

2.1 Introduction

To produce failure processes in the sample, uniaxial compression tests were used. To be able to load the sample accordingly, special equipment is required. The Rock Mechanics Laboratory of the University of Technology Graz has a servo-hydraulic rock testing system MTS 815 (shown in Figure 2), which is able to perform several test procedures including Uniaxial Compression test and Triaxial test. All tests, performed for this Master thesis were done by a Uniaxial loading. For this reason, the Uniaxial compression test and the necessary equipment for this specific test, is explained in more detail (also see 4.2).

Figure 2: MTS-UCS test

Unconfined compression test means, that a cylindrical rock sample is loaded in axial direction until failure. With the failure load and the cross-sectional area, the Uniaxial Compressive strength is obtained. According to the ÖNORM B 3124-9 [8], the l/d ratio should be 2 (for cylindrical rock samples).

The end faces of the rock sample have to be parallel and the lateral surface has to be smooth and without any irregularities. If not, the uniform stress state in the sample could be disturbed and the failure of the sample would not be representative [8].

2.2 Extensometers

To be able to record the strains in axial and circumferential direction, it is necessary to attach extensometers to the rock sample. For this purpose, the MTS Model 632.11E-90 was used for axial strains and for circumferential strain the MTS model 632.21A-01 was used.

As shown in Figure 3, elastic rubber bands are used to attach the axial extensometers to the specimen. The chain is used for recording the circumferential strains.
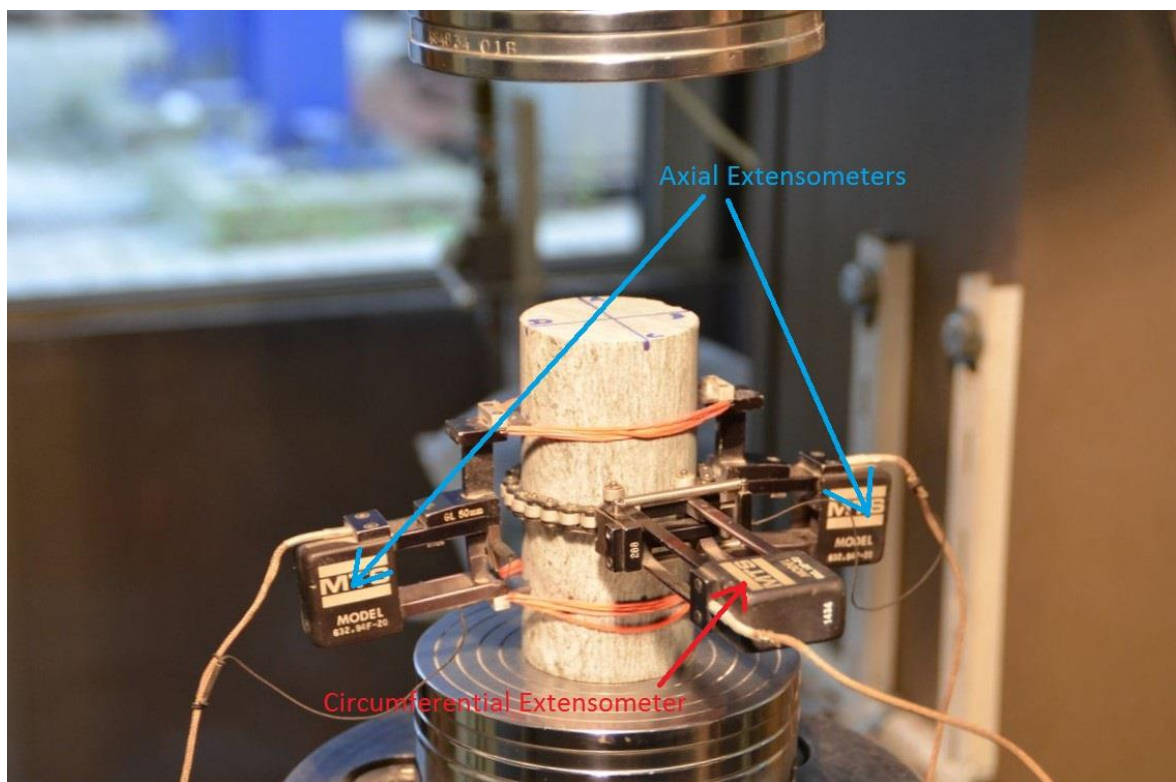
Figure 3: Extensometers attached to the a specimen

The circumferential strains are calculated, to be able to perform a post-failure test. The final point of the post-failure investigation depends on the post-failure behaviour of the sample. One goal of the post failure investigation is, to be able to calculate the destruction energy. A destruction energy till 100% ,50% and 30% of the UCS would be desirable.

2.3 Destruction Energy

$$SDE = \int \sigma \, d\varepsilon$$

Where SDE = specific destruction energy (MJ/m³) and σ = axial stress (MPa). This destruction energy is considered to give an idea about the rock cutability and is defined as the area under the stress vs. strain curve [9].
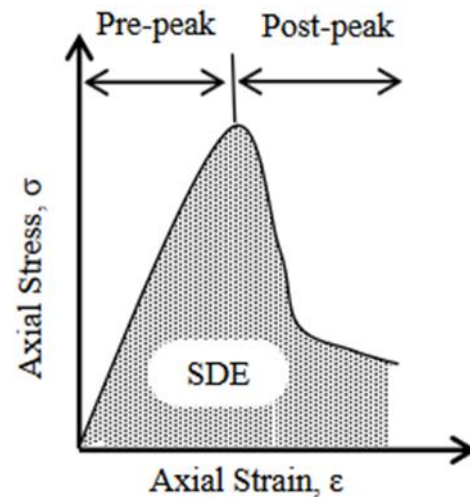
Figure 4: Stress strain curve with SDE [9]

2.4 Rock Classification

As shown in Figure 4, the stress-strain or stress-time curve consists of a pre failure part (pre-peak) and a post failure part (post-peak). Depending on the pathway of the post failure curve, two classes of rock can be distinguished, which is shown in Figure 5 .
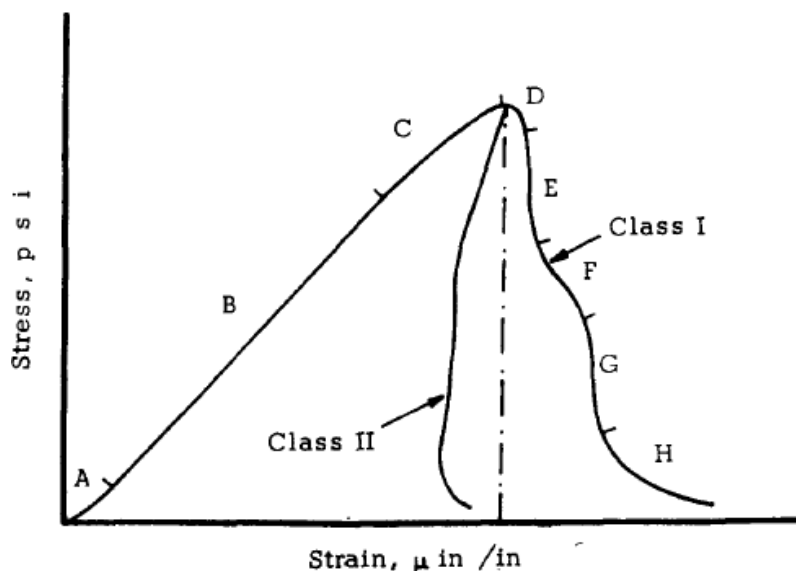
Figure 5: Two classes of rock failure behaviour [10]

According to Wawersik 1970 [10], the two classes of rock are defined as follows:

Class I rocks: If the post peak section is reached, there is still a residual strength in the rock which means that the rock behaves ductile. To further reduce this strength, it is necessary to bring additional energy into the system, which leads to a crack-development and a strain-increase.

Class II rocks: In contrast to stable fracture development, failure for class II rock is self-sustaining. In other words, the elastic strain energy stored in the sample, when the applied stress equals the compressive strength, is sufficient to maintain fracture propagation until the specimen has lost virtually all strength. This means that this leads to a sudden failure (brittle post failure behaviour) and the fracture development will be autonomous without any additional energy. To be able to record this in the laboratory, it is necessary to revoke the potential energy from the system [2].

The dividing line between class I and class II behaviour is defined by the dashed line in Figure 5, which represents the case when the stored elastic energy just balances the energy required to produce total breakdown of the specimen.

2.5 Source mechanisms

Rocks usually behave elastically at first (after the pore space is closed), this means it expands and compresses under loading and bounces back to its initial state if unloaded. The bigger the load and expansion/compression, the higher the stored elastic energy. If the elastic limit is exceeded, the material behaves plastically and if further loaded, it will fail (break). The behaviour of the material´s limits is strongly dependent on the brittleness. The failure causes a short shock, an acoustic emission event, which generates an elastic wave [11]. This AE source has its origin in the change of the stress field inside the material, which is related to the deformation processes, crack growth and dislocation movements, taking into account cracks [12]. It can be compared to an earthquake where the epicentre is the defect but in microscopic dimensions [13].

For brittle deformation, this mechanism leads to two distinctive effects:

1. It is accompanied with significant changes in the effective macroscopic elastic constants.
2. Since crack formation is generally irreversible, the process is cumulative.

In a physical experiment, a yield reduction of elastic moduli and an increase of the Poisson`s ratio during dilatancy can be observed [14].

To be able to interpret the results of a laboratory test, it is an important aspect to understand the failure mechanism. This can be done by taking a look at the volumetric strain and axial strain in relation to the axial stress. This relationship was proposed by Bieniawski, Denkhaus et.al 1969 [15] and is shown in Figure 6. Fundamental research to the rock behaviour was also done by Hudson et.al (1972).
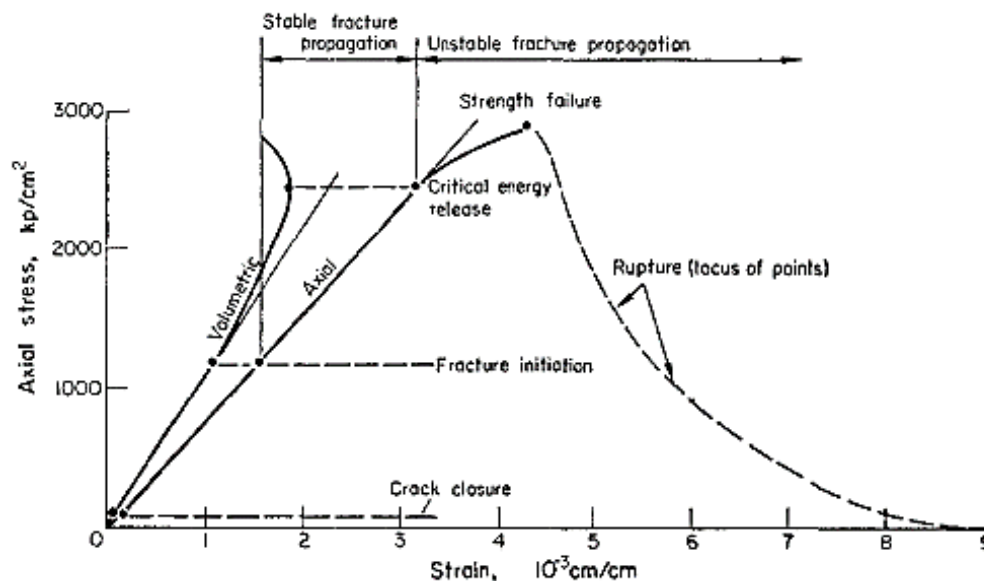
Figure 6: Brittle fracture process in rock [15]

Crack closure:

At the beginning of the loading crack closure due to pre-existing micro cracks and cavities is happening. This is the reason for the non-linear, more concave behaviour of the stress strain curve at the beginning. Other reasons for this can be non-planar or non-parallel end faces of the specimen [16].

Linear elastic behaviour:

This behaviour is the phase between the crack closure and fracture initiation and means a linear behaviour between stress and strain. Concluding that the specimen behaves totally elastic in this phase and reaches its initial state if stress is decreased again. If the point of fracture initiation is exceeded micro cracks are forming and the sample behaves non linearly.

Propagation modes:

Bieniawski 1969 [15] described two fracture propagation modes, stable and unstable fracture propagation. Stable fracture propagation is considered to be a slow process and requires an increase in stress (or strain) for an increase in crack growth. Unstable crack propagation is considered not to be controllable unless the stress is dropped. As shown in Figure 6, the point where the stable fracture propagation changes into the unstable, the axial stress-strain curve deviates from linearity. At the same time the volumetric strain reverses which results in a change from contraction to extension [17].

3 Acoustic Emission Testing

3.1 Glossary

To be able to describe and discuss the acoustic emission measurement certain terms have to be defined in advance. The following standard terms are defined in the ÖNORM EN 1330 – 9 [18].

- **AE – Acoustic emission:**
  Phenomena whereby transient elastic waves are generated by e.g. plastic deformation, crack propagation, erosion, corrosion, impact or leakage.
- **AE – event:**
  Physical phenomenon giving rise to the acoustic emission.
- **AE – source:**
  Spatial element from which one or more acoustic emissions events originate.
- **AE signal:**
  The electrical signal from an acoustic emission sensor produced by the acoustic emission wave.
- **Transient signal, continuous signal:**
  Explained in detail in chapters 3.5.1 and 3.5.2.
- **Hit:**
  Detection of one burst signal on one acoustic emission channel.
- **AE – channel:**
  Single acoustic emission sensor and related measurement and processing instrumentation.
- **AE – detection threshold:**
  Voltage level to be exceeded before a burst signal is recorded.

These terms above are the most common ones, discussing AET. Other terms – definitions can be found in the ÖNORM EN 1330 – 9 [18].

3.2 Acoustic Emission Process-Chain

With the acoustic emission testing, acoustic events can be detected and damages can be identified in an early stage. To simulate these damaging processes, uniaxial compression tests are performed in laboratories in combination with suitable measuring devices. Figure 7 describes the AE process chain for a laboratory measurement.
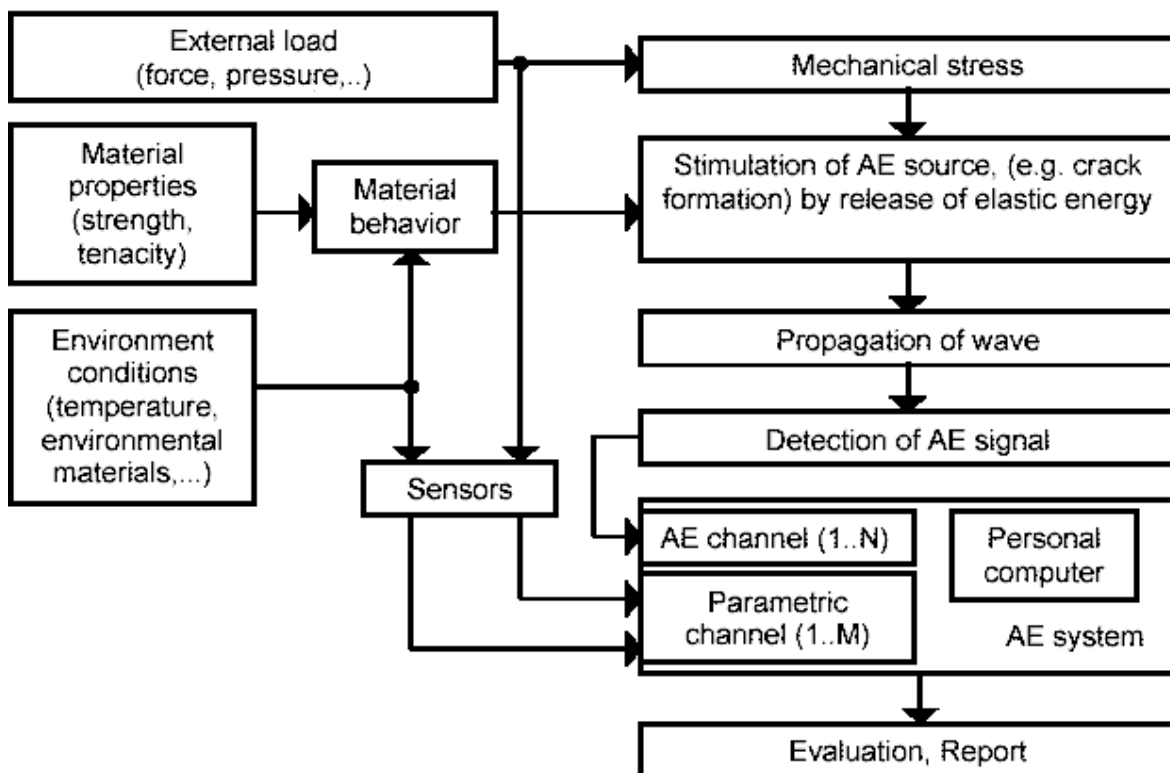
Figure 7: AE-process chain [13]

This figure gives an overview of the single steps in an AET process which consists of following links [13]:

1. **Mechanical stress:**
   ▪ Induced to test object by application of load
2. **Stimulation of AE source:**
   ▪ Release of elastic energy
3. **Propagation of wave:**
   ▪ From the source to the sensor
4. **Detection of AE signal:**
   ▪ Converting a mechanical wave into an electrical AE signal

5. **AE-System:**
   - Acquisition of measurement data
   - Converting the electrical AE signal into an electronic data set

6. **Evaluation, report:**
   - Plotting the recorded data into diagrams
   - From diagrams to a safety-relevant interpretation

3.3 Wave propagation

The wave propagation will just be discussed to some degree, to give a short introduction about this topic but since this is a very complex topic, more detailed information is beyond the scope of this master thesis.

Generally, two waveforms are distinguished:

1. Body waves
   a. P-waves
   b. S-waves
2. Surface waves
   a. Rayleigh waves
   b. Love waves

3.3.1 Body waves

<u>P-waves</u> are body waves and are considered to be the primary ones. They are compressional waves in longitudinal direction and their velocity is defined as [19] (for term explanation see chapter "Symbols"):

$$Vp = \sqrt{\frac{K + 4G/3}{\rho}}$$

These waves are the fastest waves and can travel through solids, liquids and gases.
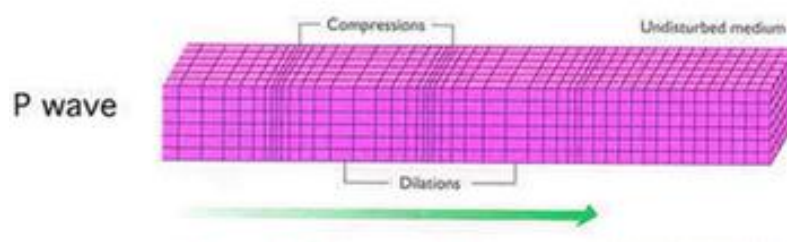
Figure 8: Schematic principle of a body wave [20]

S-waves are waves which are considered to be secondary. They are shear waves or transverse waves and their velocity is defined as:

$$Vs = \sqrt{\frac{G}{\rho}}$$

They are much slower than P-waves and they can only travel through solids.
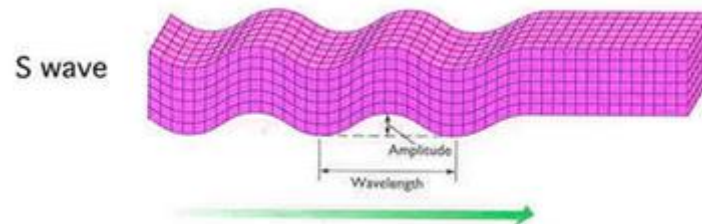
Figure 9: Schematic principle of a surface wave [20]

It can be mentioned, that compressional waves always travel faster than shear waves and if the rigidity increases, the P- and S-wave velocities also increase. The rigidity depends on the density ρ. If ρ increases, the rigidity will increase too but more rapidly. This is the reason why denser rocks have faster wave propagation velocities [19].

3.3.2 Surface waves
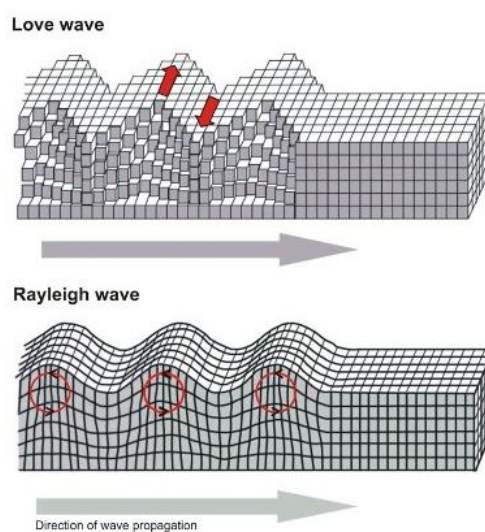
Figure 10: Schematic principle of Love- and Rayleigh-waves [21]

Love- and Rayleigh-waves are two special types of surface waves. While Rayleigh

waves exist at any free surface, Love waves can only develop if there is some kind of wave guide formed by a velocity increase with depth (gradient – or layer –wise) [19].

3.4 Detection of AE-signals

To be able to detect the acoustic emissions, piezo-electric sensors are most commonly used. This sensor type is considered to provide the most effective conversion from elastic, mechanical waves (acoustic emissions), to an electronic signal. Piezo-electric sensors are used in a frequency range from 20 kHz to 1 Mhz. These sensors consist of a piezo-electrical crystalline or ceramic element which is embedded in a protecting case (shown in Figure 11). The piezo-element detects a combination of wave-types: Compression-, shear-, surface (Rayleigh)- and plate (Lamb)- waves [22].

Figure 11: Schematic setup of an AE sensor [13]

The maximum sensibility is defined by the ratio of output-voltage to a velocity or an applied pressure in units V/(m/s) or V/kPa in a range of 0.1 mV/kPa [23]. For this reason, the sensitivity of a sensor is mostly given in decibel.

Two types of AE sensors can be distinguished, depending on their frequency characteristic:

a) Resonance sensors
b) Broadband sensors
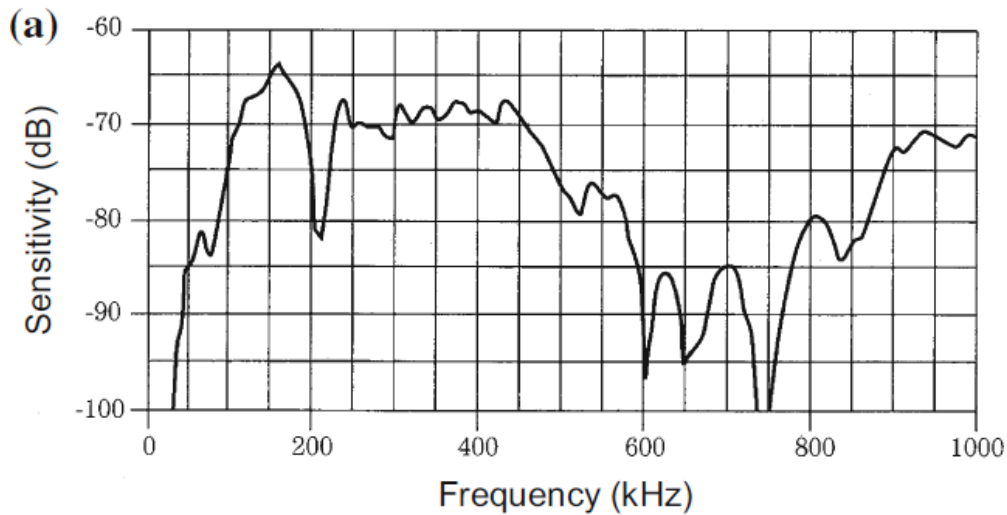
Figure 12: Frequency characteristic of a resonance sensor [23]
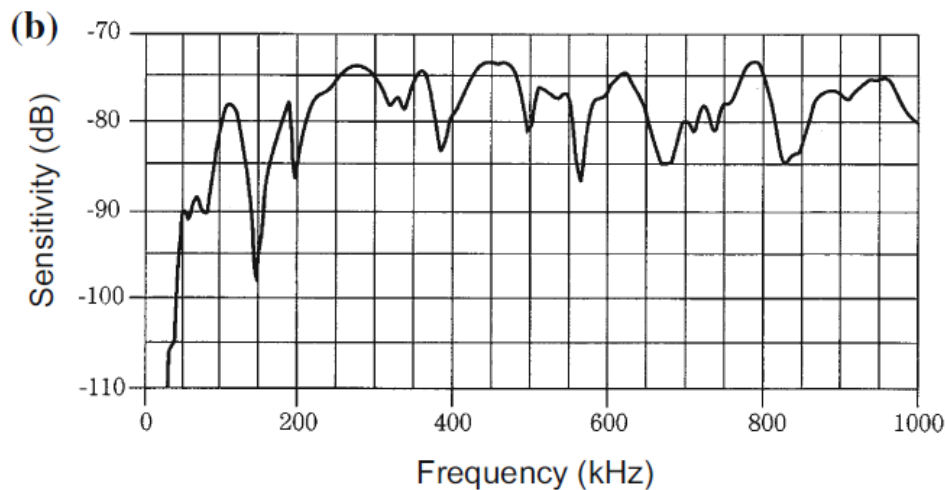
Figure 13: Frequency characteristic of a broadband sensor [23]

If the resonance sensor (Figure 12) is compared to the broadband sensor (Figure 13) it can be noticed that the broadband type sensor covers a bigger frequency spectrum than the resonance-type sensor but is not as sensitive. This means that the resonance type sensor can just be used for certain frequency spectrums. Concluding both have advantages and disadvantages, it depends on the demands and requirements particularly the expected frequency spectrum. This is the decisive factor which sensor-type is used.

For the AET conducted at the Rock mechanics laboratory of the University of Technology Graz, the sensor PAC Nano30 was used. It is a sensor with resonance characteristic and a maximum sensitivity of 62 decibels. Further information about the sensor can be found in the Appendix .

3.5 Signal types

For the acoustic emission testing (AET), different signal types (emissions) have to be distinguished. This differentiations are according to the ÖNORM EN 1330-9 [18].

3.5.1 Burst emission

The occurrence of acoustic emission events which can be separated in time. That´s because a burst signal has an identifiable beginning and end (shown in Figure 14).
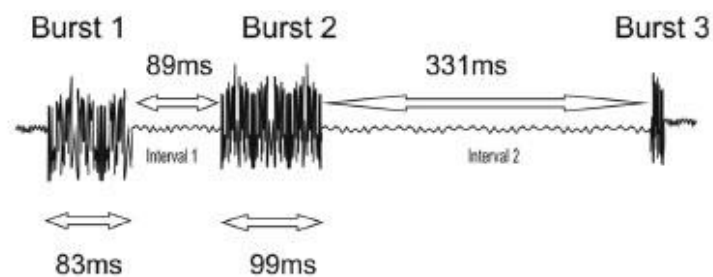
Figure 14: Schematic Illustration of burst signals and their intervals [24]

The acoustic emission detection threshold controls the voltage level, which has to be exceeded before a burst signal is recorded. If the signal is only detected on one acoustic emission channel, it is called hit. If this burst signal is detected by four or more different channels within a specific amount of time, the burst signal can be back-calculated to its spatial position. Then this burst signal is called an event and it is defined by a physical phenomenon giving rise to acoustic emissions.

3.5.2 Continuous emission

These occurrence of acoustic emission events cannot be separated in time because they have no identifiable beginning and end (shown in Figure 15).
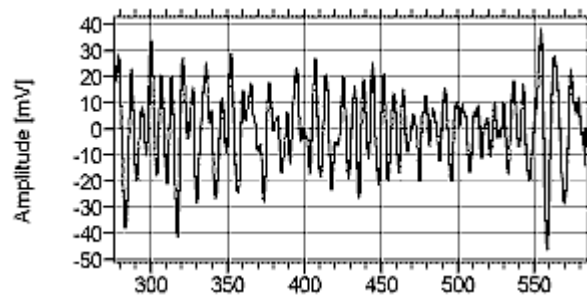
Figure 15: Continuous AE signal [13]

Amplitude and frequency variations can be seen but the signal never ends. Continuous signals are mostly unwanted (3.5.3) such as friction or electromagnetic interference [13].

3.5.3 Acoustic emission noise

Signals which are not relevant to the purpose of the test are called acoustic emission noise. Noise can have electromagnetic, thermal or mechanical origins.

3.5.4 Background noise

Acoustic emission noise which can be rejected by raising the detection threshold or by frequency filtering. These signals can be e.g. electronic noise of the preamplifier or the sensors [13].

3.5.5 Spurious noise

Spurious noise is acoustic emission noise which cannot be rejected by raising the detection threshold or frequency filtering and which might be rejected by logical filtering.

3.6 Further Measurement Equipment

3.6.1 Preamplifier

If the sensor gets a signal (see chapter 3.5), first it will be preamplified and then it will be transferred to the measurement-electronics (computer electronics and software). The preamplifier which is used for this measurement at the laboratory is the PAC-2/4/6. This preamplifier (shown in Figure 16) has the options to select between 20, 40 or 60 dB as pre-amplification. In the test procedures conducted, this level was set to 40 decibels. It has to be mentioned, that the preamplifier has a customized filter installed. Further information about the preamplifier can be found in the Appendix .

Figure 16: PAC 2/4/6 preamplifier [25]

3.6.2 PAC-PC system

This customized PC system is used for real time tracking of the AE events. To be able to track them accordingly, it is necessary to be able to set a suitable sampling rate. In the experiments conducted at the Rock Mechanics laboratory, the sampling rate was set to 10 MSPS (million samples per second). Further information about the PAC-PC system and about its calibration, can be found in Stefanie Plahs Master thesis (2015) [2].

4 Laboratory Tests

4.1 Tested samples

The samples which were tested are characterized through a brittle failure. Some of them are prone to rock burst.

Four of the 15 tested samples were post processed, due to the fact, that the goal of the thesis is to develop a post-processing-routine. These four samples then were compared to each other and conclusions were drawn. The goal is to objectively compare their AE-results and their failure behaviour. The post processed samples are:

Sample number	Rock type	Source
268.41	Marble	Drama; Greece
268.43	Marble	Carrara; Italy
268.59	Dolomite	Hochfilzen; Austria
268:67	Magnesite	Breitenau; Austria

Table 1: Post processed rock samples

All samples were drilled in the laboratory from construction-site boulders.

4.2 Test procedure

4.2.1 Test object and application of load

The test objects are cylindrical-shaped rock samples. They have to have a length (height) to diameter ratio of 2:1 and are normally around 100:50 mm in their dimensions. Their surfaces should be planar, to minimize end-face effects and uneven loading.

The loading of the sample is performed in three cycles. Ideally the first cycle is performed at about 40 to 50% of the UCS and the second and third cycle´s peak will be at about 70 to 80% of the sample`s UCS. The first cycle was used to determine the elastic rock parameters like elastic modulus E, deformation modulus V and the Poisson`s ratio υ [2]. The second and third cycle are for the evaluation of specific rock burst parameters. Additionally, the Kaiser-effect can be demonstrated during the cycles. After the third cycle the rock sample is loaded until failure. The post

failure behaviour is also investigated and the destruction energy is evaluated (see chapter 2.3). To be able to perform a post failure investigation the sample is loaded with a constant circumferential strain rate after the third cycle. Before that, the loading happens in a force controlled manner.

A typical curve for a sample loading is shown in Figure 17.
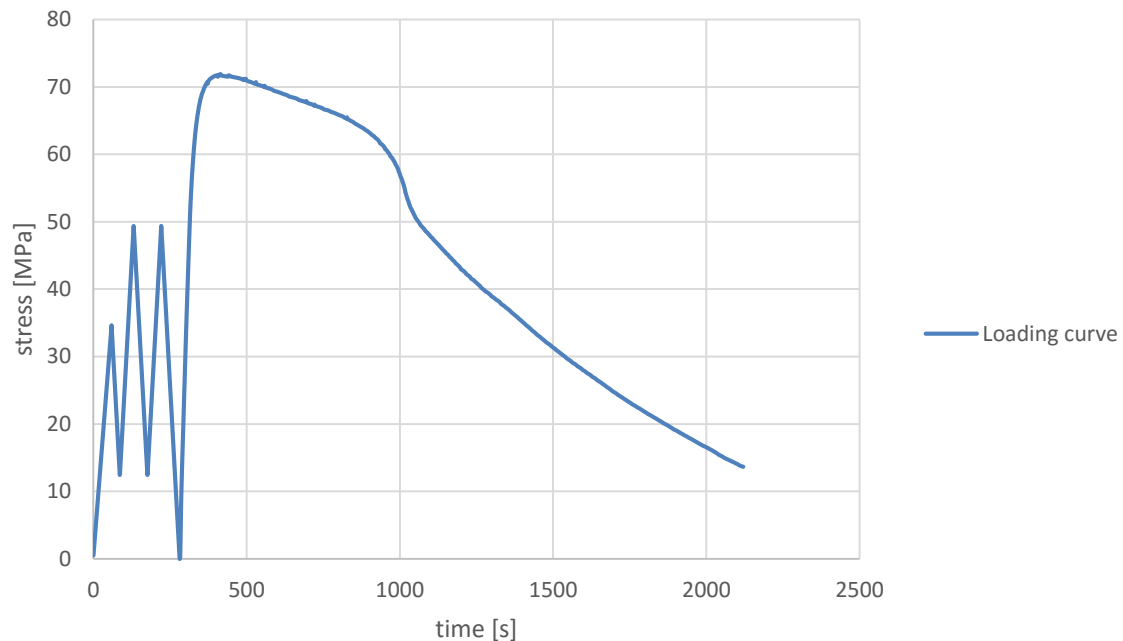
Figure 17: Typical stress vs. time curve

4.2.2   Mounting and coupling of the AE-sensors

To be able to obtain representative results, the AE-sensors have to be well coupled to the sample. For a good localisation, the sensors should be arranged in isosceles triangles around the sample (shown in Figure 18) [26].
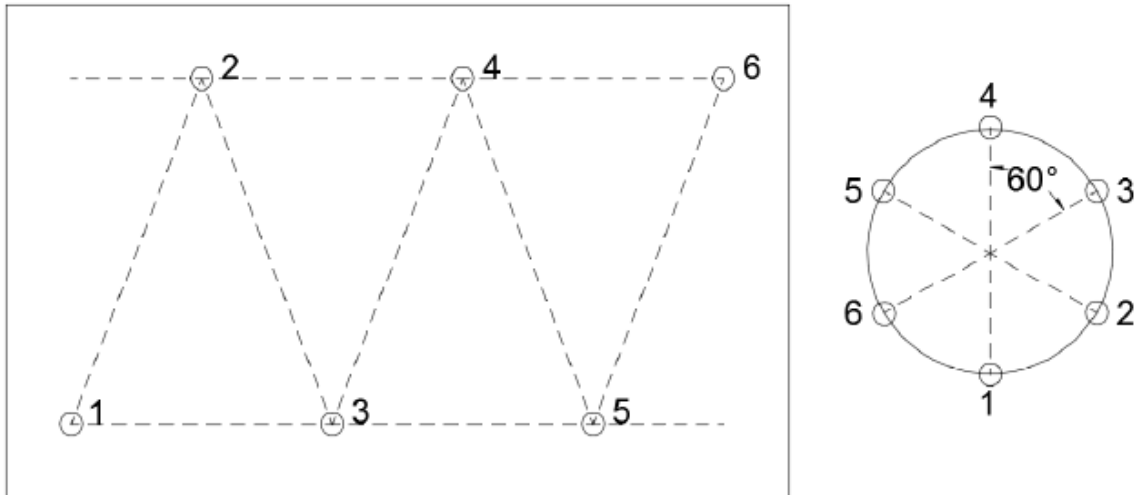
Figure 18: Arrangement of the sensors [26]

It has to be mentioned that the isosceles triangles couldn`t be achieved due to the extensometer-positions.

It is also very important that the sensors are not mounted too close to the top and the bottom, to prevent spurious noise or end effects [26]. This is why a distance of about 1.5 cm between the top/bottom and the sensors was chosen.

The acoustic waves, which propagate through the sample during the test, have to attain the sensors as undamped as possible. For this reason, the couplant plays an important part in the measuring chain.

The couplant compensates the flat AE-sensor surface and the curved sample surface. For this reason and for the reason that the sensor- and sample-surface are microscopically rough, a simple contact without any couplants would cause much lower signal amplitudes. The couplant acts as an additional layer between the sensors and the sample to optimize the sensor-measurement. Regardless of the type of the sensor-attachment to the sample, the couplant must not affect the signal and it is not allowed to damage the sample or the sensor. Following criteria have to be considered when choosing a couplant:

- Self-sticking properties to attach the sensors to the sample
- Acoustic signals must not be affected
- Couplant has to be free from dissolver
- Couplant must not exceed certain temperatures (exclusion of hot melt-adhesives)

- The couplant must not change its properties during the test (from sample preparation to disassembling of the sensors about three hours are required)
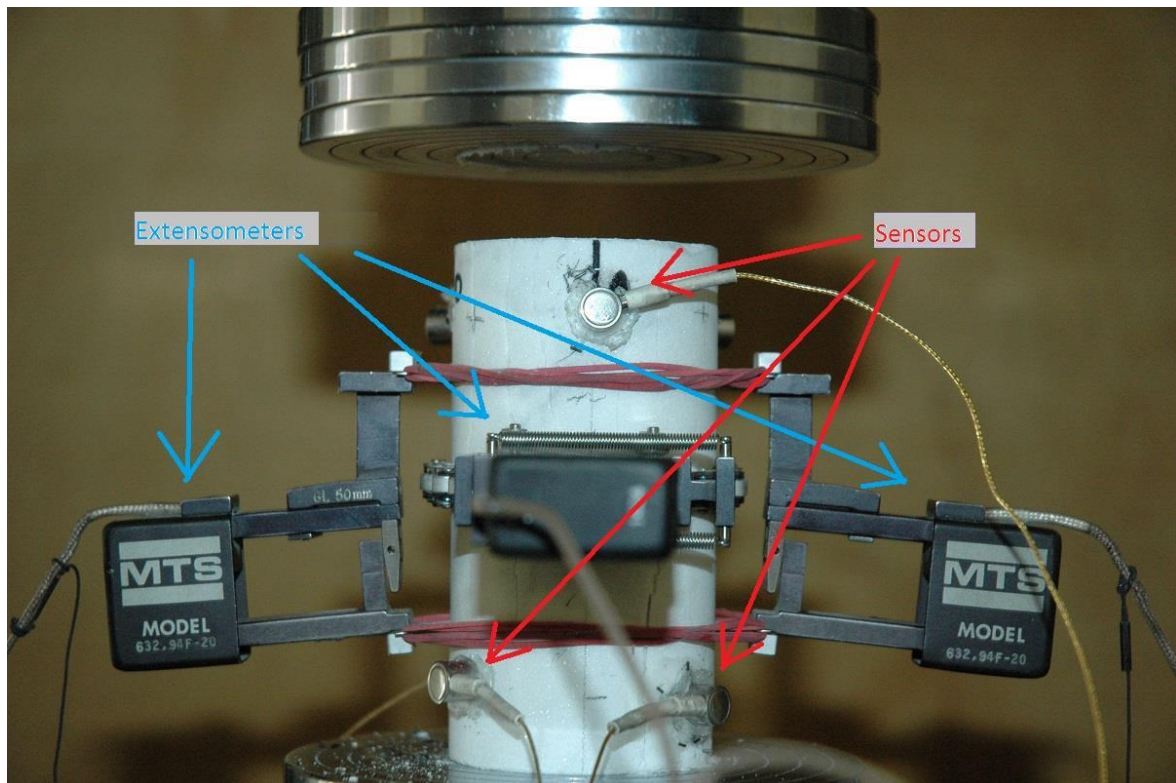
Figure 19: Testing setup, including AE-sensors

Figure 19 shows the sensor attachment to the sample with the self-sticking couplants

4.2.3 Localisation of AE-events

One goal of these tests is, to localize the failure occurrence in real time. To localize events, the p-wave velocity has to be entered into the computer program, to be able to back-calculate the spatial position of the event. It has to be mentioned that the p-wave velocity depends amongst others, on the stress applied to the rock sample. This causes an increase of the velocity with increasing pressure. Other reasons for alternating p-wave velocities are heterogeneities and pre-existing or developing cracks, in the sample. The real impact of the stress-dependence and the other factors can hardly be quantified and they change from rock to rock. For this reason, an averaged p-wave velocity with respect to the sample, was used during the whole procedure.

Also the sensor-coordinates can be possible sources of errors. For this reason, the

coordinates should be conducted as exact as possible. The literature shows two different types of localizing:

1. Iterative localizing
2. Hyperbolic method

These two methods are described in the master thesis from Stefanie Plahs (2015) [2], and won´t be further described here.

4.2.4 Kaiser effect:

The Kaiser effect takes place in rocks and materials subjected to cyclic loading/unloading. During uniaxial loading with the cycle`s peak stress increasing from cycle to cycle, the acoustic emission (AE) is zero or close to the background level, as long as the stress stays below the largest previously reached stress value. As this peak ("memorised") stress is attained, the AE activity increases dramatically. This behaviour is called Kaiser effect [27].

5 Post Processing and Results

5.1 Post processing now and then

Since the development of Acoustic Emission testing in the middle of the 20th century, the post processing was always a crucial part of this testing method. At that time, the technical state of the art was not able to record and process big data. Therefore, every signal had to be analysed per hand. This changed with the technical evolution and the ability to record and post process e.g. filter, amplify, or sort the data. The post processing depends on the type of AE-technique used:

1. Parameter based AET (large scale)
2. Signal based AET (small scale)

Parameter based AET only records chosen signal attributes (e.g. rise time, duration, peak to peak frequency, arrival time etc.) whereas signal based AET records each signal and gives the opportunity to change settings after the measurement and to apply different signal analysis tools [1].

Both AET approaches have their pros and cons (see [1]) but with further technical development, especially in sampling frequencies and storage capacity, the signal based will be the most commonly used.

Several post processing/analysis methods are mentioned in the literature:

- Energy analysis
- Volumetric strain comparison
- Pattern recognition
- Moment tensor analysis
- B-value comparison

Although there are several methods available, only the first three will be discussed in this Master-thesis. Discussing the Moment-tensor analysis and B-value comparison would be beyond the scope of this thesis. For further information take a look at Rao, 2012 [5].

5.2 Used software

For the post processing, two different software packages were used.

1. AE-Win
2. Noesis

These software packages were developed by the Mistras Group Hellas. They are specialized in non-destructive testing and monitoring services [28].

5.2.1 AE-Win

AE-Win is a signal based analysis tool. The software was used to monitor the failure occurrence in real time. This can be done by modelling the sample in the program and by entering the material data e.g. wave velocity, material and other AE relevant data. The sensor positions have to be entered additionally. If this is done correctly the visualization looks like shown in Figure 20. It can be seen that the real sensor positions are visualized and marked with the numbers 1-6, and they are evenly distributed around the rock sample (see 4.2.2).
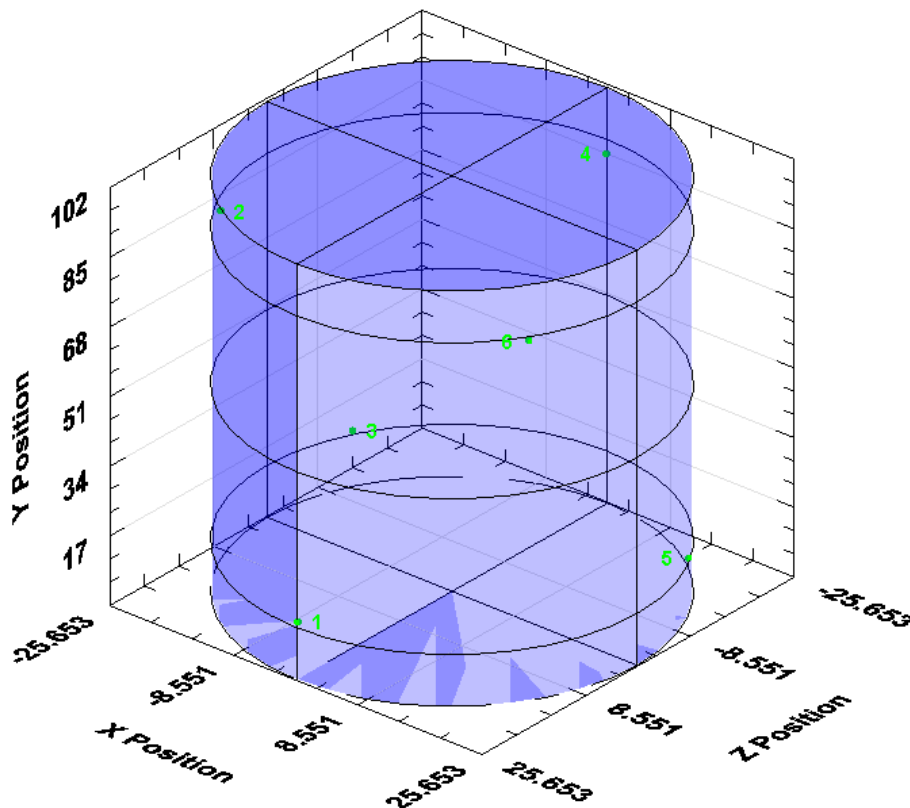
Figure 20: Visualization of a rock sample in AE-Win

5.2.2 Noesis

Noesis is also a signal based analysis tool. Compared to AE-Win, it is not able to track the event-occurrence in real time but the post processing is more convenient. A big advantage is, that Noesis is able to perform pattern recognitions. Pattern recognition is a part of Artificial-Neural-Networks and is often used for automated signal -classification and –analysis, when it comes to AE-measurements. There are two basic distinctions for pattern recognition.

1. Unsupervised pattern recognition
2. Supervised pattern recognition

To perform the first one, it is not necessary to train the program with pre-investigated features. The neural network groups the signals by means of signal characteristic. This means that the program forms a vector with the signal characteristics e.g. risetime, amplitude, energy etc.(shown in Figure 21), and weighs their "importance".

$$v_i = \begin{bmatrix} ArrivalTime \\ Param1 \\ Param2 \\ RiseTime \\ Counts \\ Amplitude \\ Duration \\ Energy \\ . \\ . \\ . \\ feature_n \end{bmatrix}$$
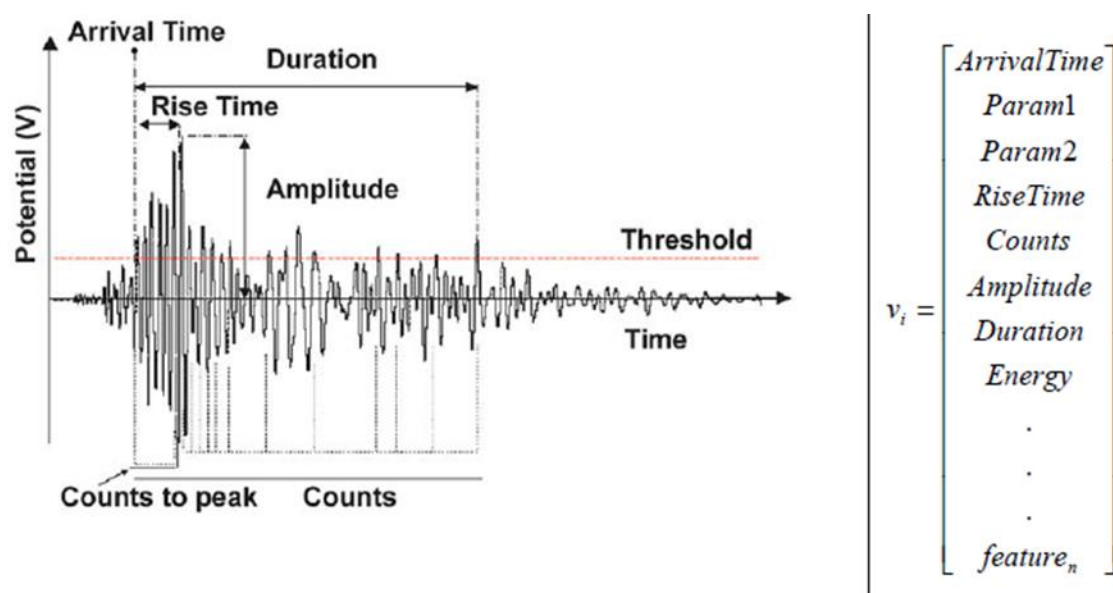
Figure 21: Schematic principle of pattern recognition [29]

This is done to every signal and through the pattern recognition, similarities between the vectors are distinguished, and alike objects are grouped. The advantage with this is that no predefined training-data is needed but the accuracy of the results depends on the input-settings and the operator`s experience.

The supervised pattern recognition works quite similar except, that a training set is needed to tell the program which signal-pattern is representative for this kind of signal. For example, a pencil break is performed and registered. Now this signal is used to train the program how the characteristic of a pencil break looks like. The

advantage with this system is, that clear distinctions between the different patterns are predefined. The big disadvantage is, that a big amount of training data is needed and then it can only be performed for one specific material. If the material changes, everything has to be done again.

For this post processing, unsupervised pattern recognition was used (see 5.3)

5.3 AE-Post processing data-sheet

This data sheet was created to be able to compare AE –results from different rock types in an objective manner. It also gives a chronology for the analysis and quantifies the many different AE-plots in a useful manner.

The AE-data sheet will be exemplarily shown and described for the test sample 268.41. This sample and additional data-sheets, obtained by the AE-measurements, will be found in the Appendix . For a better overview, the data-sheet will be explained in several parts.

Part 1:

Analysis Sheet

Sample Information		
Sample Nr.	268.41	
Rock type	Marble	
Length	101.42	[mm]
Diameter	50.73	[mm]
Weight	553.2	[g]
Density	2.698	[kg/dm³]
p-wave velocity	6.5	[mm/μsec]
Used channels for analysis	6	

UCS Values, Elastic Parameters and Destruction Energy				
σcs	71.88			[MPa]
25%	17.97			[MPa]
40-50%	28.8	-	35.94	[MPa]
70-80%	50.3	-	57.50	[MPa]
E-Modulus			87.52	[GPa]
V-Modulus			82.09	[GPa]
Poisson`s ratio			0.33	[-]
Destruction-energy	100%	50%	30%	[-]
	50.64	72.09	75.5	[kJ/m³]

Table 2: General sample information

Table 2 gives a general overview of the sample`s rock properties. It should be mentioned that the p-wave velocity is the velocity which was used in the software to back calculate the events. Also worth mentioning is the section "Used channels for analysis". This section describes the amount of channels which can be taken into account for the post processing. Six is the maximum number due to the six sensors (=channels) attached to the sample. In the post processing the results will then be divided trough the number of "useable" channels to get a representative result. If for example, one sensor is decoupled during the pre-failure measurement due to

spalling, the sensor won´t get any more signals and the whole test results (e.g. number of hits, absolute energy) will be divided by 5 instead of 6.

The "UCS-Values, Elastic Parameters and Destruction Energy" section gives an overview of the rock`s strength and properties. Several levels of σ_{CS} are shown, to be able to compare these levels with the AE-results. Although the post-failure AE-results are not elaborated, the uniaxial compression test was operated into the post-failure range too, to additionally determine the destruction-energy. Like shown in Figure 22, the destruction energy (see 2.3) was calculated for three stages:

1. 100% (till 100% of UCS)
2. 50% (till Sigma 1 reaches 50% of UCS in the post-failure stage)
3. 30% (till Sigma 1 reaches 30% of UCS in the post-failure stage)

It should be mentioned that the total destruction-energy is also calculated, but it is not representative because it depends on the moment the test has been stopped. It should be mentioned that this Figure 22 is not shown on the analysis-sheet, but it is displayed in the appendix. Following destruction energy shows a Class I rock.
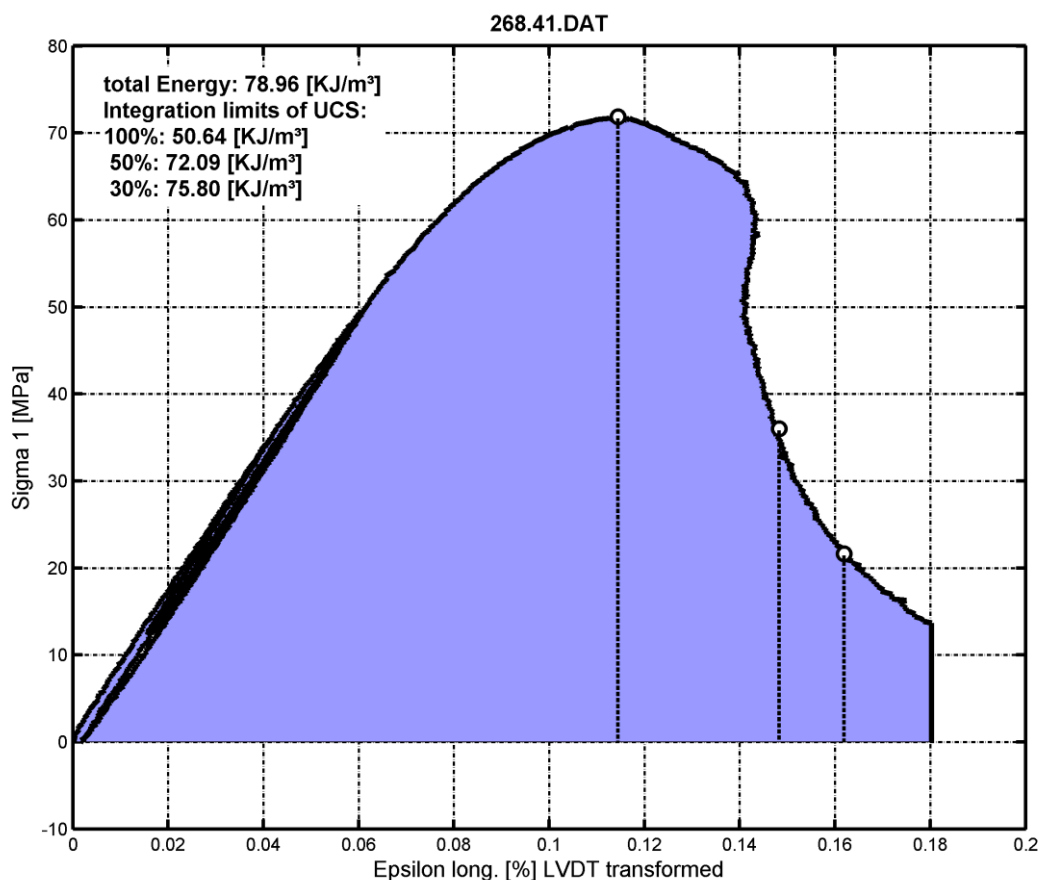

Figure 22: Destruction-energy for rock sample 268.41

Part 2:

Number of Hits in relation to their signal strength (pre failure)							
UCS [%]	Amplitude [Decibel]						
	30-40	41-50	51-60	61-70	71-80	81-90	91-100
0-25% of UCS	402	59	6	0			
>25-50% of UCS	983	151	19	2			
>50-80% of UCS	3452	601	104	12	1		
>80-100% of UCS	8270	1079	134	14	1		
Sum:	13106	1889	264	28	2		
						Total:	15288

Table 3: Hits related to their signal strength (268.41)

Table 3 shows the relation between the amount of hits in relation to the different UCS stages and their signal strength. As mentioned earlier, only pre failure hits are taken into account. Another important thing to mention is, like described in "part 1, that the amount of "useful" channels is six in this case. So every result in the table above was divided by six to get a representative number and make it comparable with other test results. It is important to know that the divided results were rounded mathematically to integer numbers. So for example 0.5 equals 1 and 4.4 equals 4. Notice that most of the hits happen between 80% and 100% of the UCS and most of them have a signal strength between 30 and 40 decibels. Table 3 is also visualized in a graph shown in Figure 23. Note that the amplitude scale starts at 30 db. This is because of the threshold, which was set to exclude noise from the records. This threshold level had been tested in advance.
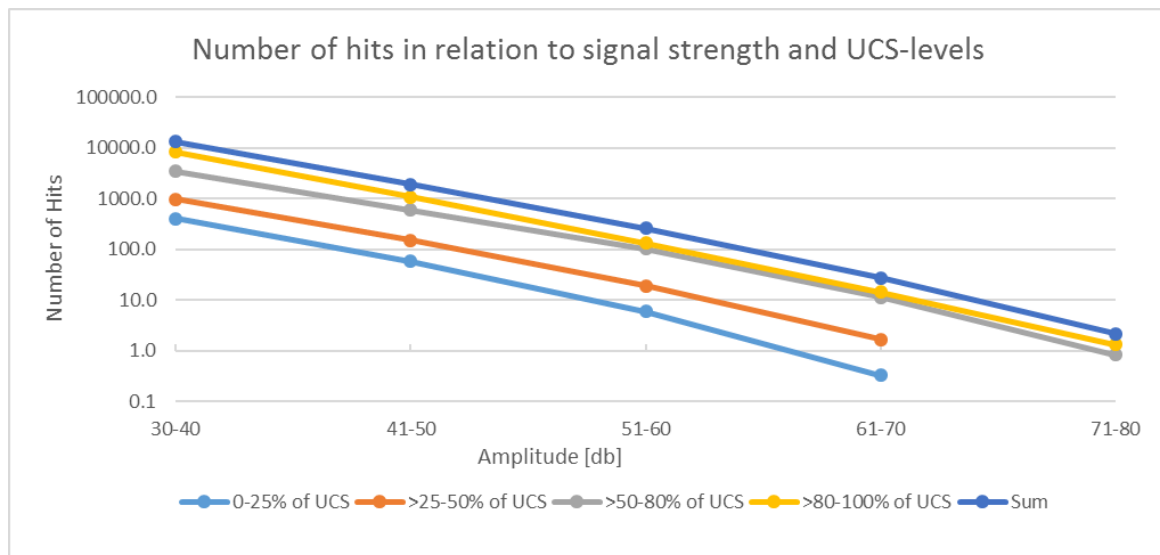
Figure 23: Relation between amount of hits and signal strength respective to an UCS level

It should be mentioned that the y-axis in Figure 23 is in logarithmic scale, otherwise small numbers can hardly be displayed in this graph because of the big difference between the highest and the smallest numbers. Notice that the graph displays the real and not the rounded numbers.

Part 3:

Analysis Parameter (pre failure) including cycles					
Values till % UCS	25%	50%	80%	100%	
Number of Hits	466.8	1621.5	5790.3	15288.3	[-]
Number of Events	5	36	179	412	[-]
Absolute Energy [aJ]	8.10E+03	3.50E+04	1.85E+05	3.70E+05	[aJ]
Cumulative Hits [%]	3%	11%	38%	100%	[-]
Cumulative Events [%]	1%	9%	43%	100%	[-]
Cumulative Energy [%]	2%	9%	50%	100%	[-]

Table 4: Hits, Events and Energy

This Table 4 gives a comparison between hits, events and energy respective to the different UCS stages. These numbers were then normalized to be able to compare them with different test results and rock types. It can be seen, that nearly 50%, of the energy released by the cracking, happens in the last 20% of the UCS and even a bigger amount of hits and events develop in this stage. These values are also displayed in Figure 27 which is also included in the analysis sheet. Also worth mentioning is, that the data which is displayed in Table 4, includes the cycles. Due to the Kaiser effect (see chapter 4.2.4) the difference is relatively low (e.g. <2%). These data are then compared with the different fracture stages described in the literature (see [30]; [17]).

Part 4:

Crack level indicators by $\Delta V/V$ Analysis					
derived through graphic solution					
	Stress [% - from UCS]	ε_{axial} [%]	$\varepsilon_{lateral}$ [%]	$\Delta V/V$ [%]	Determination
σcc	4.5	0.003	-0.001	0.002	non linear to this point
σci	43.5	0.0375	-0.013	0.0125	lateral strain departs from linearity
σcd	76.5	0.069	-0.025	0.018	derrived from volumetric strain reversal

Table 5: Volumetric strain results (268.41)

These values are derived by a graphical solution shown in Figure 25. With this graphical approach it is possible to derive the three indicators for the different stress levels. These indicators are partially derived trough the axial strain, the lateral strain and the volumetric strain itself. Note that, although these indicators are derived at different strains, they are representing a stress level. These stress levels can be compared with the different regions derived through the AE-measurements (Figure 24) and should be similar. Note that the colour in the upper left corner refers to the categorisation with this analysis in Figure 27.
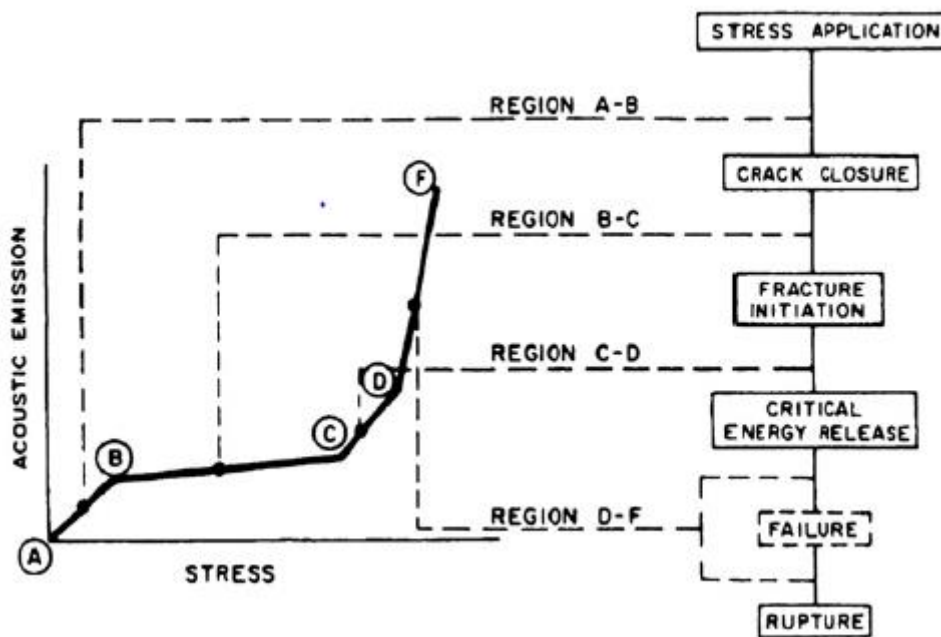

Figure 24: Failure states from AE-measurements [31]

σcc: Also called "crack closure stress", is the point (volumetric stress level) where the axial strain (green line) migrates from a non-linear to a linear part at the beginning of the loading. For brittle rocks, this part is hard to discover because of a very linear increase at the beginning. If this is enlarged, it is easier to distinguish a

slight curve. The part represents the closure of existing micro-cracks depending on initial crack -density and -geometry.

σ_{CI}: Also called "crack initiation stress" is the point (volumetric stress level) where the later strain (orange line) departs from linearity. This part between σ_{CC} and σ_{CI} is considered to be the elastic part of the rock sample and the elastic rock properties can be determined from this stage. It has to be mentioned that this dilation can only be registered in the lateral strain gauge and therefore reflects the growth of axial cracks [30].

σ_{CD}: Also called "crack damage stress", is the point where the volumetric strain reverses its direction and loads above would result in damage to the material under a permanent load. As visible in Figure 25 the cycles were filtered out, to show a smooth strain increase.
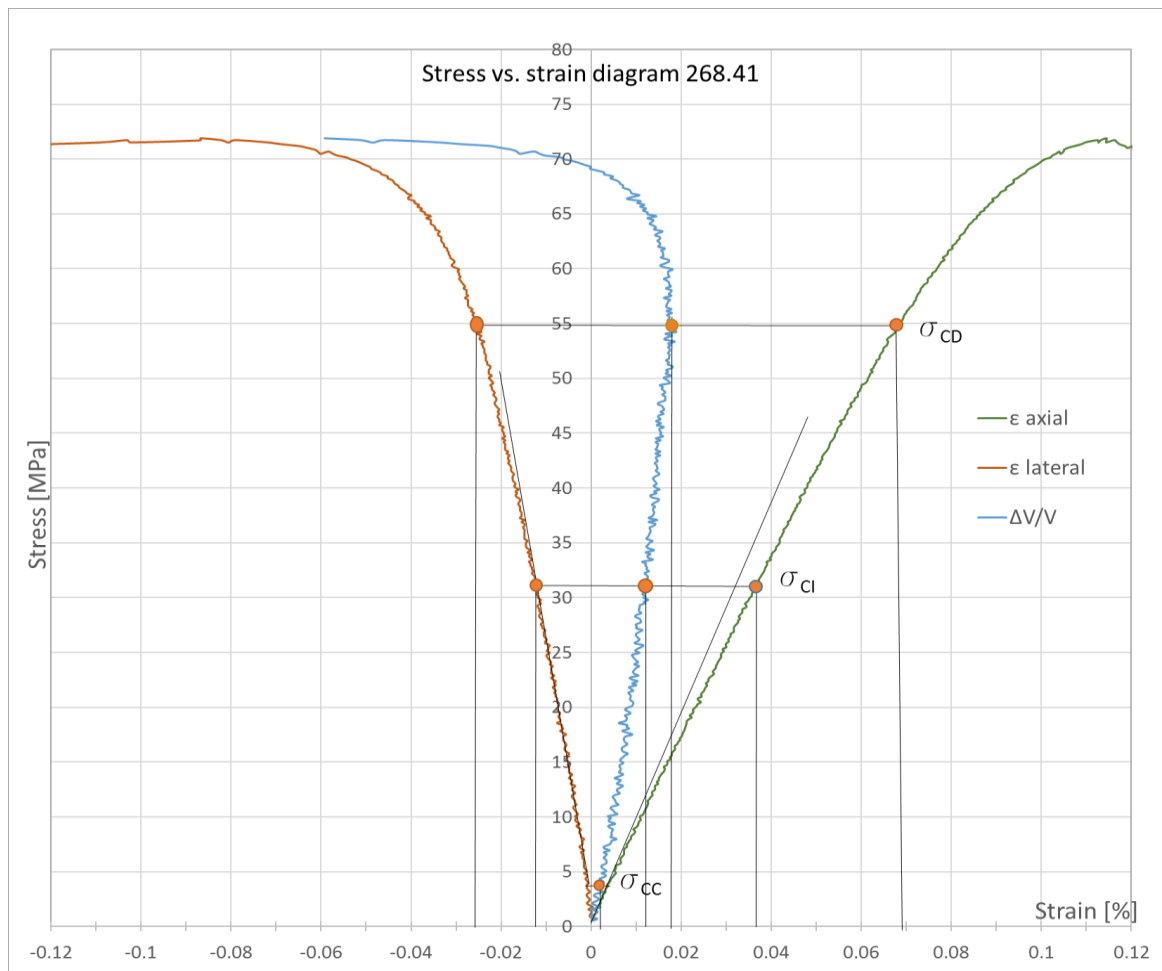

Figure 25: ΔV/V graphical solution

Part 5:

Crack level indicators by $\mathbb{AE}$ Analysis		
derived through graphic solution		
	Stress [%-from UCS]	Determination
σcc	5	the point where the cumulative energy becomes linear for the first time
σci	38.5	the point where the cumulative energy deviates from linearity
σcd	74.5	not eactly established, very uncertain point derived from AE signals

Table 6: Crack level indicators by AE-analysis (268.41)

The values from Table 6 were evaluated with the two programs described in 5.2. After this, the results are displayed in an Excel diagram (Figure 27) to compare the different crack-level indicators. As shown, the independently derived classification from the volumetric strain and the AE-results are similar to each other (<1.5%) in this post processing. It should be mentioned, that the recorded events were not taken into account because their amount and occurrence strongly depends on the entered p-wave velocity (>50% difference by 0.5mm/µs increase). Figure 27 also shows each hit and its absolute energy, which gives a good overview where, how much energy was released by the hits. It has to be mentioned that every hit, including the his in-between the cycles, were taken into account for these values. As mentioned before, due to the Kaiser effect, the error is very small (<2%).

Part 6:

This part of the analysis sheet tries to verify the recently conducted crack-level indicators via pattern recognition. Like described in chapter 5.2.2, Noesis is able to perform such operations.
Several different kinds of the "Unsupervised pattern recognition" can be performed with Noesis:

- Max-Min Distance
- K-Means
- Forgy
- Cluster Seeking
- Isodata
- Agglomerative
- CAM
- L.V.Q. Net

Although there are several options available, only the "K-means method" will be described in this thesis. Due to the fact that pattern recognition is a relatively complex field, the "K-means" method can be used by operators with not much previous experience regarding this topic. It is a simple iterative algorithm, aiming to minimize the square error for a given number of clusters. The algorithm starts with the initial clusters specified and assigns the remaining points to one of the predefined clusters, by nearest neighbour classification. The cluster centers are updated and the process continues until none of the patterns changes class membership [32]. The input parameters are:

1. Distance type: (Euclidian, City Block, Square and Octagonal can be chosen) Refers to the similarity metric used by the method when comparing two vectors (hits, centers, clusters etc.).

2. Initial Partitioning: (Random, N-First Points, Time Distribution, Nearest Mean, Furthest Mean, Current Centers).
   It describes how the method will be initialized, which means that it defines the initial cluster-centers acting as starting points for the method [32].

3. Initial clusters: It has to be defined with how many clusters the algorithm should start calculating.

4. Iterations: Defines the number of iterations done by the computer. If a convergence is reached before the amount of defined iterations, the algorithm will terminate [32].

Like described before, only the "K-Means method" was used to cluster the hits and following input parameters were used:

1. Euclidean
2. Time Distribution
3. 4 (in the K-Means, the amount of initial clusters is equal to the amount of resulting clusters.)
4. 100 (default)

With these input parameters it was attempted to find the four different failure regions and confirm them with the already conducted results from $\triangle V/V$ and the AE-analysis. The results of such a plot can be seen in Figure 26 below.
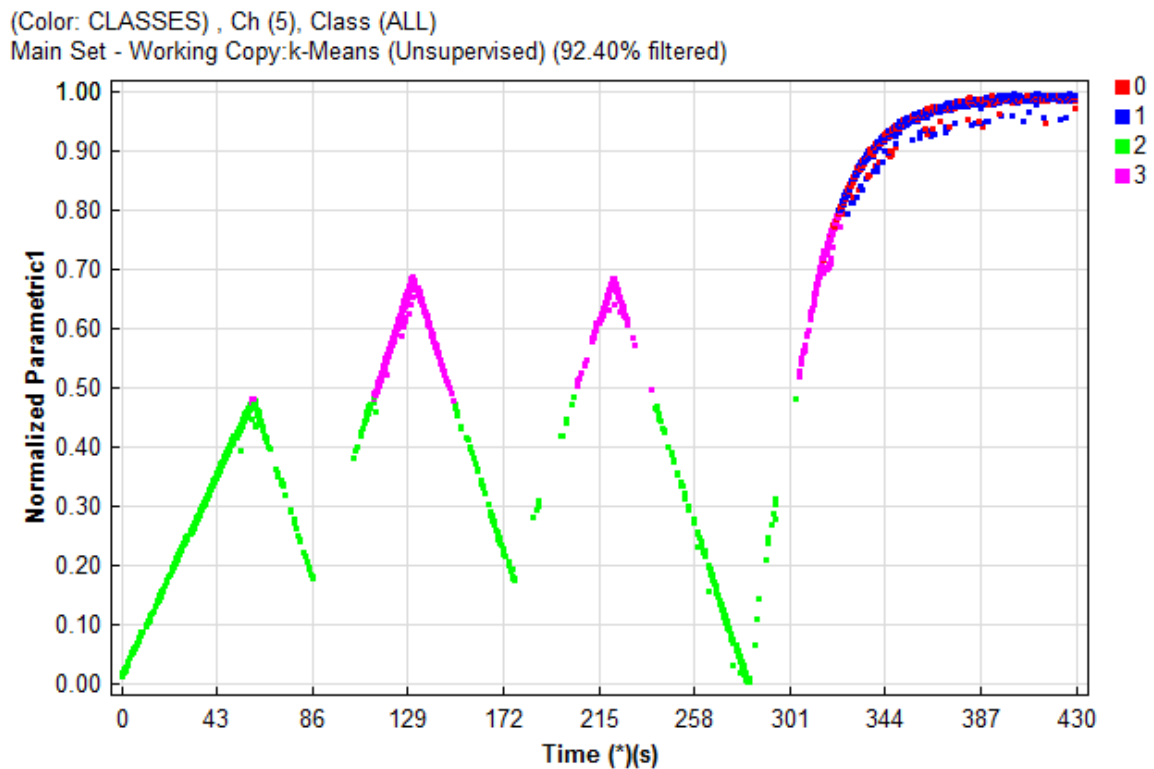

Figure 26: Pattern recognition results for 268.41

It has to be mentioned, that there are only three distinctive sections (red and blue are referring to the same region) clustered by the algorithm. If the boundaries of the pattern recognition-sections are evaluated it can be seen (that they are similar to the ones from $\triangle V/V$ and the AE-analysis. Although two boundaries are similar, the first region (crack closure region) is not present in this plot.

As mentioned earlier, pattern recognition is a part of neural networks. The problem with neural networks is, that they have a "black box" character. This means, that it is hard to comprehend the results and classification steps, done by this program [33]. Subsequently, another method is necessary to confirm the results. For this reason, the pattern recognition classification for the crack-level indicators, should be compared with either the AE-analysis or with the ΔV/V-analysis.
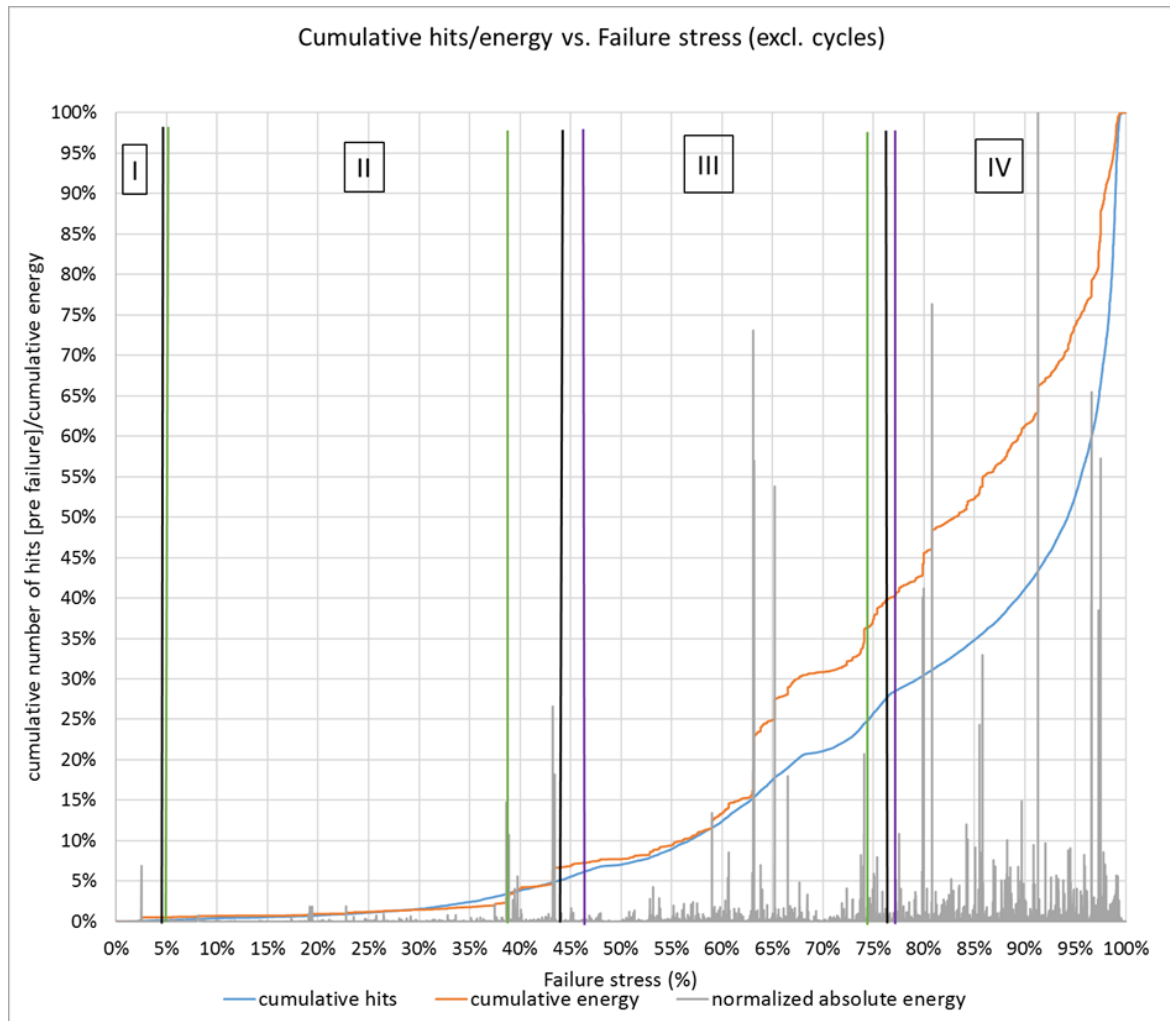

Figure 27: Different failure states due to energy analysis ΔV/V and PR for 268.41

It has to be mentioned that a comparison of the different crack level indicators for one test can be found in the chapter "AE-Post processing data-sheet".

In Figure 27, several vertical lines separate the different sections. As mentioned before, the colours of these lines are indicators of the analysis-method used:

Black: Crack level indicators via Volumetric strain-analysis

Green: Crack level indicators via AE-analysis

Purple: Crack level indicators via pattern recognition

Figure 27 also shows a correlation between hits and energy. They tend to rise similarly. At the beginning, the two lines proceed parallel (in this cases they overlap). In later stages a gradual increase of hits also results in a gradual increase of energy. It has to be mentioned, that either a few energetic hits, or many hits without much energy, offset the two lines from parallelism. This can be observed in every post processed sample.

In section one, the crack closure can be observed. It is characterized by a very small, non-linear increase of hits at the beginning. If the section until the first crack level indicator is zoomed out, this behavior can be seen.

Section two indicates the crack initiation part. In this part small cracks start to form. The hits, which indicate the crack initiation, normally do not have much energy. This can be observed by the parallel behavior of the hits and energy curve. If the sample is very stiff, this behavior cannot be observed (see Appendix, sample number 268.67). There is a gradual increase in hits, but their energy in relation to the total energy is relatively low.

The third part is the critical energy part. It can be seen that much more energetic hits can be found in this section. It is the part where normally the two curves start to offset from parallelism because of high energetic hits. This causes a terrace shaped increase in energy.

The last part indicates the foreseeable failure of the sample. In this section, normally the steepest increase of hits and energy can be observed.

5.4 Useful visualization

To be able to draw some additional conclusions (in addition to the data sheet chapter- 5.3) some visualizations, conducted from the software, are displayed and described below. These were created for each post processed sample and can be found in the Appendix . Exemplarily the visualizations for sample 268.41 will be displayed, and the pros and cons of each plot will be described below.

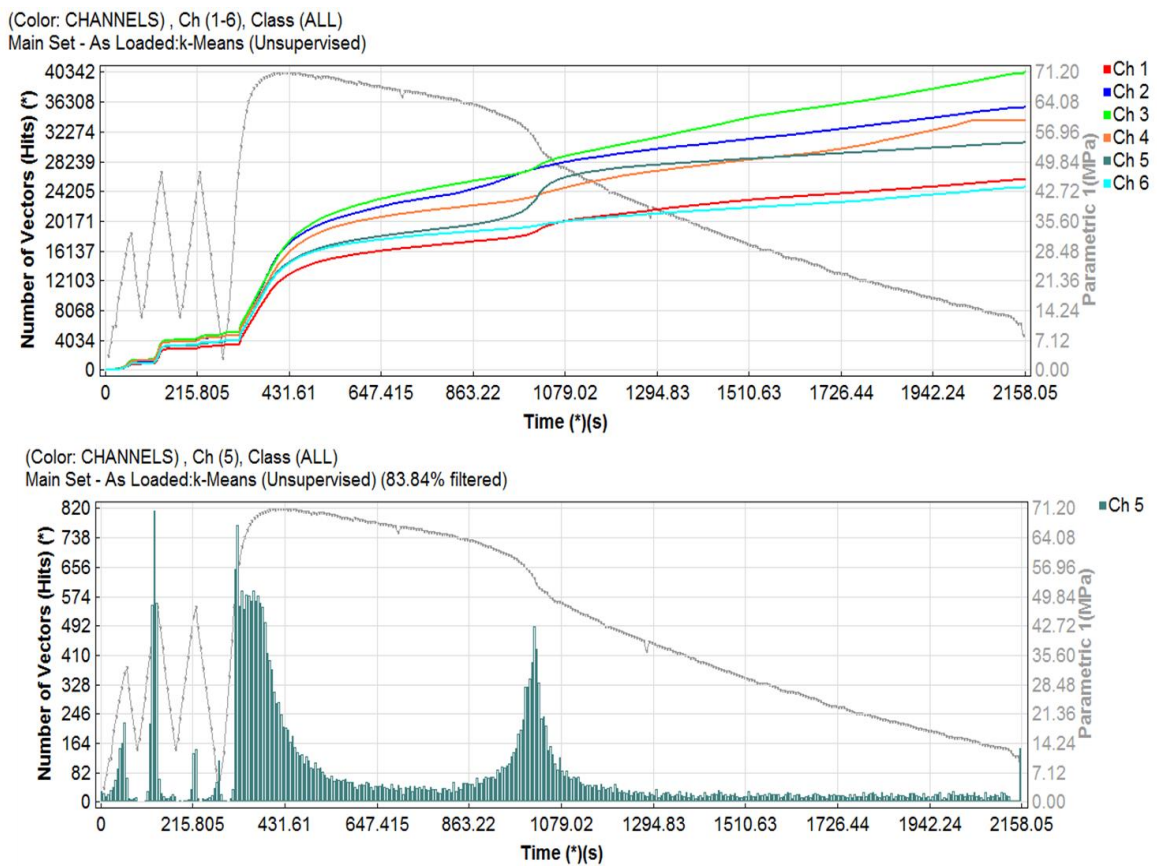### 5.4.1 Overview of hits vs. time (whole test incl. post failure)

Figure 28: Hits vs. time; with post failure

The upper part of Figure 28 shows the cumulative hits of each channel, while the lower part shows the number of hits of a representative channel (in this case channel 5). The grey line in the background represents the stress-path.

Pros:

Figure 28 gives a good overview of the connectivity for each sensor throughout the whole test (incl. post failure). It is also a good visualization of the AE-activity compared to the stress level.

Cons:

Contains no information about the amplitude of each hit.

As shown in the plot, each sensor stayed connected during the displayed test (except channel 4 – last 150 seconds → straight line). Each of the sensors behaves similar (relatively parallel) which means that the amount of counted hits is relatively similar (except for the post failure due to the fractured rock sample).

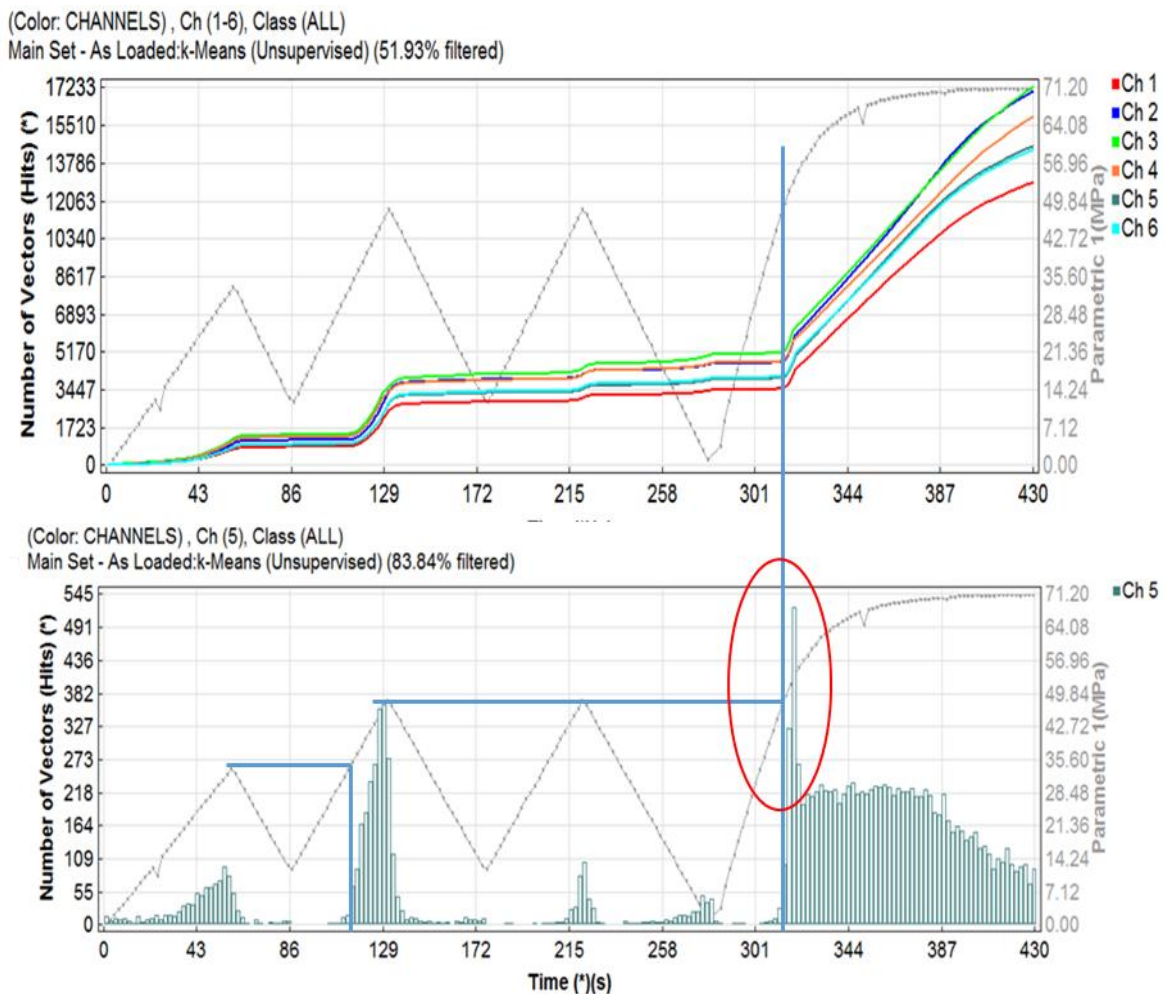### 5.4.2 Overview of hits vs. time (pre failure)

Figure 29: Hits vs. time; without post failure

Figure 29 shows the same as Figure 28, except that only the pre failure region is shown, to better visualize the behaviour of the sample before the actual failure. As highlighted with a red circle there is a high rise before the failure which is a distinct property of the sample.

Pros:

It confirms, that every sensor was properly attached in the pre-failure test-stage. The Kaiser effect can be observed with marginal hits in between (<1%). As visible, only small AE-amplitudes are visible between the stress peaks. If the previous stress peak is surpassed, the AE-amplitudes are much higher, which means that much more hits are registered (see blue lines in the lower part of Figure 29).

Cons:

This plot contains no information about the strength (amplitude) of each hit.
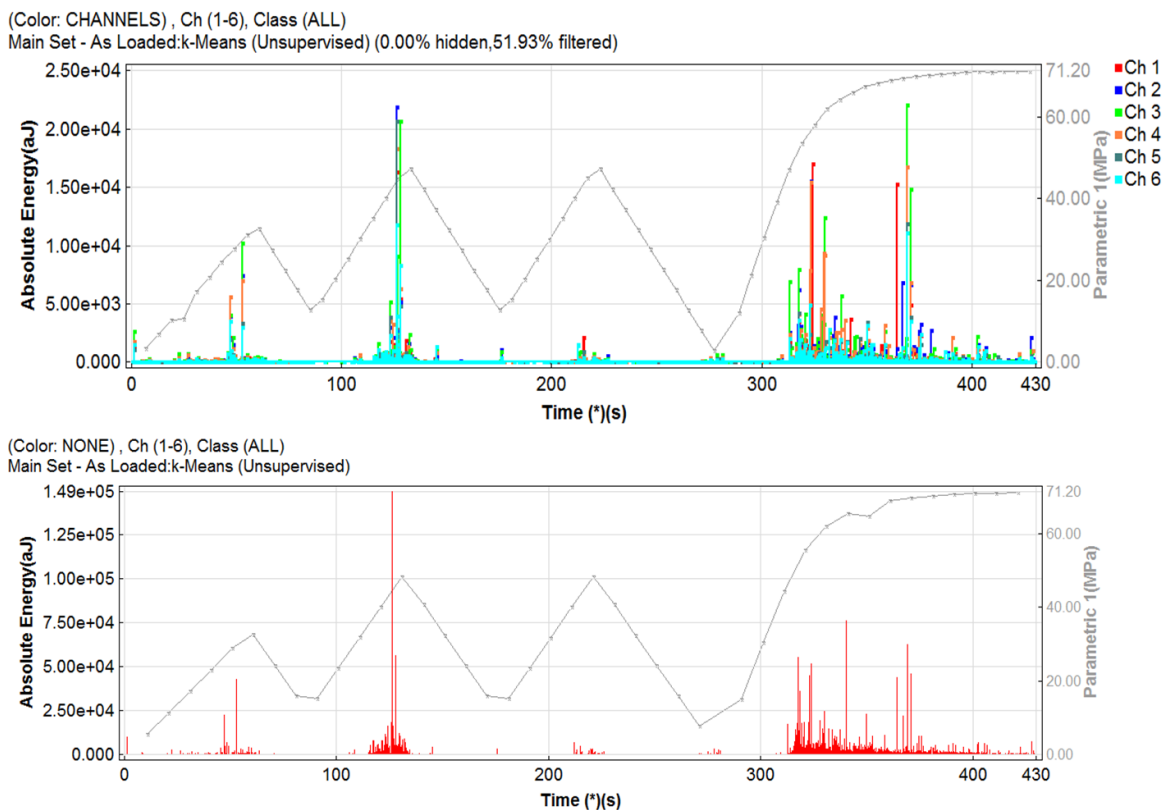
5.4.3 Overview of energy vs. time

Figure 30: Energy vs. time; without post failure

The upper part of Figure 30 shows the strength of a single AE-hit for each channel, compared to the stress level (grey line). The lower part of this plot shows the cumulative energy of all channels, which is also displayed in Figure 27 as normalized energy (grey bars). It should also be mentioned that the energy is displayed in [aJ] = atto-Joule (10^{-18}) which is a common unit for AE-measurements.

Pros:

The plot is a good visualization of the energy behaviour with the progressing stress. The "Kaiser effect" can also be observed in this visualization.

Cons:

Figure 30 only contains information of energy vs. time with no respect to the amount of hits. That's the reason Figure 28 was created to give a summarized and representative overview of all these characteristics.

5.4.4 Events vs. time visualization

Another interesting visualization is the event appearance with progressing stress level. Like mentioned earlier, the event appearance is depending on the used p-wave velocity in the analysis. The visualisation underlying this parameter and Table 4, are shown in Figure 31.
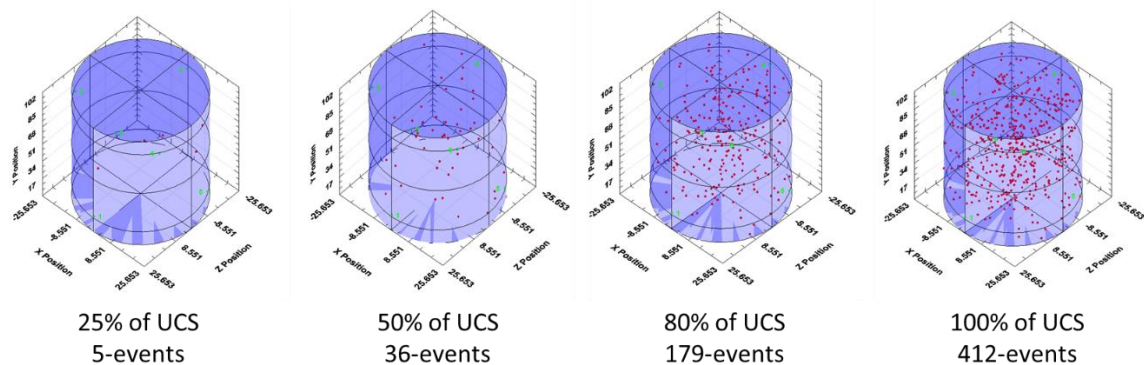

| 25% of UCS | 50% of UCS | 80% of UCS | 100% of UCS |
| 5-events | 36-events | 179-events | 412-events |

Figure 31: Visualization of events depending on stress level

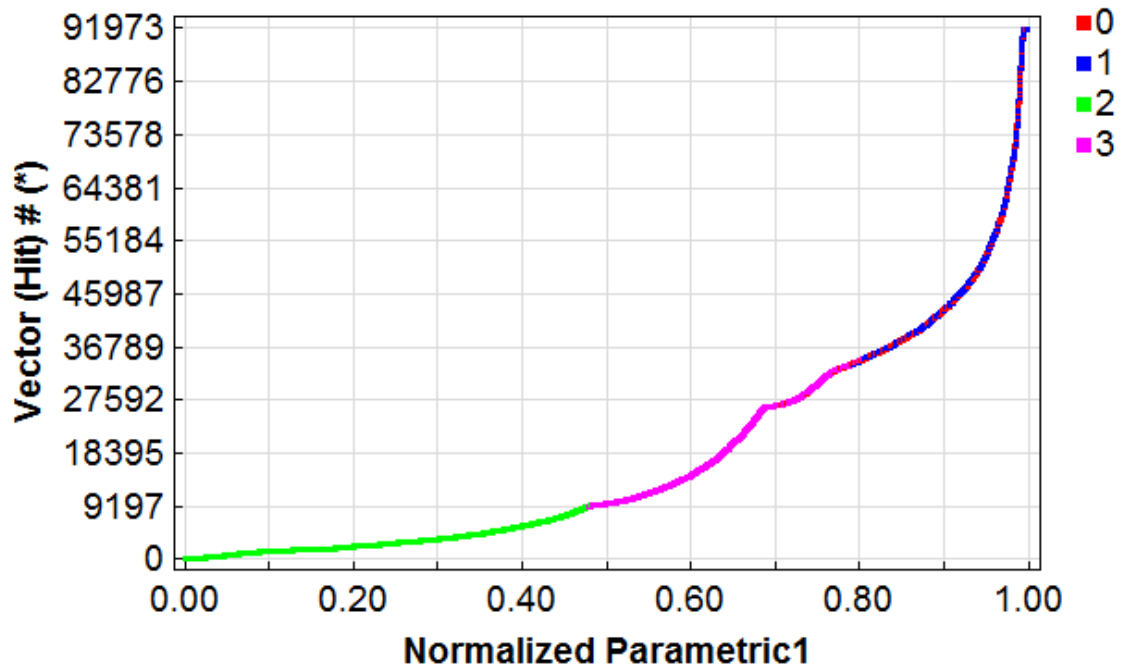### 5.4.5 Pattern recognition plot

Figure 32: Hits vs. Stress clustered with pattern recognition

Figure 32 shows the cumulative hits ("Vector (Hit) #") vs. normalized stress diagram ("Normalized Parametric1") and its classification by the pattern recognition. It visualizes, at which normalized stress state the classification changes.

Pros:

A good visualization of the boundaries with respect to the stress level. Easy and fast way to distinguish two of the three crack-level boundaries.

Cons:

Only two of the three crack level-boundaries could be visualized with the pattern recognition. Pre-processing of the data is necessary to be able to get conclusive results.

6 Interpretation

In this chapter the post-processed samples will be compared. The values which are shown in the figures below, are taken from their respective part of the data-sheet (see chapter 5.3). As an overview, the UCS values, elastic parameters and the specific destruction energy for each post-processed sample, will be displayed in Figure 33:
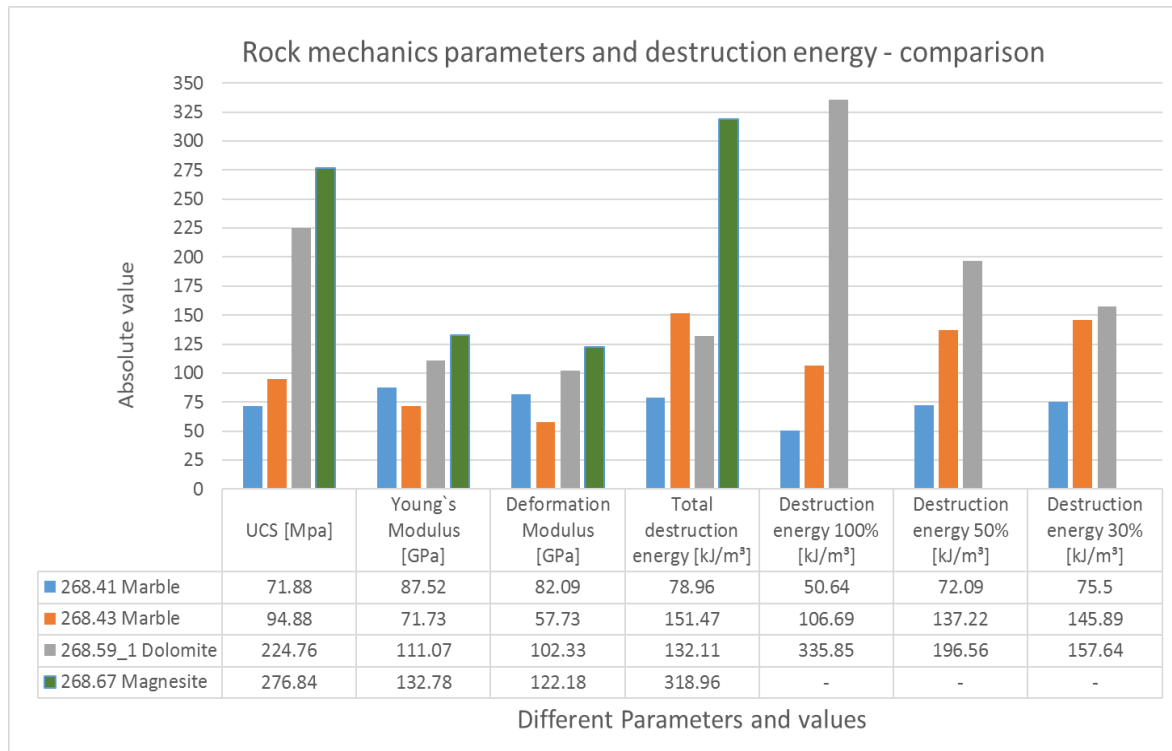
Figure 33: Parameter comparison and specific destruction energy of the post processed samples

As mentioned in chapter 4.1, these are the samples which were post-processed. Two marbles, a dolomite and a magnesite were chosen and their results can be found in the Appendix. It has to be mentioned that the test from sample 268.59 was interrupted at about 30% of the UCS value and was started again under the reference number 268.59_1. This means, because of the pre-loading, the results from this sample are not 100% representative for this rock type. Nevertheless, the Kaiser effect could be visualized as well (see "Hits vs. time" diagram for the sample 268.59_1 in the Appendix).

In the following figures the absolute and normalized values from hits, events and energy will be displayed and compared.

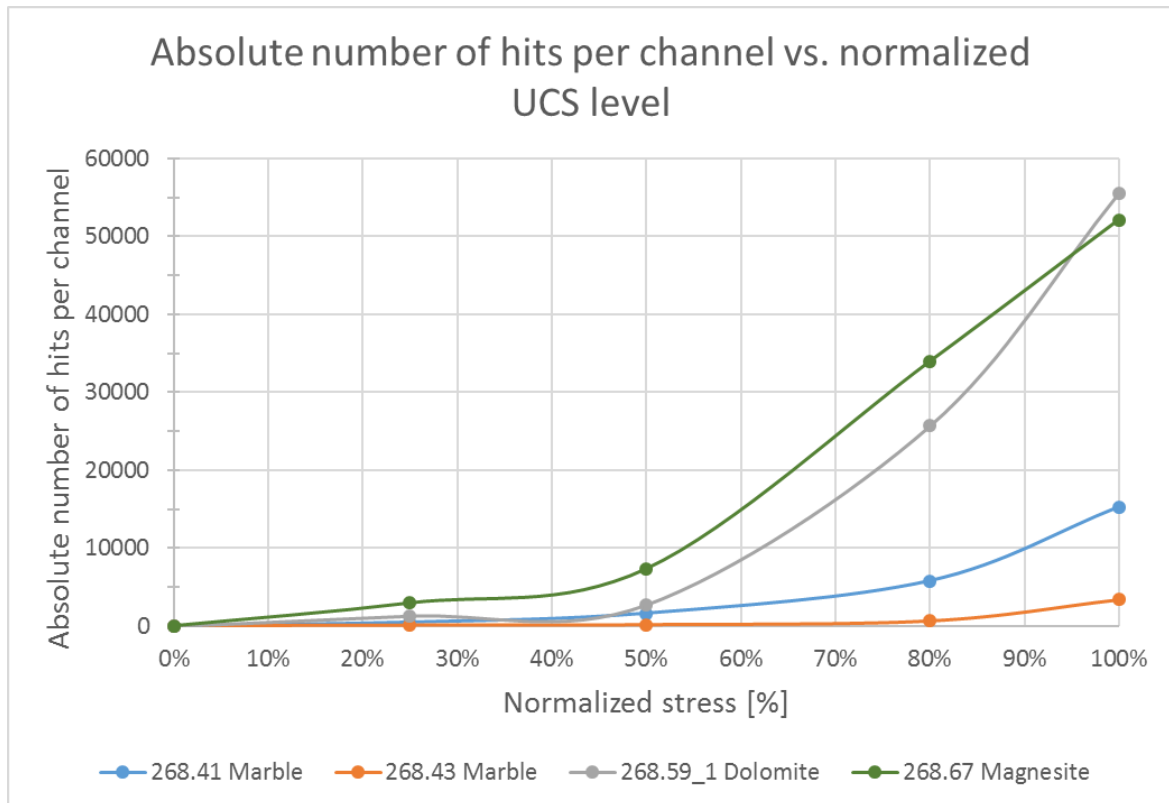## 6.1 Absolute Hits comparison

Figure 34: Absolute hits comparison

The figure above shows the absolute number of hits for each rock type, respectively to their normalized UCS levels. As visible in Figure 34, there is a big difference in the amount of absolute hits between samples with a UCS >200MPa and rock samples <100MPa. Due to the trend of the destruction energy in Figure 33 (100% - 30%), a rock classification can be distinguished. It can be observed, that the samples with lower UCS values and hits are Class I rocks and the dolomite is a Class II rock (see chapter 2.4). Unfortunately, the rock class for the magnesite could not be distinguished, but it is considered to be a Class II rock.

Due to the fact that sample 268.59_1 was pre-loaded, the amount of hits should be even higher for this sample. Up to this point, no correlation of the absolute amount of hits and the sample`s elastic parameters can be observed. To be able to correlate the absolute amount of hits with the UCS values and elastic parameters, more data is necessary, especially from samples of the same rock type.
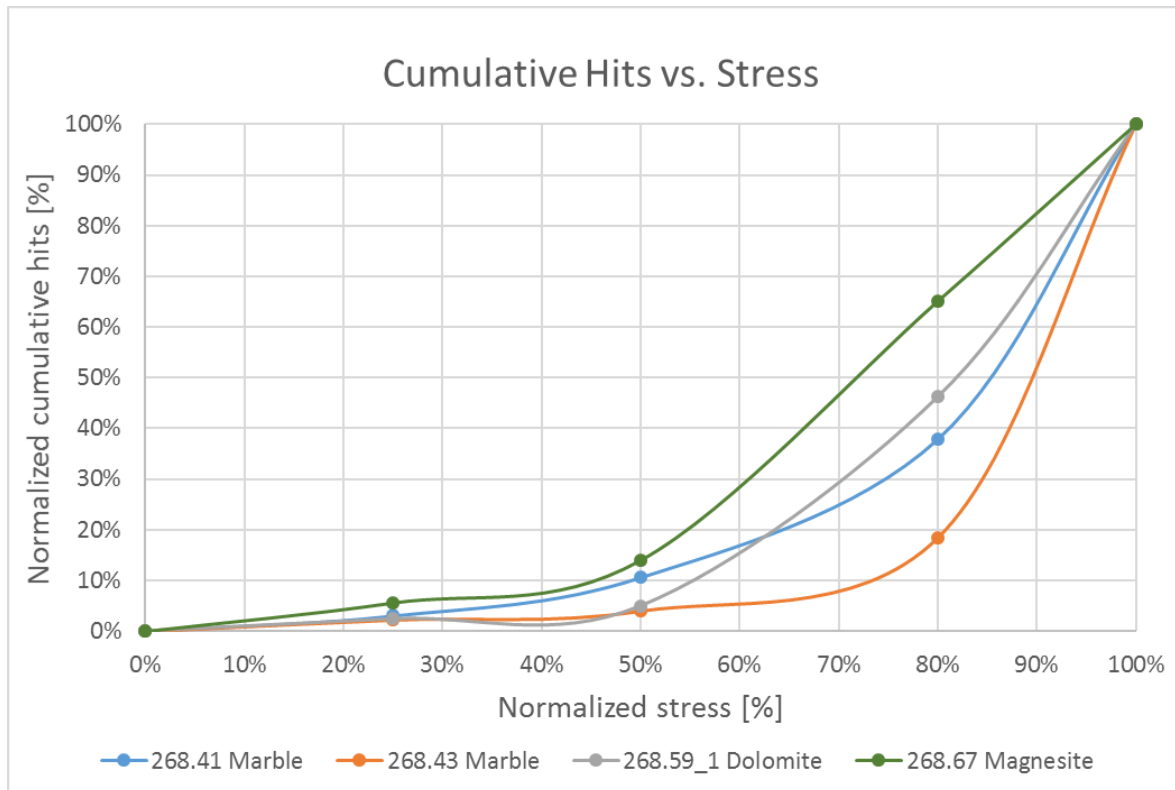
6.2 Normalized Hits comparison

Figure 35: Normalized cumulative hits comparison

As shown in the figure above, the normalized cumulative hits in relation to their normalized UCS levels are displayed. This was done, to be able to compare different rock types with different amount of hits and UCS values. What can be seen in Figure 35 is, that each rock sample shown, behaves relatively similar till 50% of the UCS. Most definitely can be said, that the cumulative hits from sample 268.59_1 would be much higher without the pre-stressing (at least till 30% of the UCS). The reason for this is, that the hits which had occurred during the first loading, were not replicable during the second loading (Kaiser effect).

Also visible in Figure 35 is, that the marble rock samples (268.41 and 268.43) generate more than 50% of their hits in the range of 80% and 100% of their maximum stress (except for 268.59_1; due to interrupted test, the real amount of hits could not be displayed here). The sample 268.43 is the sample with the lowest elastic parameters but with the steepest curve in the last 20% of the UCS.
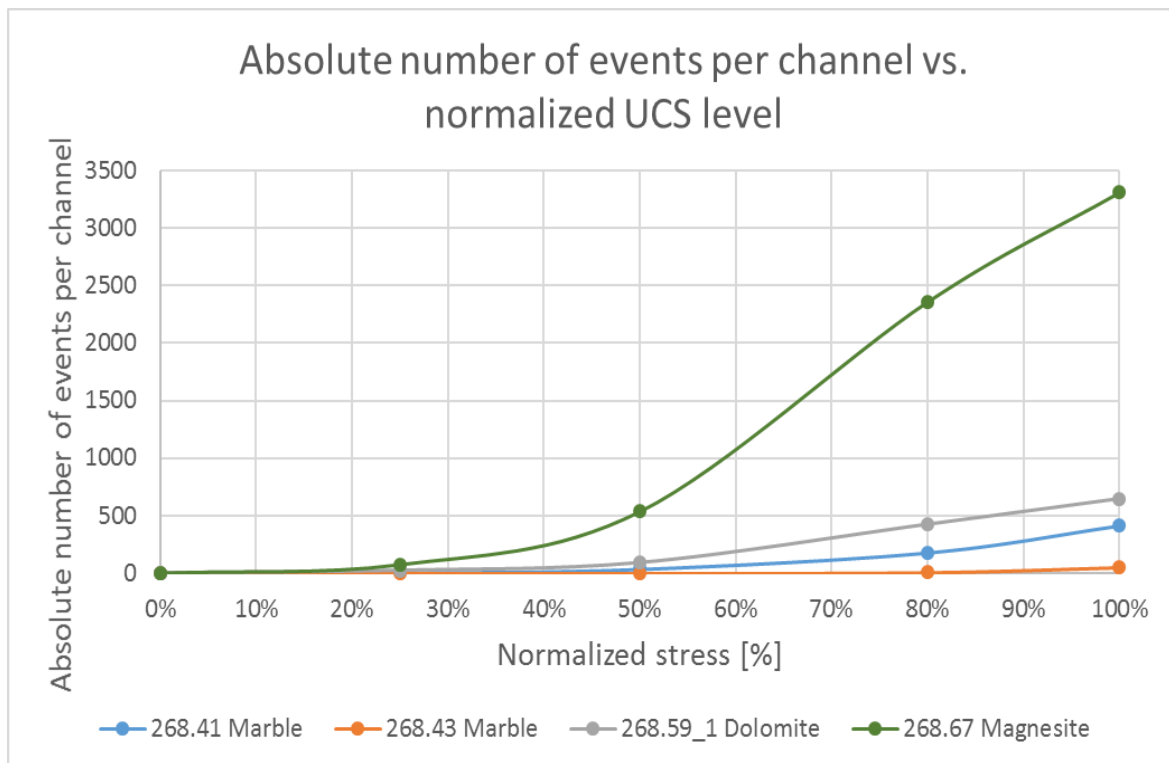
6.1 Absolute Events comparison

Figure 36: Absolute events comparison

As mentioned before, the number of events depends, amongst others, on the entered p-wave velocity in AE-Win. Due to this fact, an objective comparison between different rock types is difficult. Events are back-calculated from the hits. For this reason Figure 36 should look similar to Figure 34. The fact that these two figures do not look similar verifies the assumption, that an absolute events-comparison cannot be performed between different rock types at this point.

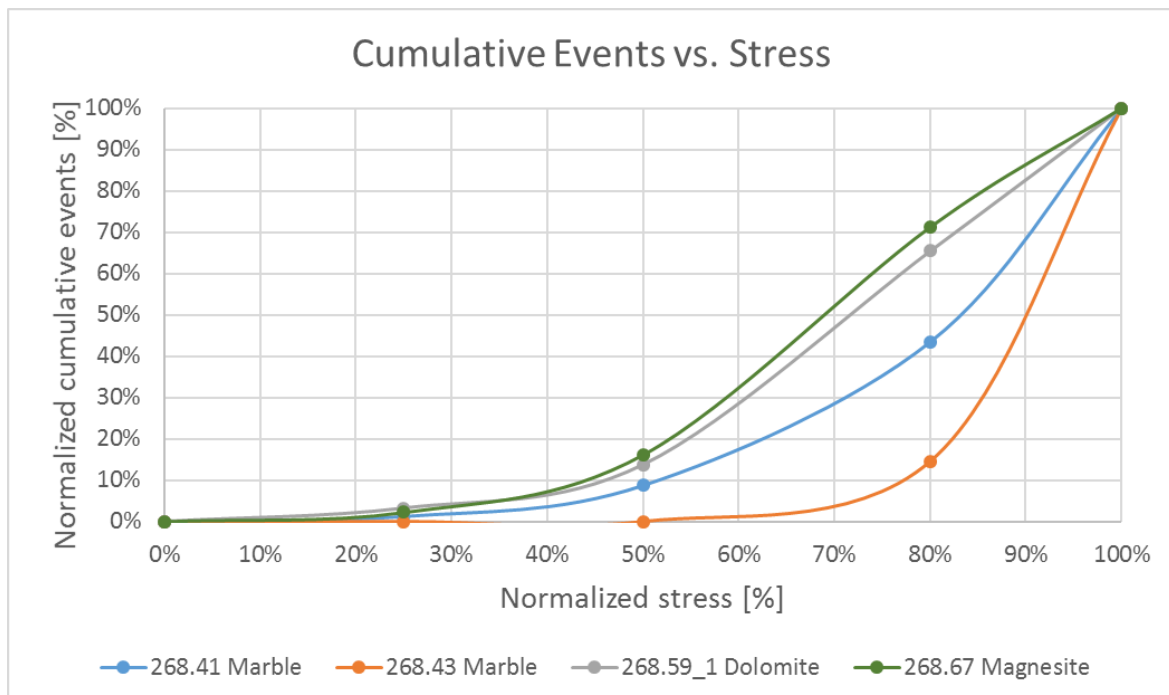## 6.2 **Normalized Events comparison**

Figure 37: Normalized cumulative events comparison

Although samples 268.59_1 and 268.67 behave similar in this plot, it has to be considered that the grey line is not representative at the beginning (until 30% of the maximum loading →pre-loading level). This would mean that without pre-loading of the sample, the results of sample 268.59_1 would be higher, especially in the beginning. What can be seen is, that they behave very similar after 50% of the maximum loading.

It can also be observed, that the order of the cumulated events, in the last 20%, is the same as in Figure 35. This can also be traced back to the fact that the events are back-calculated from the hits. Due to the uncertainty in the p-wave velocity in different directions and its stress dependence it can be said, that it is better to compare hits with other samples, not events.

6.1 Absolute Energy comparison

The following graphs show the absolute cumulative energy of the hits. This should not be mistaken with the SDE (see chapter 2.3).

It is safe to say, that hits from stiffer rocks (and with higher UCS) in general release more energy until the failure, than softer rocks. This can be observed in Figure 38. The absolute energy of the samples 268.59_1 and 268.67 is higher by a factor of 10^4, which makes it hard to compare them with the marbles (268.41 and 268.43).
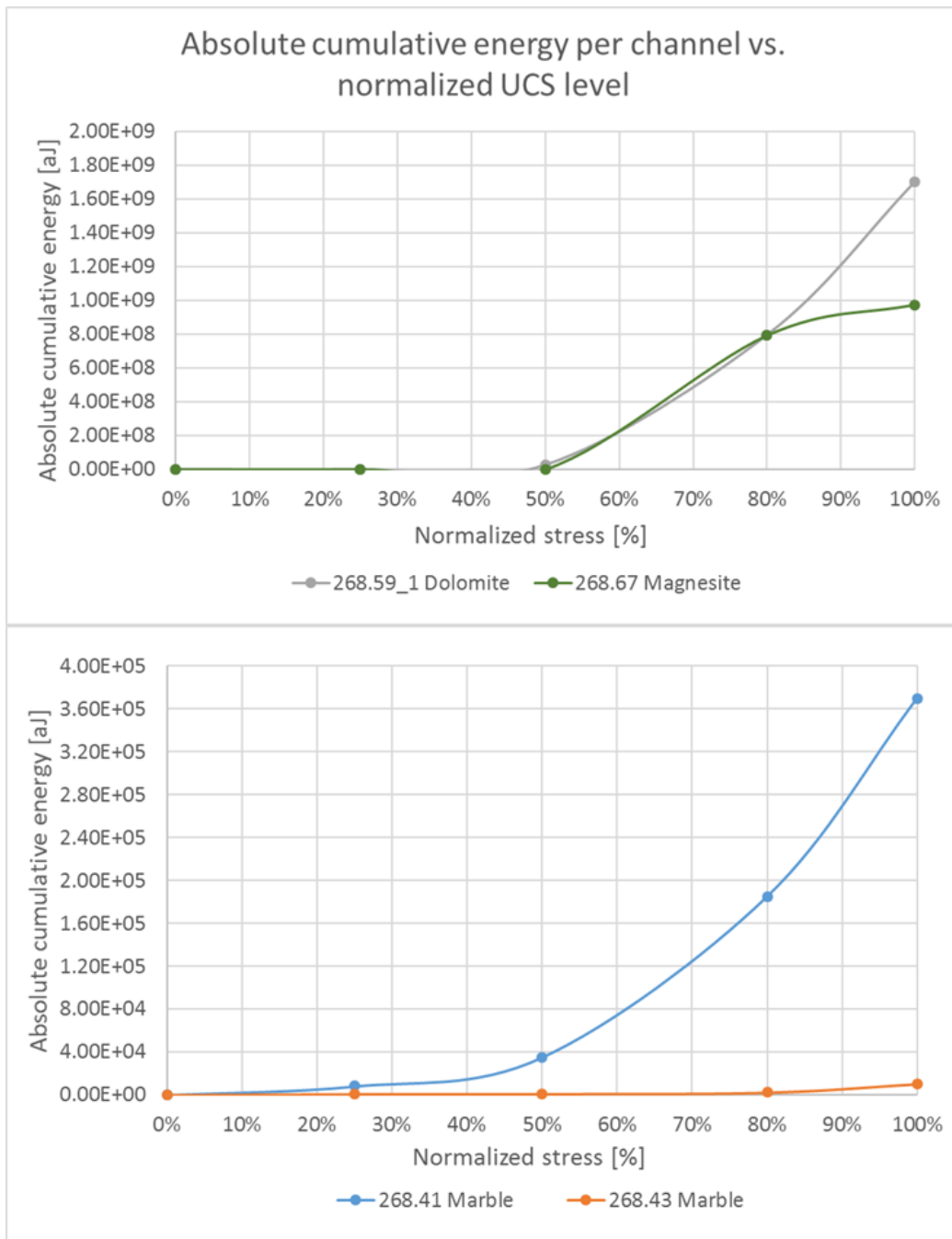
Figure 38: Absolute energy comparison

In can be seen, that the dolomite (sample 268.59_1) released the most energy throughout the test. It has to be mentioned again, that the energy is released by the formation and propagation of cracks. It should not be mistaken with the SDE. It is also visible, that the magnesite behaves similar till 80% of the UCS, then releases only a low amount of energy. A pre-healed crack was observed at sample 268.67. This pre-healed crack could be the reason for the shape of its energy curve.

Due to this magnesite-behaviour, several failure mechanisms could be possible:

1. Sliding along the crack. A big amount of hits, but small amplitudes and energy would be the result. This would lead to shown behaviour of the flattening curve (268.67) in Figure 38 and Figure 39.

2. Stress concentrations caused by heterogeneities. A small amount of hits, but with high amplitudes and energy would be the result.
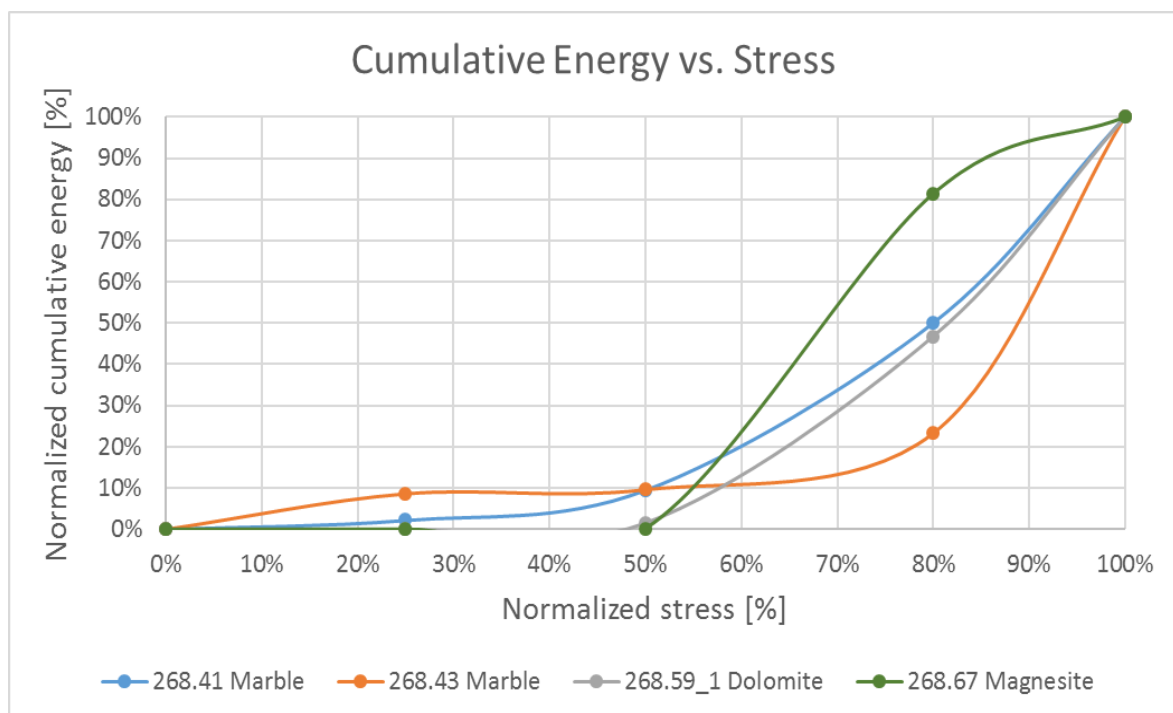
6.2 Normalized Energy comparison

Figure 39: Normalized cumulative energy comparison

Interesting in the normalized cumulative energy plot is, that the sample with the lowest elastic parameters (268.43) releases relatively the most energy in the last 20% of the UCS. It can also be observed, that the stiffest and the sample with the highest UCS (268.67), generates 80% of its energy before the last 20% of the UCS. The reason for that could be, as mentioned, the influence mechanism of the healed

crack. An indicator for such a behaviour is the occurrence of just a few hits, which generate more than 80% of the energy (see the results of 268.67 in the Appendix). Also noticeable is, that these were high-amplitude- (>90db) and high-energetic - hits (>10^8 aJ).

It has to be mentioned, that a high amplitude has to be seen relative to the sample`s average, but normally it is above 85db. Due to the fact that a high-amplitude correlates with high absolute energy, it can be concluded, that the amount of absolute energy released by a single hit is an indicator for the amplitude of this hit. If the "Energy vs. Time" diagrams from samples 268.59_1 and 268.67 are compared (see Appendix), it can be seen, that sample 268.59_1 generates the high amplitude hits above 80% of the UCS value. This leads to the conclusion, that no pre-healed crack or bigger heterogeneities appear in the sample and a sudden failure is going to occur soon.
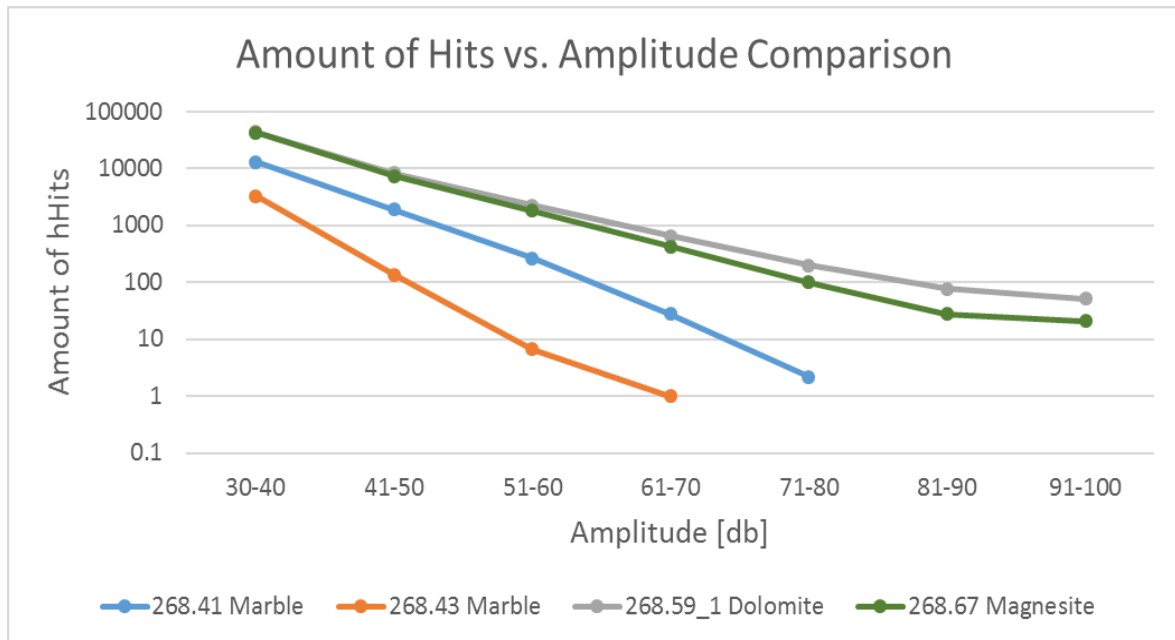
6.3 Amplitude comparison

Figure 40: Amplitude comparison

The figure above shows the amount of hits relative to their amplitude. It clearly shows, that the most hits are low-amplitude hits between 30db and 40db.The vertical axis is displayed in a logarithmic scale, to be able to visualize the amount of high energetic hits (>80db). Note that the amplitude scale starts at 30db. This is because of the threshold, which was set to exclude noise from the records.

As visible in Figure 40, the only similar behaviour between the hit´s amplitude is between the last two samples (268.59_1 and 268.67). These are also the samples with the highest UCS values.

As visible in Figure 40, the two samples are the only ones with amplitudes higher than 80db and 90db. This leads to the conclusion that rocks with amplitudes higher than 85db are highly prone to rock burst. These hits normally occur at about 80% and higher of the UCS, which indicates a soon failure.

7 Summary

The goal of this master thesis was, to find a post-processing routine and to be able to compare different rocks, tested and measured with the AE-measurement. During the test procedure, the Kaiser effect was visible. For determining the crack level indicators (see Figure 27) all three types of analysis techniques were applied. For the first stage (σ_{cc}), the AE-energy analysis is the best option. The energy-plot in this area can be enlarged to see a slight curve, and the transition from non-linear to linear can be observed easily.

For the second stage (σ_{ci}), pattern recognition should be used. Due to the fact that the AE-results are not easy to interpret in this area and the volumetric strain analysis is also depending on the operator's skills, pattern recognition is the best option for determining this indicator.

The last indicator (σ_{cd}) can easily be observed with the volumetric strain comparison. There is just one point where the volumetric strain reverses its direction, which makes it easy to distinguish. This point can also be double-checked by applying the pattern recognition. The "K-means" method was applied in this thesis and the results from the volumetric strain and AE-energy analysis could be confirmed.

As the development of the post processing routine has shown, it is not easy to compare different samples. Four overall comparisons have been looked at in more detail:

1. Hits comparison
2. Events comparison
3. Energy comparison
4. Amplitude comparison

These four were compared by the absolute values as well as the normalized values. The event comparison is not suitable for comparing different rock-samples objectively at this point. It is related to the hits comparison but with the error of uncertain p-wave velocity. Although the amplitude comparison shows similarities between the samples 268.59_1 and 268.67, more samples have to be analysed to be certain, that a comparison between samples with similar amplitude characteristic is possible.

Best results showed the hits comparison and the energy comparison. In the course of post processing, the rock samples showed some good correlations with parameters like stiffness and UCS value.

AE-measurements in general are very complex. Due to the high sensitivity of the measurement and instruments, results can easily get distorted. Another challenging part of this measurement technique are the results itself. Especially the amount of hits and data in general can be challenging. It is safe to say that a test includes hundreds of thousands of hits with different signal-characteristics. The proposed analysis methods and the developed data sheet provide a good basis for evaluation and interpreting AE results.

8 Outlook

This thesis is only considered to provide a step by step analysis and post processing routine. The next steps should be, that more samples are post-processed and their results are compared afterwards. If a high amount of post processed results is available, there is a possibility other correlations can be distinguished. To be able to compare the different events, the change of p-wave velocity should be investigated in detail. This could also lead to a better localisation of the events.

The hits comparison and the energy comparison should also be further investigated. As mentioned, two other analysing-routines haven´t been further addressed in this thesis. The "b-value" analysis and the "moment tensor" analysis could be performed and the results could be compared with the already evaluated methods.

Further investigations in the pattern recognition are also strongly recommended. Like described in this thesis, only the "K-means" method was used. This is the most user-friendly one, but as shown, it was not able to distinguish all three cack level indicators. If additional effort is put into this topic, all crack level indicators and additional signal types, e.g. EMI or reflexions, could be classified and filtered if needed.

9 References

[1] Grosse, C., Ohtsu, M., *Acoustic Emission Testing: Basics for Research - Applications in Civil Engineering*, Springer-Verlag, Berlin, Heidelberg 2008.

[2] Plahs, S., Schallemission von Bruchereignissen in Gesteinen. Master Thesis 2015.

[3] He, M. C., Miao, J. L., Feng, J. L., Rock burst process of limestone and its acoustic emission characteristics under true-triaxial unloading conditions. *International Journal of Rock Mechanics and Mining Sciences* 2010, *47*, 286–298.

[4] Cheng, W., Wang, W., Huang, S., Ma, P., Acoustic emission monitoring of rockbursts during TBM-excavated headrace tunneling at Jinping II hydropower station. *Journal of Rock Mechanics and Geotechnical Engineering* 2013, *5*, 486–494.

[5] Rao, M., *Acoustic Emission Signatures of Microcrack Damage in Rock: Laboratory Investigations*, LAP Lambert GmbH, Saarbrücken, Germany 2012.

[6] Lockner, D., The Role of Acoustic Emission in the Study of Rock Fracture 1993.

[7] Wevers, M., Lambrighs, K., Working principle of the AE method. [Internet], 2009 [cited 2017 Dec 28]. Available from: https://www.researchgate.net/figure/230258957_Figure-1-Working-principle-of-the-AE-method.

[8] ÖNORM B 3124-9: Prüfung von Natursteinen; Mechanische Gesteinseigenschaften, Elastizitätsmodul, Arbeitslinie, Verformungsmodul und Querdehnzahl bei einaxialer Druckbelastung 1986.

[9] Su, O., Genis, M., Variation of specific destruction energy depending on particle and bond prperties 2016.

[10] Wawersik, W. R., Fairhurst, C., A study of brittle rock fracture in laboratory compression experiments. *International Journal of Rock Mechanics and Mining Sciences & Geomechanics Abstracts* 1970, *7*, 561–575.

[11] Vallen, H., Schallemissionsprüfung: Grundlagen - Gerätetechnik - Anwendungen [Internet], DGZfP-Jahrestagung, Berlin 2001 [modified 2006 Aug 15; cited 2017 Dec 28]. Available from: http://www.ndt.net/article/dgzfp01/papers/v15/v15.htm.

[12] Filipussi, D. A., Guzmán, C. A., Xargay, H. D., Hucailuk, C. et al., Study of

Acoustic Emission in a Compression Test of Andesite Rock. *Procedia Materials Science* 2015, *9*, 292–297.

[13] Vallen, H., AE Testing Fundamentals, Equipment, Applications [Internet], 7th Ed., Icking, Germany 2002 [modified 2006 Aug 15; cited 2017 Dec 29]. Available from: http://www.ndt.net/article/v07n09/05/05.htm.

[14] Cox, S. J. D., Meredith, P. G., Microcrack formation and material softening in rock measured by monitoring acoustic emissions. *International Journal of Rock Mechanics and Mining Sciences & Geomechanics Abstracts* 1993, *30*, 279.

[15] Bieniawski, Z. T., Denkhaus, H. G., Vogler, U. W., Failure of fractured rock. *International Journal of Rock Mechanics and Mining Sciences & Geomechanics Abstracts* 1969, *6*, 323–341.

[16] Schubert, W., Skriptum Tunnelbau und Felsmechanik: Vorlesungsunterlagen, University of Technology Graz, Austria 2014.

[17] Amann, F., Button, E. A., Evans, K. F., Gischig, V. S. et al., Experimental Study of the Brittle Behavior of Clay shale in Rapid Unconfined Compression. *Rock Mech Rock Eng* 2011, *44*, 415–430.

[18] ÖNORM EN 1330-9: Non-destructive testing - Terminology - Part 9: Terms used in acoustic emission testing 2009.

[19] Bormann, P., Engdahl, B., Kind, R., Seismic wave propagation and Earth models.

[20] Difference Between S Waves, P Waves, Body Waves [Internet], 2016, June 27 [cited 2018 Jan 2]. Available from: https://byjus.com/physics/p-wave/.

[21] Lamit Company, Earthquake Early Warning System. SOS-LIFE Quake Detector [Internet], 2014 [modified 2014 Jan 6; cited 2018 Jan 2]. Available from: http://www.lamit.ro/earthquake-early-warning-system.htm.

[22] ÖNORM EN 13477 - 1: Non-destructive testing - Acoustic emission - Equipment characterization - Part 1: Equipment description 2001.

[23] Ishida, T., Labuz, J. F., Manthei, G., Meredith, P. G. et al., ISRM Suggested Method for Laboratory Acoustic Emission Monitoring. *Rock Mech Rock Eng* 2017, *50*, 665–674.

[24] Spadotto, A. A., Components of the acoustic swallowing signal: preliminary study [Internet], Jornal da Sociedade Brasileira de Fonoaudiologia, Sao Paulo 2012 [cited 2017 Dec 29]. Available from: http://www.scielo.br/scielo.php?pid=S2179-

64912012000300006&script=sci_arttext&tlng=en.

[25] Physical Acoustics, Physical Acoustics 2/4/6 -preamplifier: Switch Selectable Gain Single Ended and Differential Preamplifier [Internet], Physical Acoustics [cited 2018 Jan 3]. Available from: http://www.physicalacoustics.com/by-product/2-4-6/.

[26] Peintner, C., Investigations on artificial samples with different aggregates regarding rockburst proneness. Master Thesis 2017.

[27] Lavrov, A., The Kaiser effect in rocks: Principles and stress estimation techniques. *International Journal of Rock Mechanics and Mining Sciences* 2003, *40*, 151–171.

[28] MISTRAS Group, Our Mission Statement [Internet] [cited 2018 Jan 24]. Available from: http://www.mistrasgroup.com/company/mission.aspx.

[29] Athanasios Anastasopoulos, Pattern Recognition Techniques for Acoustic Emission Based Condition Assessment of Unfired Pressure Vessels.

[30] Derek, M., Chandler,Neil,A., The progressive fracture of Lac du Bonnet granite. *International Journal of Rock Mechanics and Mining Sciences & Geomechanics Abstracts* 1994, *31*, 643–659.

[31] Lehtonen, A., Cosgrove, J. W., Hudson, J. A., Johansson, E., An examination of in situ rock stress estimation using the Kaiser effect. *Engineering Geology* 2012, *124*, 24–37.

[32] Kattis, S., Noesis - Manual Rev.16: Advanced Acoustic Emission Data Analysis Pattern Recognition & Neural Networks Software 2013.

[33] Heinert, M., Künstliche Neurale Netze: Ein Blick in die Black Box.

Appendix

Nano30 sensor datasheet:

MISTRAS — A World of NDT Solutions | Products & Systems Division

PHYSICAL ACOUSTICS CORPORATION

Nano30 Sensor
**Medium Frequency Resonant Miniature Sensor**

DESCRIPTION AND FEATURES

The Nano-30 miniature AE sensor has a resonant response at 300Khz and a good frequency response over the range of 125 – 750 kHz. Its size makes the sensor an ideal candidate for applications where small size is important. The sensor features a small, 1 meter, integral coax cable, which exits from the side of the sensor with a BNC connector on the end.

APPLICATIONS

The sensor can be used in any application requiring a small, mid-band frequency response. It can easily be mounted using epoxy and can be mounted in small and tight spaces.
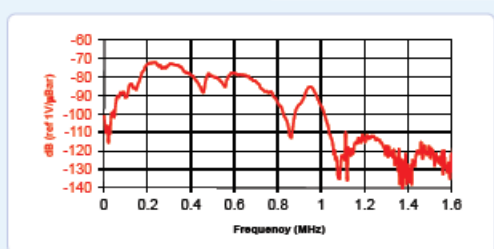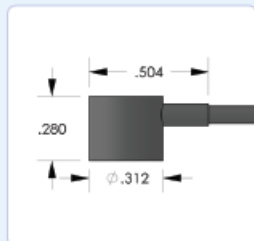
OPERATING SPECIFICATIONS

Dynamic
Peak Sensitivity, Ref V/(m/s) .... 62 dB
Peak Sensitivity, Ref V/µbar ....-72 dB
Operating Frequency Range .... 125-750 KHz
Resonant Frequency, Ref V/(m/s) .... 140 KHz
Resonant Frequency, Ref V/µbar .... 300 KHz
Directionality ....+/- 1.5 dB

Environmental
Temperature Range ....-65 to 177ºC
Shock Limit ....500 g
Completely enclosed crystal for RFI/EMI immunity

Physical
Dimensions.......................................0.3"OD X 0.3"H
....8 mm OD X 8 mm H
Weight .... 2 grams (8 with cable & connector)
Case Material.....................................Stainless steel
Face Material....................................... Ceramic
Connector .... BNC
Connector Locations...Side

ORDERING INFORMATION AND ACCESSORIES
Nano30...Nano30
Cable (specify cable length in meters)................. 1 m
Preamplifier.. 0/2/4, 2/4/6
Amplifier Subsystems AE2A, AE5A
Preamp to System Cable (specify length in 'm') 1234-X

Sensors include
NIST Calibration Certificate & Warranty

Product data sheet of the PAC 2/4/6 preamplifier

MISTRAS
A World of NDT Solutions | Products & Systems Division

2/4/6 Preamplifier

Description:

The 2/4/6 preamplifier was designed to be used with all available AE systems that have power supplied via the output signal BNC. It is supplied with 20/40/60 dB gain (switch selectable) and operates with either a single ended or differential sensor. Plug in filters provide the user with flexibility to optimize sensor selectivity and noise rejection. These filters are provided in the Low Pass (LP), High Pass (HP), and Band Pass (BP) configurations, and offers constant insertion loss for easy filter swapping without the need for recalibration. Automatic Sensor Test (AST) is standard. This option provides the sensor with the ability to characterize its own condition as well as send out a simulated acoustic emission wave that other sensors can detect.

Features:

- 20/40/60 Selectable Gain
- Wide Dynamic Range > 90dB Standard
- Low Noise < 2∞V (With Standard* Filter & Input Shorted)
- Large Output Signal 20Vpp into 50∞
- Single Power/Signal BNC or Optional Separate Power/ Signal BNC
- Plug-in Filters (Utilizes the same filter as the SPARTAN 2000)
- High Input Impedance
- Standard Auto Sensor Test
- Input Protection

Electrical Specifications:

- Gain Selectable: 20/40/60 dB + 0.5% dB
- Input Impedance: $10K\Omega$ // 15pF
- Power Required: 18-28V DC
- Operating Current: 30mA (With AST Installed)
-                        28mA (Without AST Installed)
- Dynamic Range: 80dB (Utilizing an R15 Sensor)
                         90dB (50Ω Input)

Environmental Specifications:

- Temperature: -40 C to +65 C

Gain Selection	20dB	40dB	60dB
Bandwidth (-3dB):	10kHz-2.5MHz	10kHz-2.0MHz	10kHz-900kHz
Output Voltage (50Ω Load):	6Vpp	20Vpp	20Vpp
CMRR (500kHz):	42dB	42dB	42dB
Noise (RMS rti):			

Filter Frequency Response Hz	20dB With R15 Sensor	40dB With R15 Sensor	60dB With R15 Sensor	20dB Input Shorted	40dB Input Shorted	60dB Input Shorted
135k-185k	3 µV	1.4 µV	1.5 µV	2.0 µV	0.6 µV	0.42 µV
100k-300k*	3 µV	1.8 µV	1.8 ∞V	2.3 µv	1 µV	0.8 µV
10k-2.0M	5 µV	4 µV	3 µV	4 µV	3 µV	2.5 µV

*Standard filter

195 Clarksville Road, Princeton Junction, NJ 08550 USA
Phone: (609) 716-4000 • Fax: (609) 716-0706
Email: sales.systems@mistrasgroup.com • www.mistrasgroup.com

Analysis sheet sample 268.41

Analysis Sheet

Sample Information		
Sample Nr.	268.41	
Rock type	Marble	
Length	101.42	[mm]
Diameter	50.73	[mm]
Weight	553.2	[g]
Density	2.698	[kg/dm³]
p-wave velocity	6.5	[mm/μsec]
Used channels for analysis	6	

UCS Values, Elastic Parameters and Destruction Energy				
σcs	71.88			[MPa]
25%	17.97			[MPa]
40-50%	28.8	-	35.94	[MPa]
70-80%	50.3	-	57.50	[MPa]
E-Modulus			87.52	[GPa]
V-Modulus			82.09	[GPa]
Poisson`s ratio			0.33	[-]
Destruction-energy	100%	50%	30%	[-]
	50.64	72.09	75.5	[kJ/m³]

Number of Hits in relation to their signal strength (pre failure)							
UCS [%]	Amplitude [Decibel]						
	30-40	41-50	51-60	61-70	71-80	81-90	91-100
0-25% of UCS	402	59	6	0			
>25-50% of UCS	983	151	19	2			
>50-80% of UCS	3452	601	104	12	1		
>80-100% of UCS	8270	1079	134	14	1		
Sum:	13106	1889	264	28	2		
						Total:	15288

Analysis Parameter (pre failure) including cycles					
Values till % UCS	25%	50%	80%	100%	
Number of Hits	466.8	1621.5	5790.3	15288.3	[-]
Number of Events	5	36	179	412	[-]
Absolute Energy [aJ]	8.10E+03	3.50E+04	1.85E+05	3.70E+05	[aJ]
Cumulative Hits [%]	3%	11%	38%	100%	[-]
Cumulative Events [%]	1%	9%	43%	100%	[-]
Cumulative Energy [%]	2%	9%	50%	100%	[-]

Crack level indicators by ΔV/V Analysis					
derived through graphic solution					
	Stress [% - from UCS]	ε_{axial} [%]	$\varepsilon_{lateral}$ [%]	ΔV/V [%]	Determination
σcc	4.5	0.003	-0.001	0.002	non linear to this point
σci	43.5	0.0375	-0.013	0.0125	lateral strain departs from linearity
σcd	76.5	0.069	-0.025	0.018	derrived from volumetric strain reversal

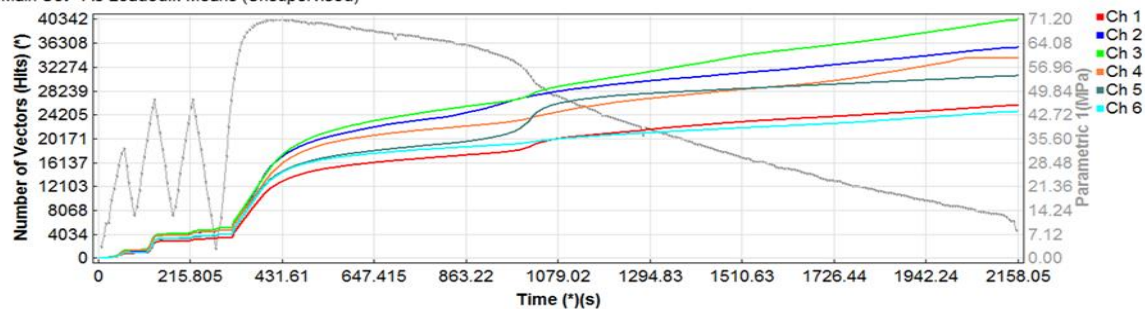| Crack level indicators by AE Analysis		
derived through graphic solution		
	Stress [%-from UCS]	Determination
σcc	5	the point where the cumulative energy becomes linear for the first time
σci	38.5	the point where the cumulative energy deviates from linearity
σcd	74.5	not eactly established, very uncertain point derived from AE signals

Crack level indicators by the pattern recognition		
derived through pattern recognition		
	Stress [%-from UCS]	Determination
σcc	unknown	due to the pattern recognition, the 1st phase was not detected
σci	47	derived through the pattern recognition
σcd	77	derived through the pattern recognition

Number of hits in relation to signal strength and UCS-levels

Cumulative hits/energy vs. Failure stress (excl. cycles)

Hits vs. time (incl. post-failure) 268.41

Hits vs. time (pre-failure) 268.41
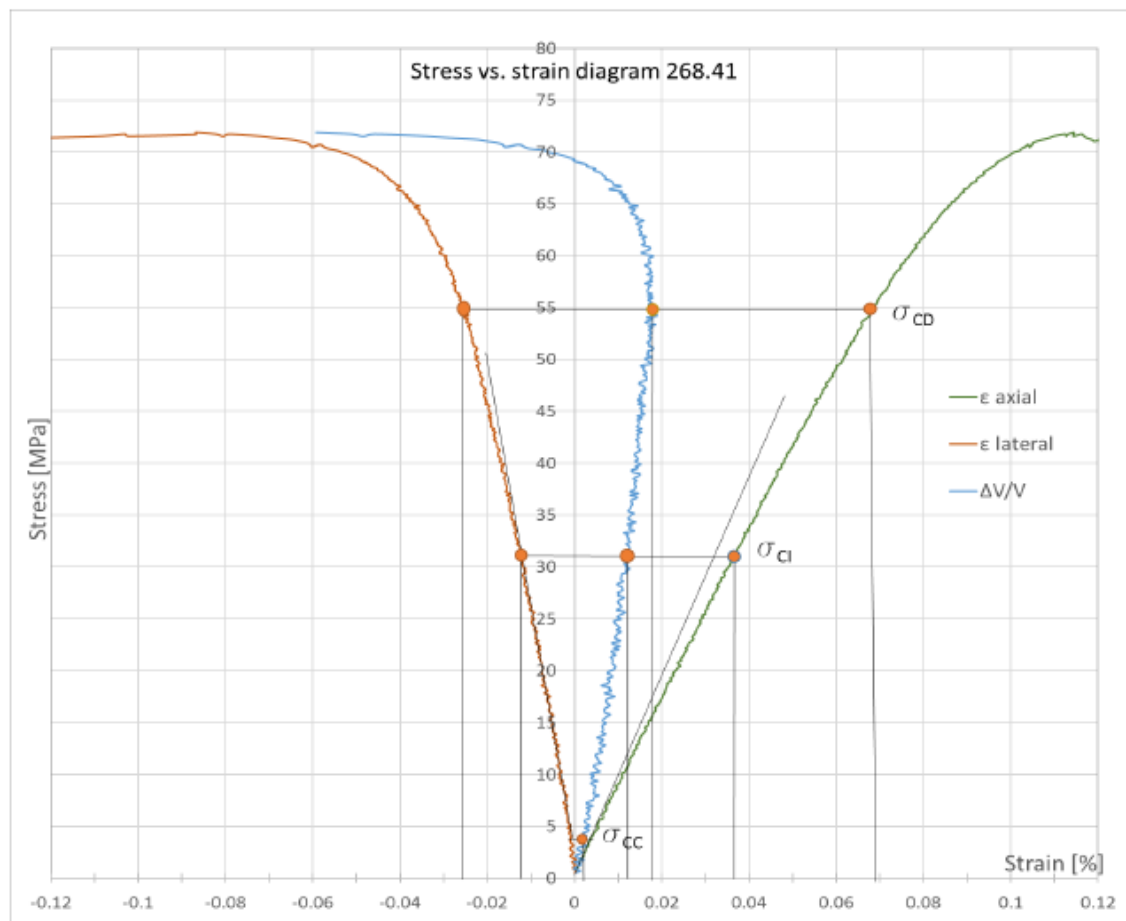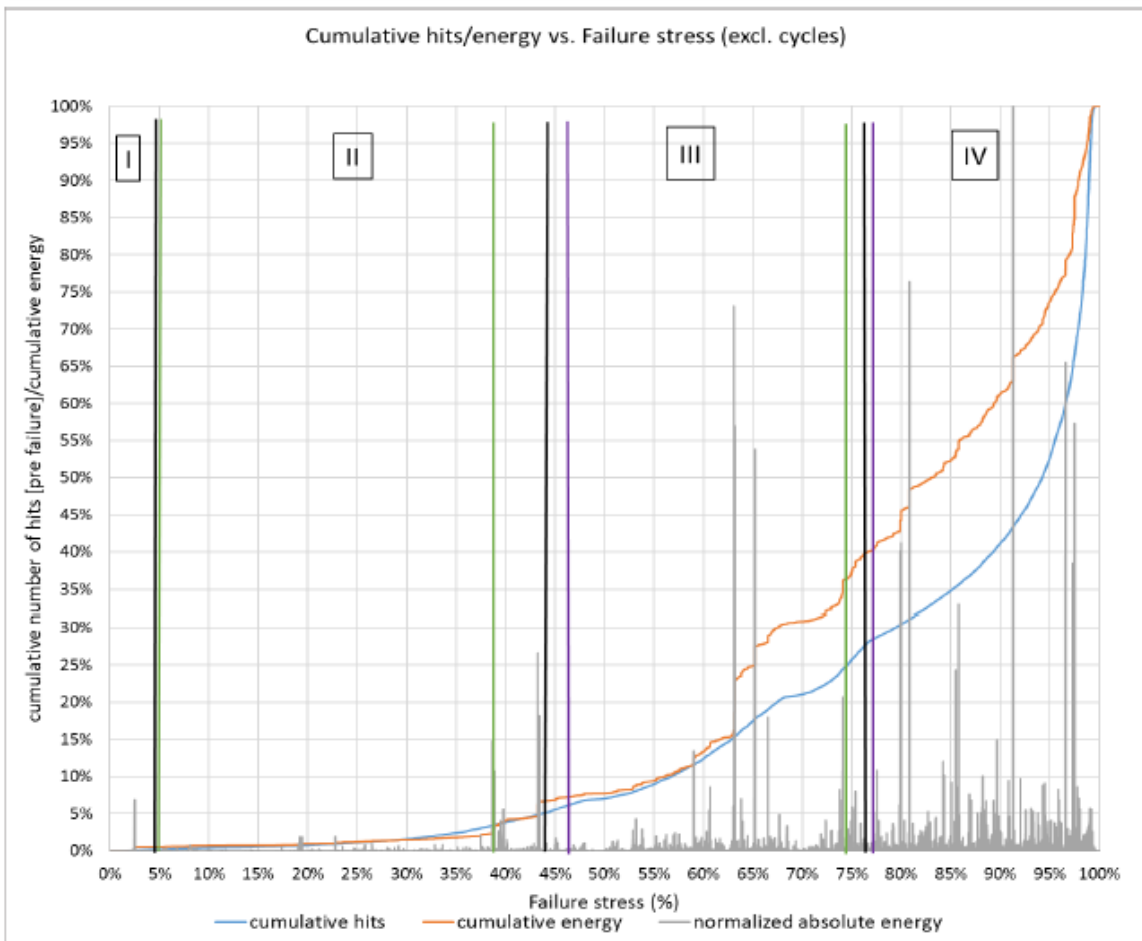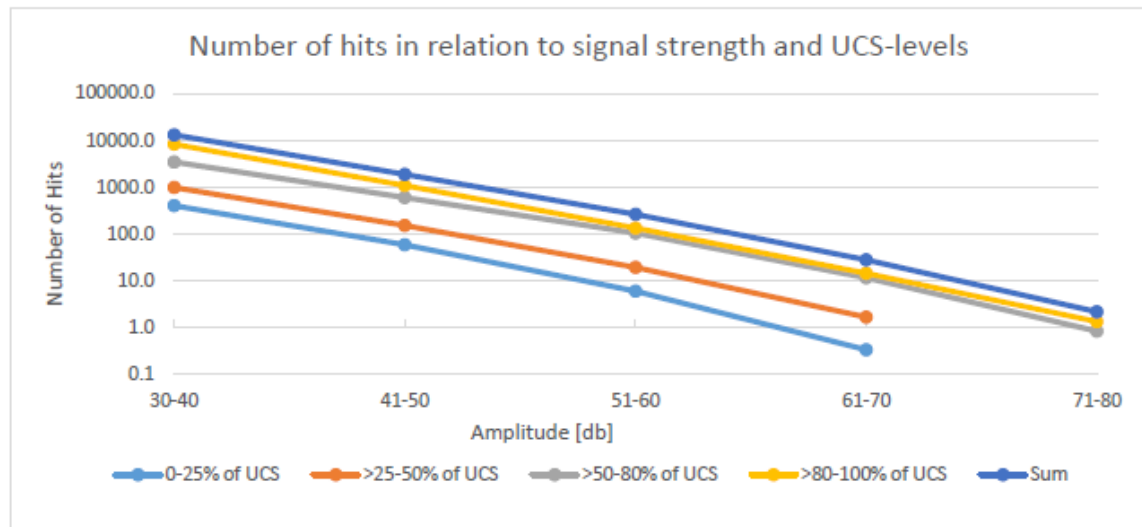
Energy vs. time (pre-failure) 268.41

(Color: CHANNELS) , Ch (1-6), Class (ALL)
Main Set - As Loaded:k-Means (Unsupervised) (0.00% hidden,51.93% filtered)
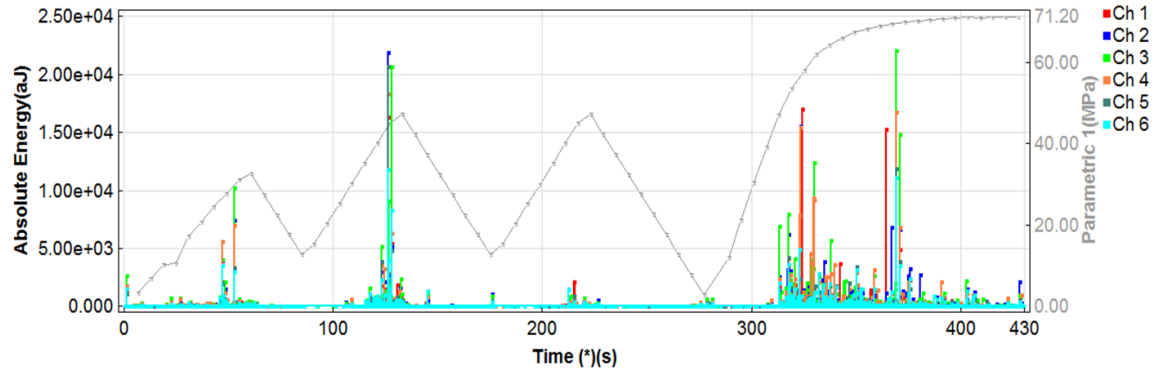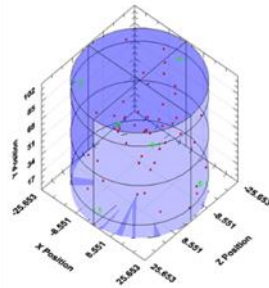

(Color: NONE) , Ch (1-6), Class (ALL)
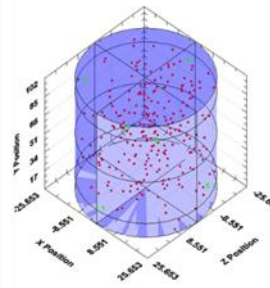Main Set - As Loaded:k-Means (Unsupervised)
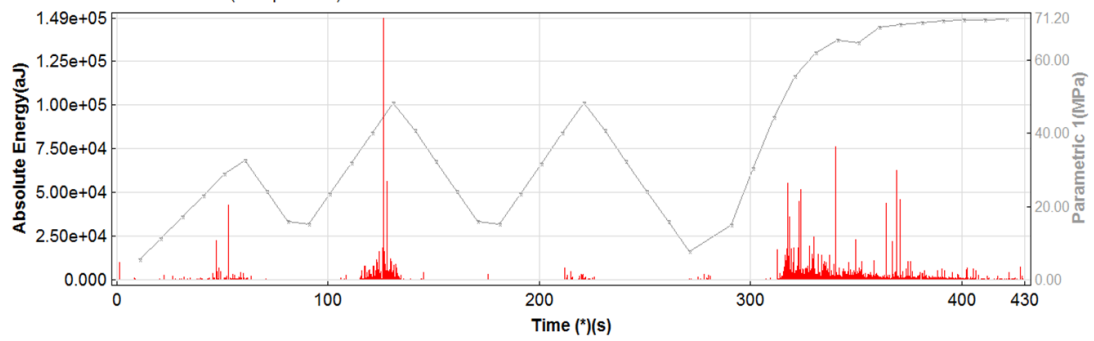
Events vs. time visualization 268.41
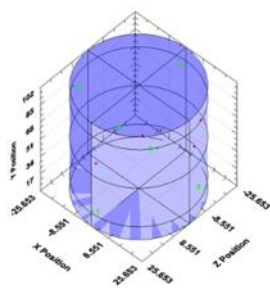
25% of UCS
5-events

50% of UCS
36-events

80% of UCS
179-events
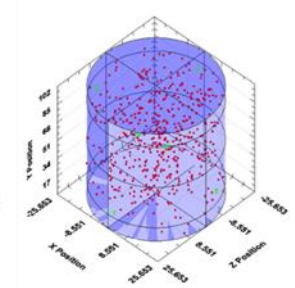
100% of UCS
412-events

Pattern recognition plot 268.41

(Color: CLASSES) , Ch (1-6), Class (ALL)
Main Set - Working Copy:k-Means (Unsupervised)
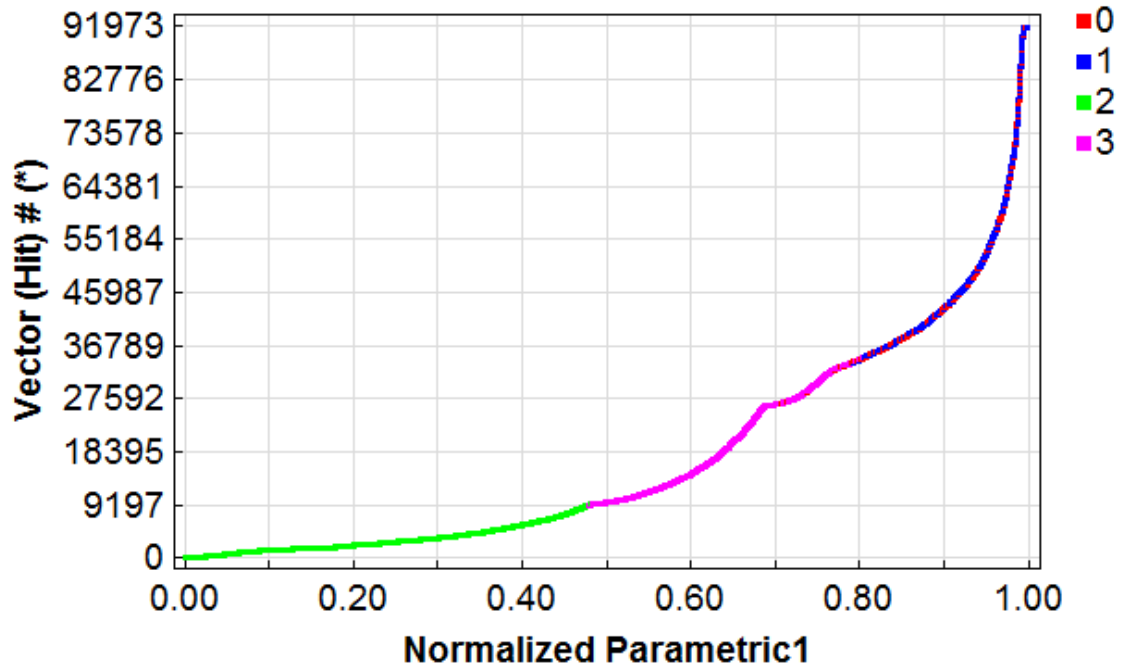
Destruction energy from the sample 268.41
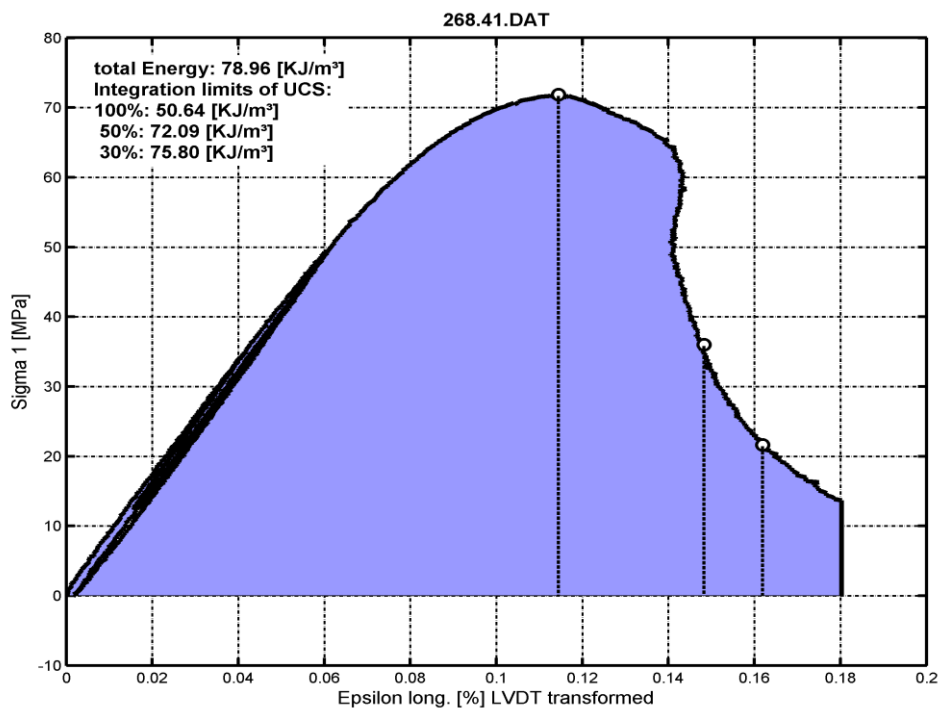
Analysis sheet 268.43

Analysis Sheet

Sample Information		
Sample Nr.	268.43	
Rock type	Marble	
Legth	101.8	[mm]
Diameter	50.7	[mm]
Weight	555	[g]
Density	2700	[kg/dm³]
p-wave velocity	5.6	[mm/μsec]
Used channels for analysis	6	

UCS Values, Elastic Parameters and Destruction Energy				
σcs	94.88			[MPa]
25%	23.72			[MPa]
40-50%	38.0	-	47.44	[MPa]
70-80%	66.4	-	75.90	[MPa]
E-Modulus			71.73	[GPa]
V-Modulus			57.73	[GPa]
Poisson`s ratio			0.3	[-]
Destruction-energy	100%	50%	30%	[-]
	106.69	137.22	145.89	[kJ/m³]

Number of Hits in relation to their signal strength (pre failure)							
UCS [%]	Amplitude [Decibel]						
	30-40	41-50	51-60	61-70	71-80	81-90	91-100
0-25% of UCS	71	5	2	0			
>25-50% of UCS	59	2	0	0			
>50-80% of UCS	472	22	1	0			
>80-100% of UCS	2680	106	4	0			
Sum:	3281	134	7	0	0		
						Total:	3422

Analysis Parameter (pre failure) including cycles					
Values till % UCS	25%	50%	80%	100%	
Number of Hits	77	137	632	3422	[-]
Number of Events	0	0	7	48	[-]
Absolute Energy [aJ]	8.50E+02	9.47E+02	2.28E+03	9.82E+03	[aJ]
Cumulative Hits [%]	2%	4%	18%	100%	[-]
Cumulative Events [%]	0%	0%	15%	100%	[-]
Cumulative Energy [%]	9%	10%	23%	100%	[-]

Crack level indicators by ΔV/V Analysis					
derived through graphic solution					
	Stress [% - from UCS]	ε_{axial} [%]	$\varepsilon_{lateral}$ [%]	ΔV/V [%]	Determination
σcc	10.5	0.016	-0.005	0.005	non linear to this point
σci	44.2	0.069	-0.021	0.028	lateral strain departs from linearity
σcd	82.2	0.135	-0.046	0.041	derrived from volumetric strain reversal

| Crack level indicators by AE Analysis		
derived through graphic solution		
	Stress [% from UCS]	Determination
σ cc	9.5	the point where the cumulative energy becomes linear for the first time
σ ci	47.5	the point where the cumulative energy deviates from linearity
σ cd	88	not eactly established, very uncertain point derived from AE signals

Crack level indicators by the pattern recognition		
derived through pattern recognition		
	Stress [% from UCS]	Determination
σ cc	unknown	due to the pattern recognition, the 1st phase was not detected
σ ci	43.2	derived through the pattern recognition
σ cd	83.7	derived through the pattern recognition

Stress-Strain diagram 268.43

Number of hits in relation to signal strength and UCS-levels

Cumulative hits/energy vs. Failure stress (excl. cycles)
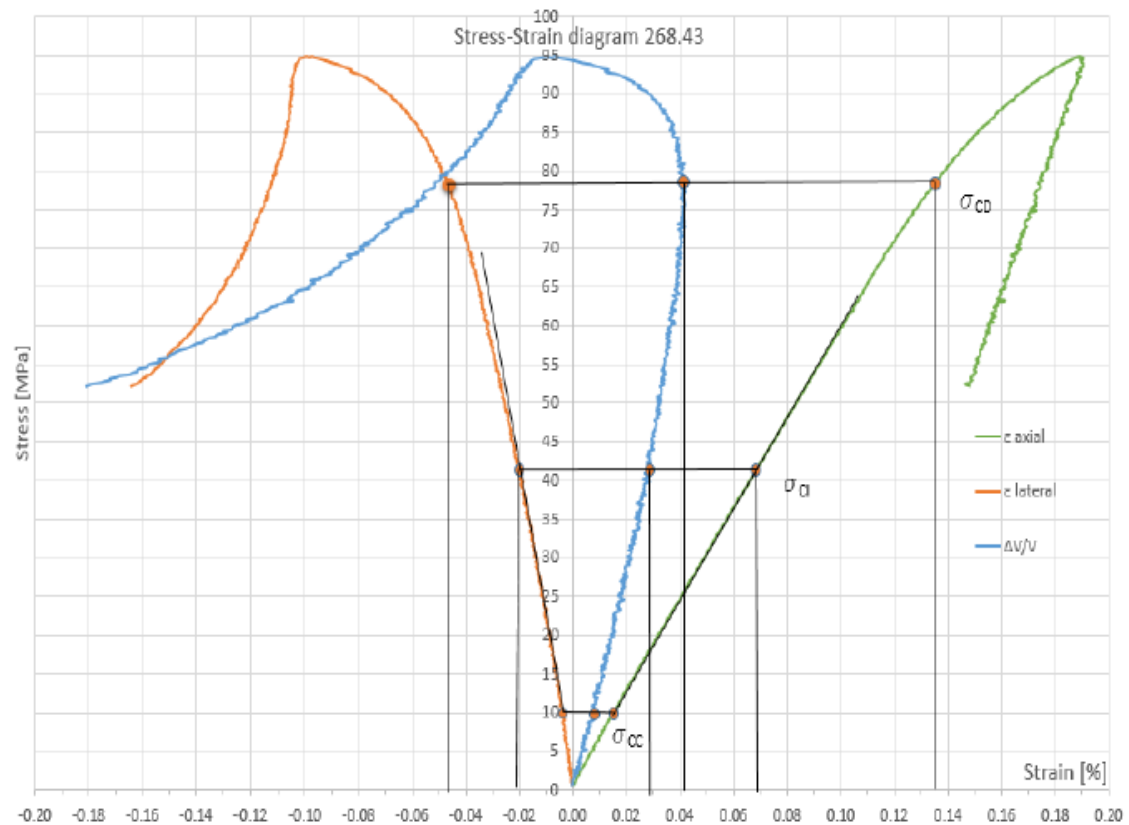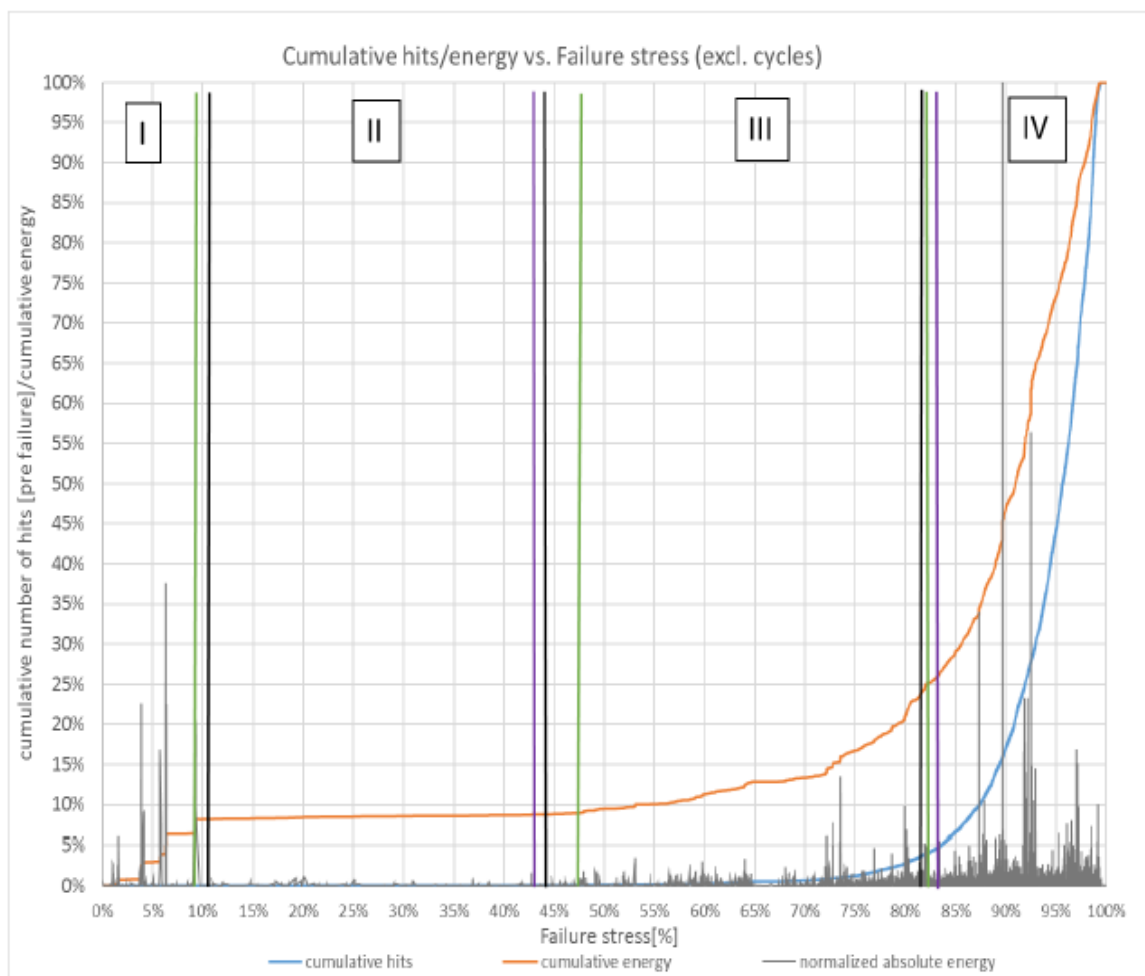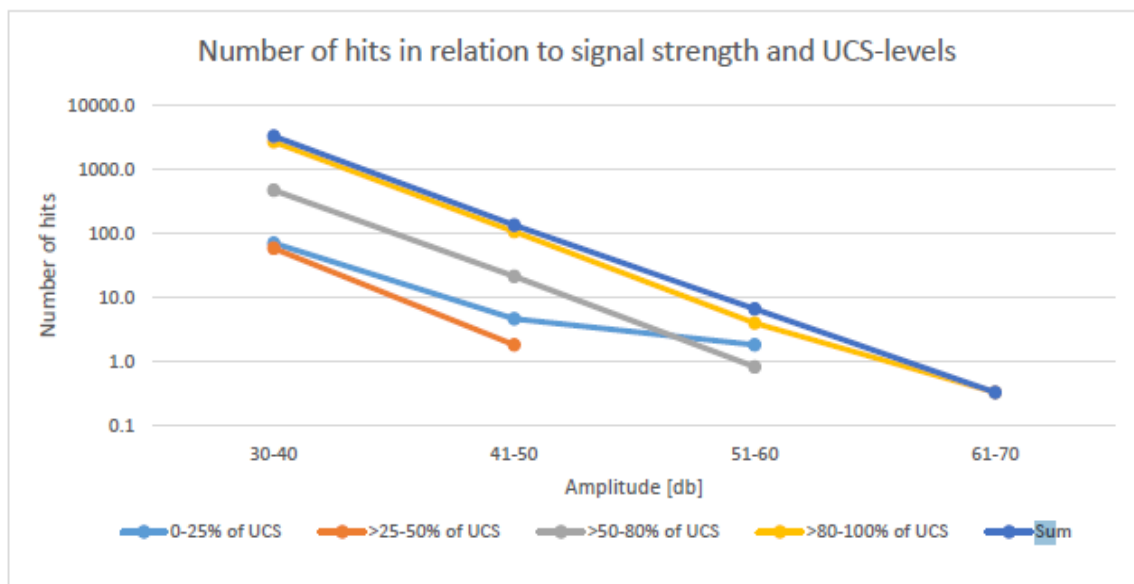
Hits vs. time (incl. post-failure) 268.43

(Color: CHANNELS) , Ch (ALL), Class (ALL)
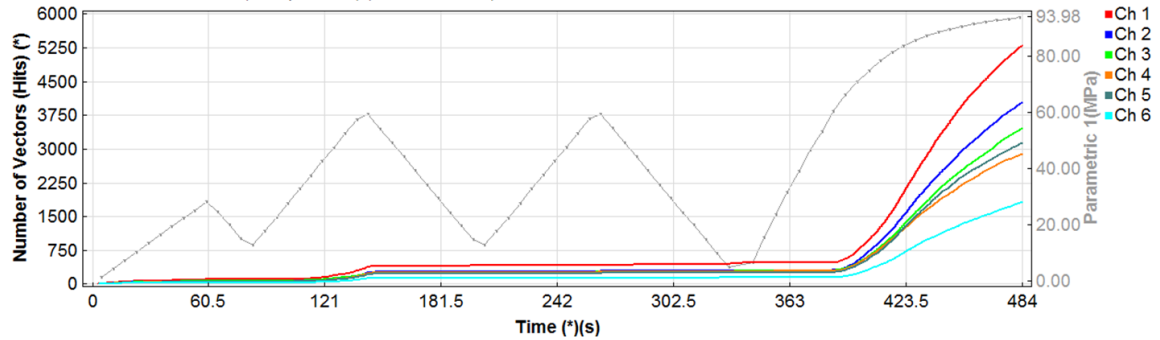Main Set - As Loaded:k-Means (Unsupervised) (100.00% hidden)
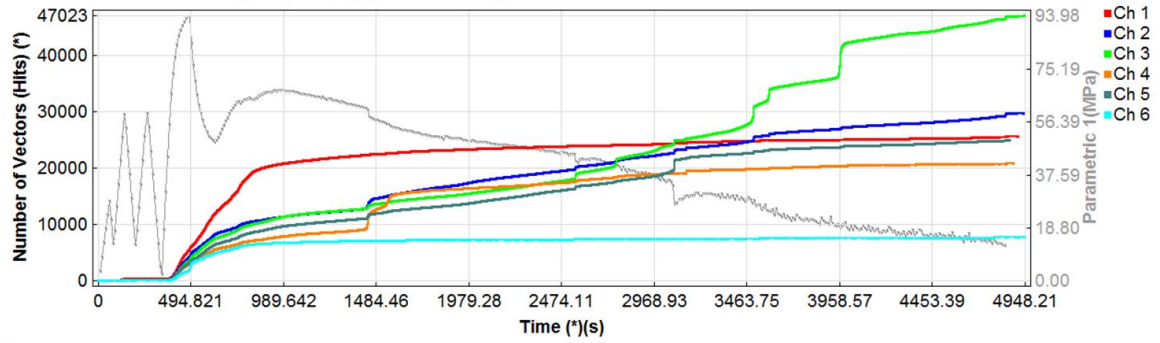
(Color: CHANNELS) , Ch (3), Class (ALL)
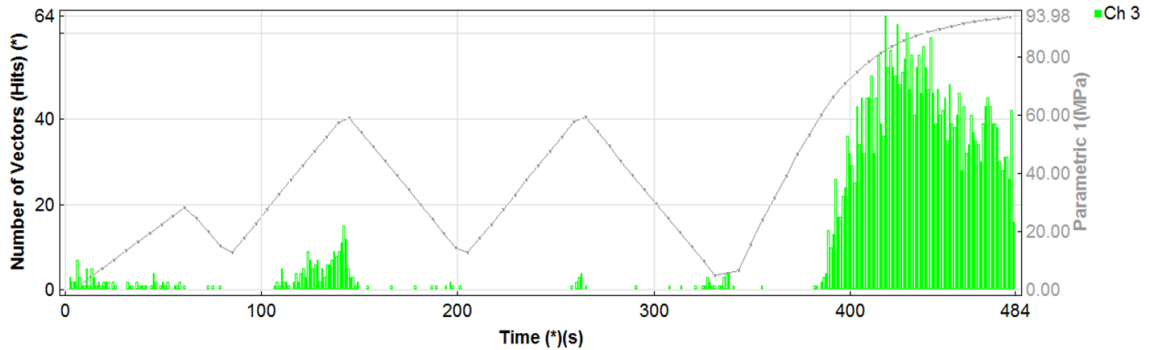Main Set - As Loaded:k-Means (Unsupervised) (69.88% filtered)
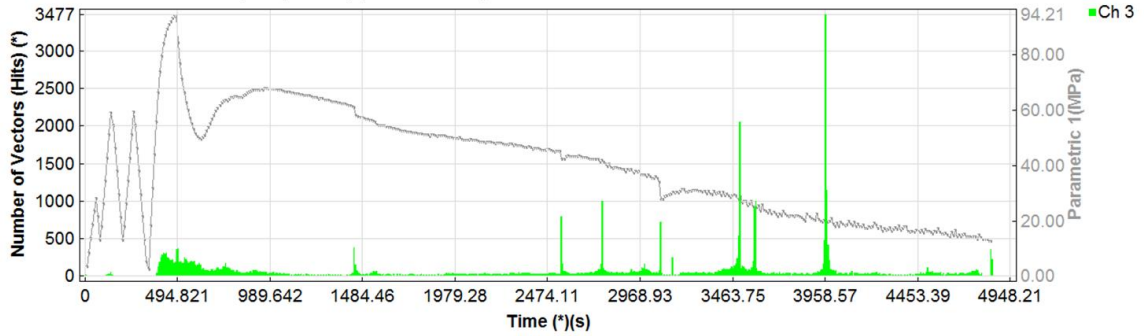
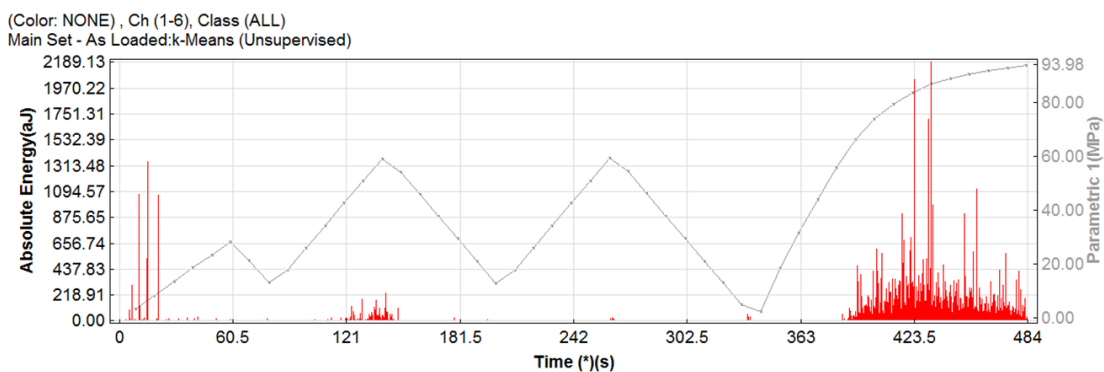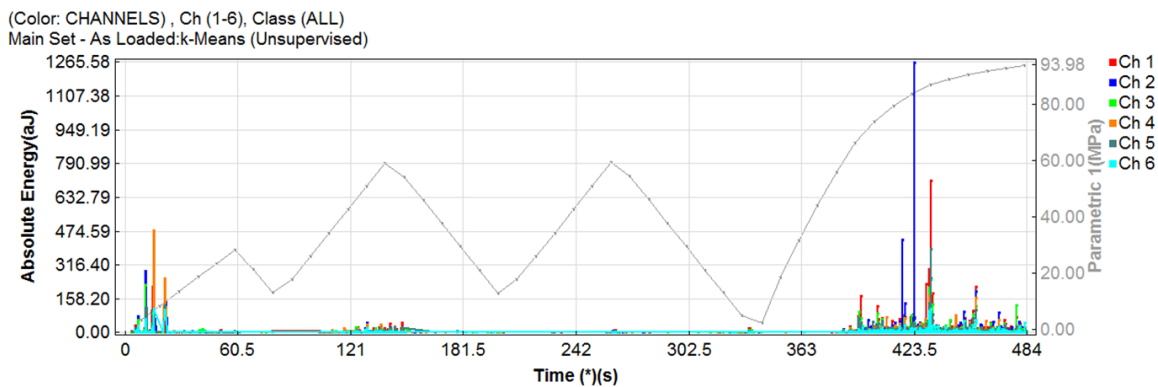## Hits vs. time (pre-failure) 268.43

(Color: CHANNELS) , Ch (1-6), Class (ALL)
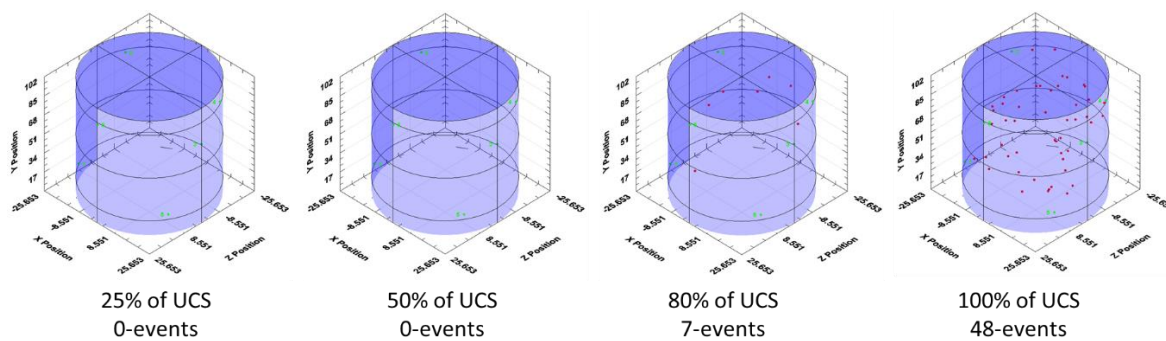Main Set - As Loaded:k-Means (Unsupervised) (86.82% filtered)

(Color: CHANNELS) , Ch (3), Class (ALL)
Main Set - As Loaded:k-Means (Unsupervised) (27.91% hidden,69.88% filtered)

Energy vs. time (pre-failure) 268.43

(Color: CHANNELS) , Ch (1-6), Class (ALL)
Main Set - As Loaded:k-Means (Unsupervised)

(Color: NONE) , Ch (1-6), Class (ALL)
Main Set - As Loaded:k-Means (Unsupervised)

Events vs. time visualization 268.43

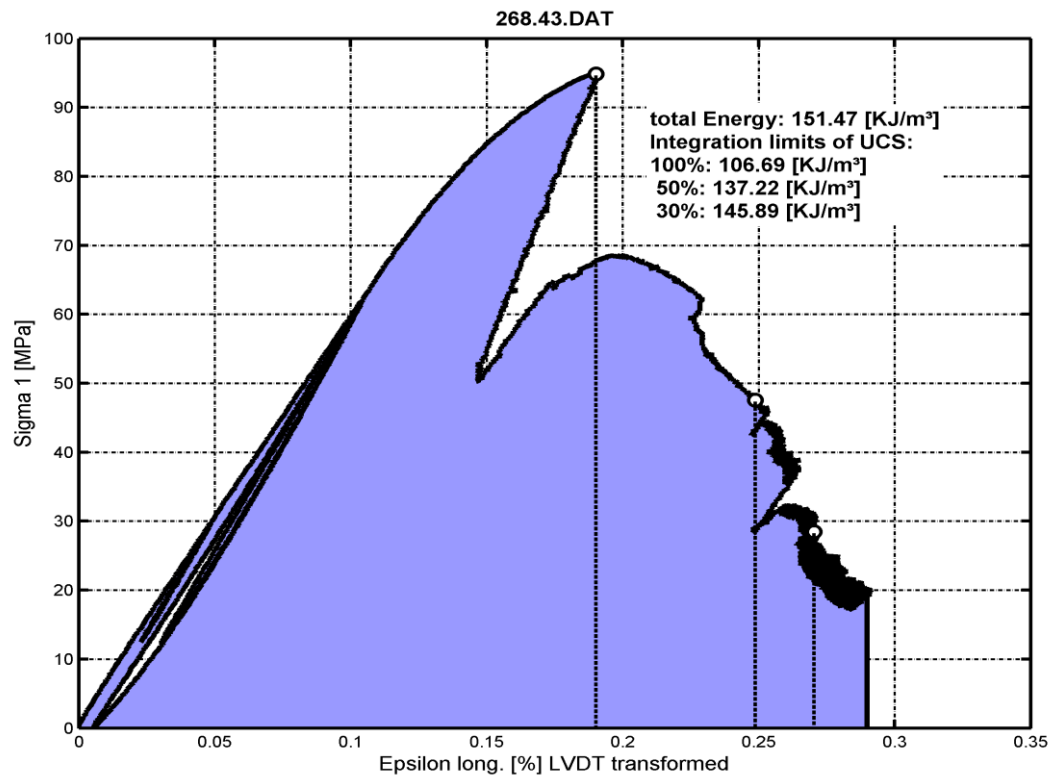| 25% of UCS | 50% of UCS | 80% of UCS | 100% of UCS |
| 0-events | 0-events | 7-events | 48-events |

Pattern recognition plot 268.43

(Color: CLASSES) , Ch (1-6), Class (ALL)
Main Set - Working Copy:k-Means (Unsupervised)
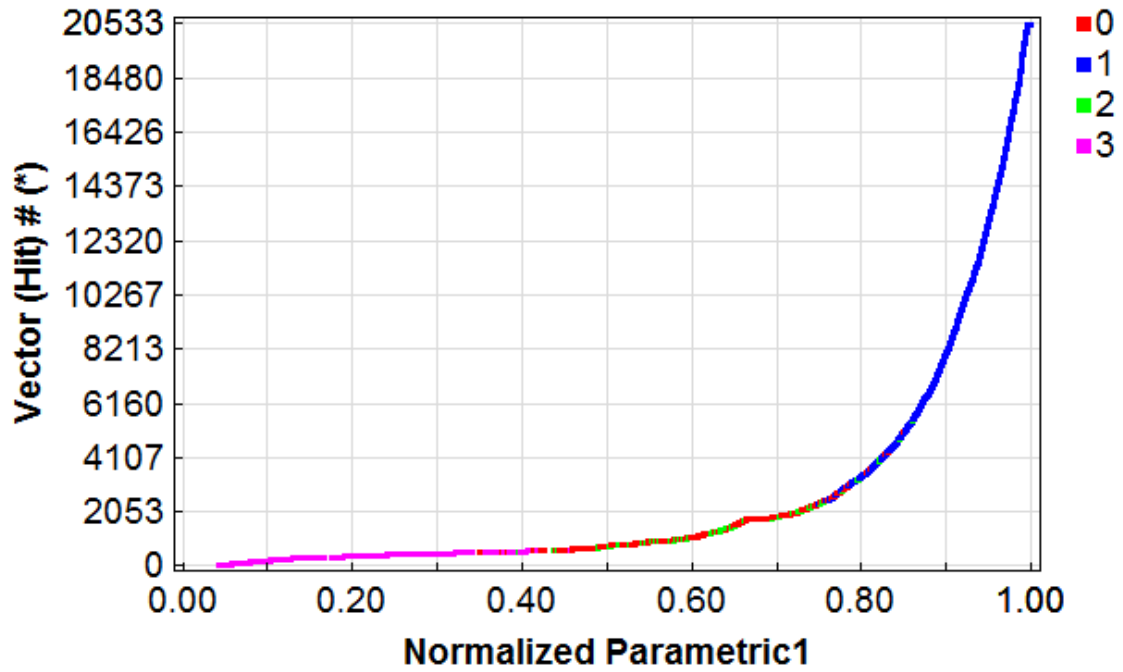
Destruction energy from the sample 268.43

Analysis sheet 268.59_1

Analysis Sheet

Sample Information		
Sample Nr.	268.59_1	
Rock type	Dolomite	
Length	101.18	[mm]
Diameter	50.7	[mm]
Weight	580.9	[g]
Density	2.843	[kg/dm³]
p-wave velocity	6	[mm/μsec]
Used channels for analysis	5	

UCS Values, Elastic Parameters and Destruction Energy				
σ_{cs}	224.76			[MPa]
25%	56.19			[MPa]
40-50%	89.9	-	112.38	[MPa]
70-80%	157.3	-	179.81	[MPa]
E-Modulus			111.07	[GPa]
V-Modulus			102.33	[GPa]
Poisson`s ratio			0.27	[-]
Destruction-energy	100%	50%	30%	[-]
	335.85	196.56	157.64	[kJ/m³]

Number of Hits in relation to their signal strength (pre failure)							
UCS [%]	Amplitude [Decibel]						
	30-40	41-50	51-60	61-70	71-80	81-90	91-100
0-25% of UCS	1193	116	14	1	0	0	0
>25-50% of UCS	1165	188	42	10	4	2	1
>50-80% of UCS	18244	3365	903	266	87	38	24
>80-100% of UCS	23412	4616	1276	371	107	37	26
Sum:	44015	8284	2234	647	198	77	51
						Total:	55508

Analysis Parameter (pre failure) including cycles					
Values till % UCS	25%	50%	80%	100%	
Number of Hits	1323	2735.2	25662.2	55507.6	[-]
Number of Events	21	89	422	645	[-]
Absolute Energy [aJ]	2.26E+04	2.62E+07	7.96E+08	1.70E+09	[aJ]
Cumulative Hits [%]	2%	5%	46%	100%	[-]
Cumulative Events [%]	3%	14%	65%	100%	[-]
Cumulative Energy [%]	0.001%	1.54%	47%	100%	[-]

Crack level indicators by ΔV/V Analysis					
derived through graphic solution					
	Stress [% from UCS]	ε_{axial} [%]	$\varepsilon_{lateral}$ [%]	ΔV/V [%]	Determination
σ_{cc}	not useable	Due to the fact that this sample had been stressed before, this volumetric strain analysis cannot be applied. σ_{CD} should be around 75% of the UCS (due to the pattern recognition) but it is at 18%.			
σ_{ci}	not useable				
σ_{cd}	not useable				

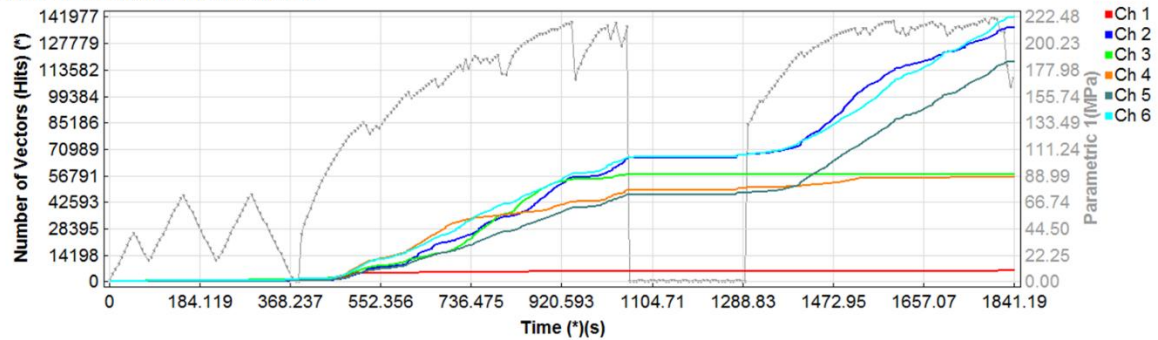| Crack level indicators by $\mathbb{AE}$ Analysis		
derived through graphic solution		
	Stress [% from UCS]	Determination
σcc	15	due to the pattern recognition, the 1st phase was not detected
σci	39	the point where the cumulative energy deviates from linearity
σcd	75	not eactly established, very uncertain point derived from AE signals

Crack level indicators by the pattern recognition		
derived through pattern recognition		
	Stress [%- from UCS]	Determination
σcc	unknown	due to the pattern recognition, the 1st phase was not detected
σci	37.5	derived through the pattern recognition
σcd	75	derived through the pattern recognition

Stress vs. strain diagram 268.59_1

Number of hits in relation to signal strength and UCS-levels

Cumulative hits/energy vs. Failure stress (excl. cycles)

Hits vs. time (incl. Post-failure) 268.59_1

(Color: CHANNELS) , Ch (1-6), Class (ALL)
Main Set - As Loaded:<No Classification>
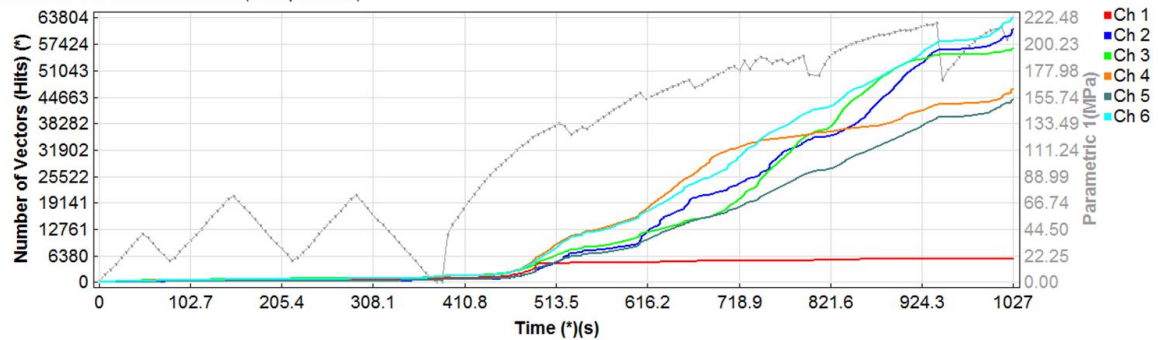

(Color: CHANNELS) , Ch (2), Class (ALL)
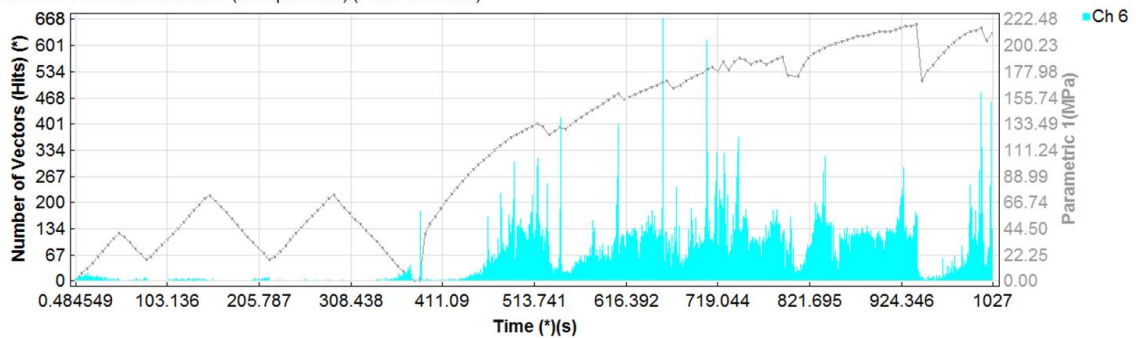Main Set - As Loaded:<No Classification> (73.58% filtered)
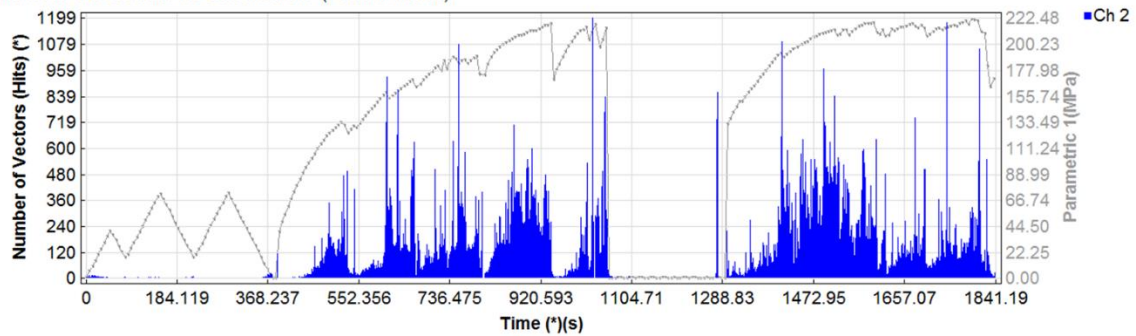
Hits vs. time (pre-failure) 268.59_1

(Color: CHANNELS) , Ch (1-6), Class (ALL)
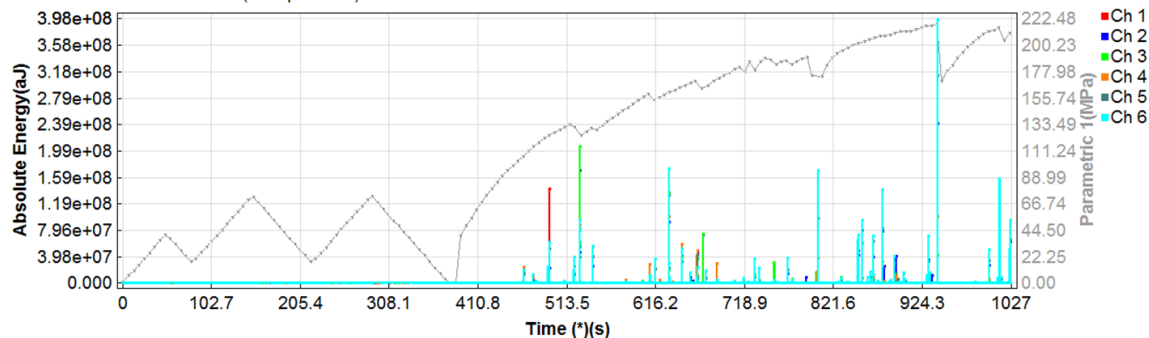Main Set - As Loaded:k-Means (Unsupervised)

(Color: CHANNELS) , Ch (6), Class (ALL)
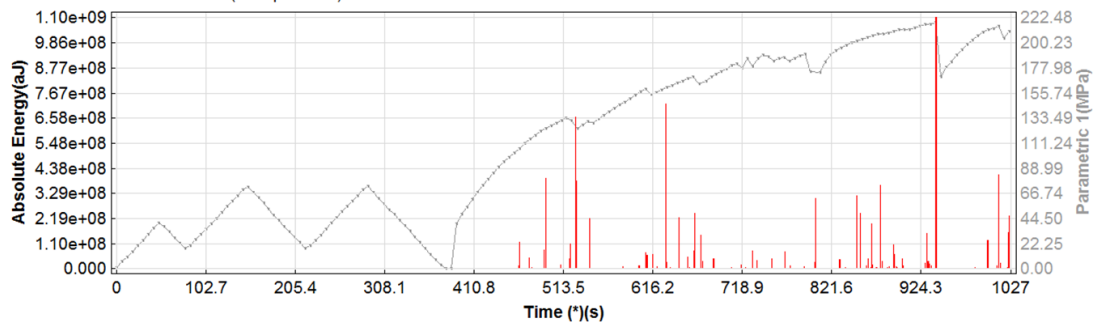Main Set - As Loaded:k-Means (Unsupervised) (77.01% filtered)

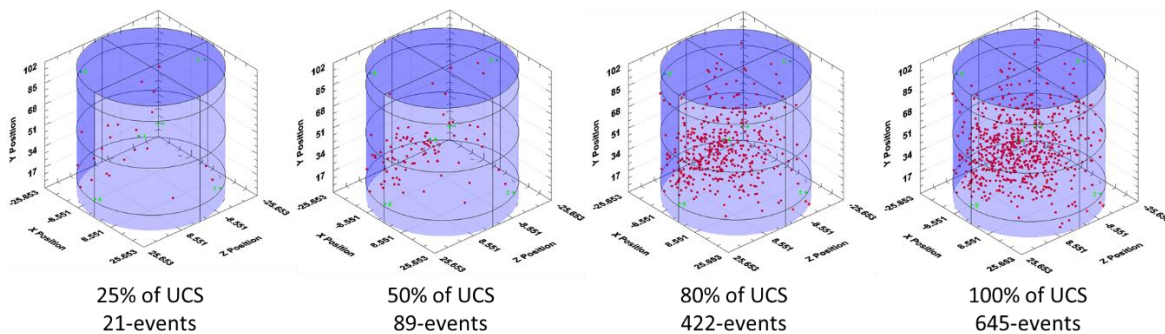## Energy vs. time (pre-failure) 268.59_1

(Color: CHANNELS) , Ch (1-6), Class (ALL)
Main Set - As Loaded:k-Means (Unsupervised)

(Color: NONE) , Ch (1-6), Class (ALL)
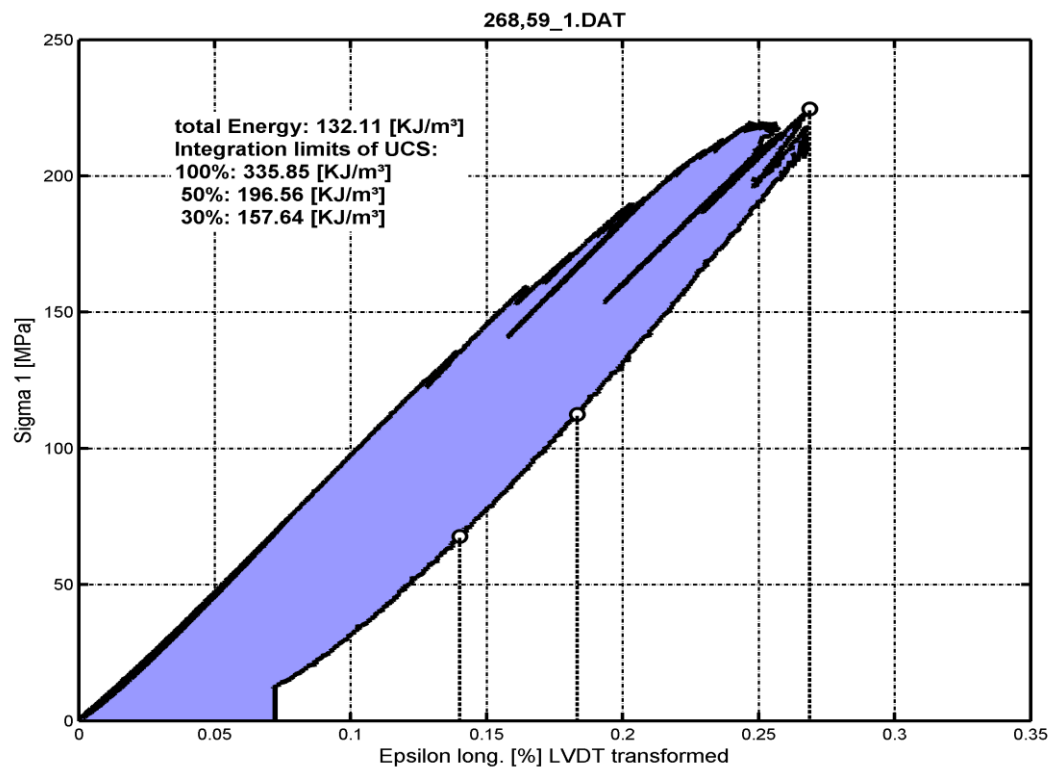Main Set - As Loaded:k-Means (Unsupervised)

Events vs. time visualization 268.59_1

| 25% of UCS | 50% of UCS | 80% of UCS | 100% of UCS |
| 21-events | 89-events | 422-events | 645-events |

Pattern recognition plot 268.59_1

(Color: CLASSES) , Ch (1-6), Class (ALL)
Main Set - Working Copy:k-Means (Unsupervised)
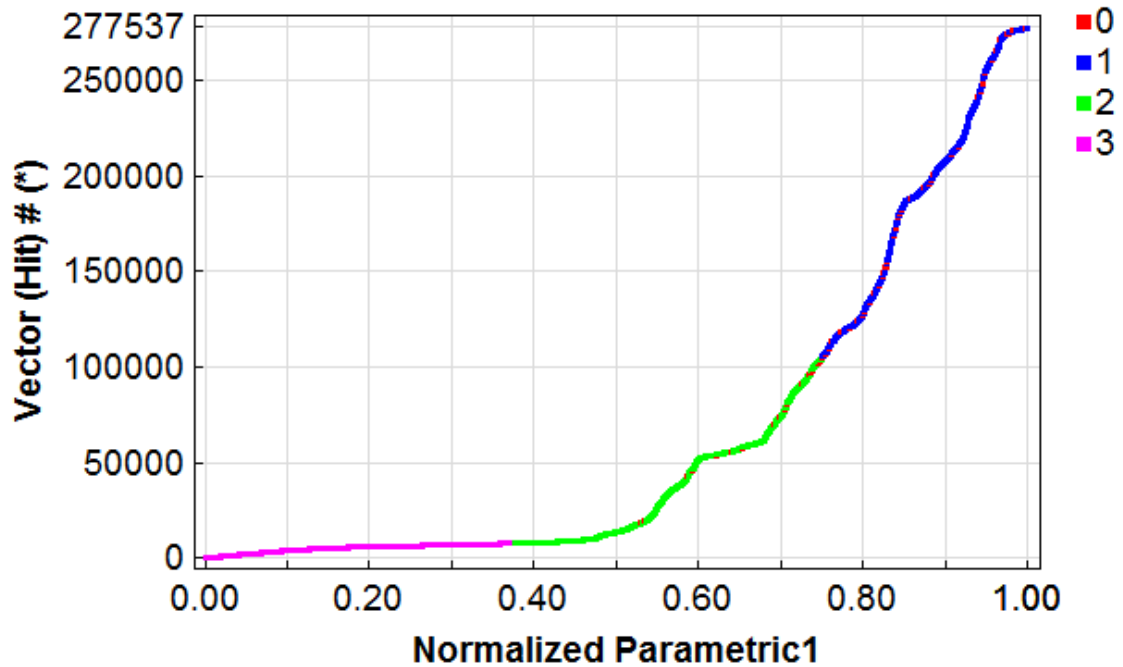
Destruction energy from the sample 268.59_1

Analysis sheet 268.67

Analysis Sheet

Sample Information		
Sample Nr.	268.67	
Rock type	Magnesite	
Length	101.83	[mm]
Diameter	50.72	[mm]
Weight	612.8	[g]
Density	2.978	[kg/dm³]
p-wave velocity	5	[mm/μsec]
Used channels for analysis	6	

UCS Values, Elastic Parameters and Destruction Energy				
σcs	276.84			[MPa]
25%	69.21			[MPa]
40-50%	110.7	-	138.42	[MPa]
70-80%	193.8	-	221.47	[MPa]
E-Modulus			132.78	[GPa]
V-Modulus			122.18	[GPa]
Poisson`s ratio			0.25	[-]
Destruction-energy	total			[-]
	318.96			[kJ/m³]

Number of Hits in relation to their signal strength (pre failure)							
UCS [%]	Amplitude [Decibel]						
	30-40	41-50	51-60	61-70	71-80	81-90	91-100
0-25% of UCS	2562	319	43	5	1	0	
>25-50% of UCS	3630	589	118	27	4	0	
>50-80% of UCS	21487	3826	948	248	65	22	13
>80-100% of UCS	14643	2655	684	141	30	5	8
Sum:	42322	7389	1792	420	100	28	21
						Total:	52072

Analysis Parameter (pre failure) including cylcles					
Values till % UCS	25%	50%	80%	100%	
Number of Hits	2929.3	7297.8	33906.7	52072.3	[-]
Number of Events	74	535	2359	3311	[-]
Absolute Energy [aJ]	42000	4.50E+05	7.92E+08	9.73E+08	[aJ]
Cumulative Hits [%]	6%	14%	65%	100%	[-]
Cumulative Events [%]	2%	16%	71%	100%	[-]
Cumulative Energy [%]	0.0%	0.0%	81%	100%	[-]

Crack level indicators by ΔV/V Analysis					
derived through graphic solution					
	Stress [% from UCS]	ε_{axial} [%]	$\varepsilon_{lateral}$ [%]	ΔV/V [%]	Determination
σcc	9	0.022	0.00625	0.013	non linear to this point
σci	46.2	0.115	0.03	0.12	lateral strain departs from linearity
σcd	79.1	0.194	0.06	0.18	derrived from volumetric strain reversal

| Crack level indicators by AE Analysis		
derived through graphic solution		
	Stress [% from UCS]	Determination
σcc	10	the point where the cumulative energy becomes linear for the first time
σci	44	the point where the cumulative hits deviate from linearity
σcd	75	not eactly established, very uncertain point derived from AE signals

Crack level indicators by the pattern recognition		
derived through **pattern recognition**		
	Stress [%- from UCS]	Determination
σcc	unknown	due to the pattern recognition, the 1st phase was not detected
σci	46.5	derived through the pattern recognition
σcd	80	derived through the pattern recognition

Stress vs. Strain diagram 268.67

Number of hits in relation to signal strength and UCS-levels

Cumulative hits/energy vs. Failure stress (excl. cycles)
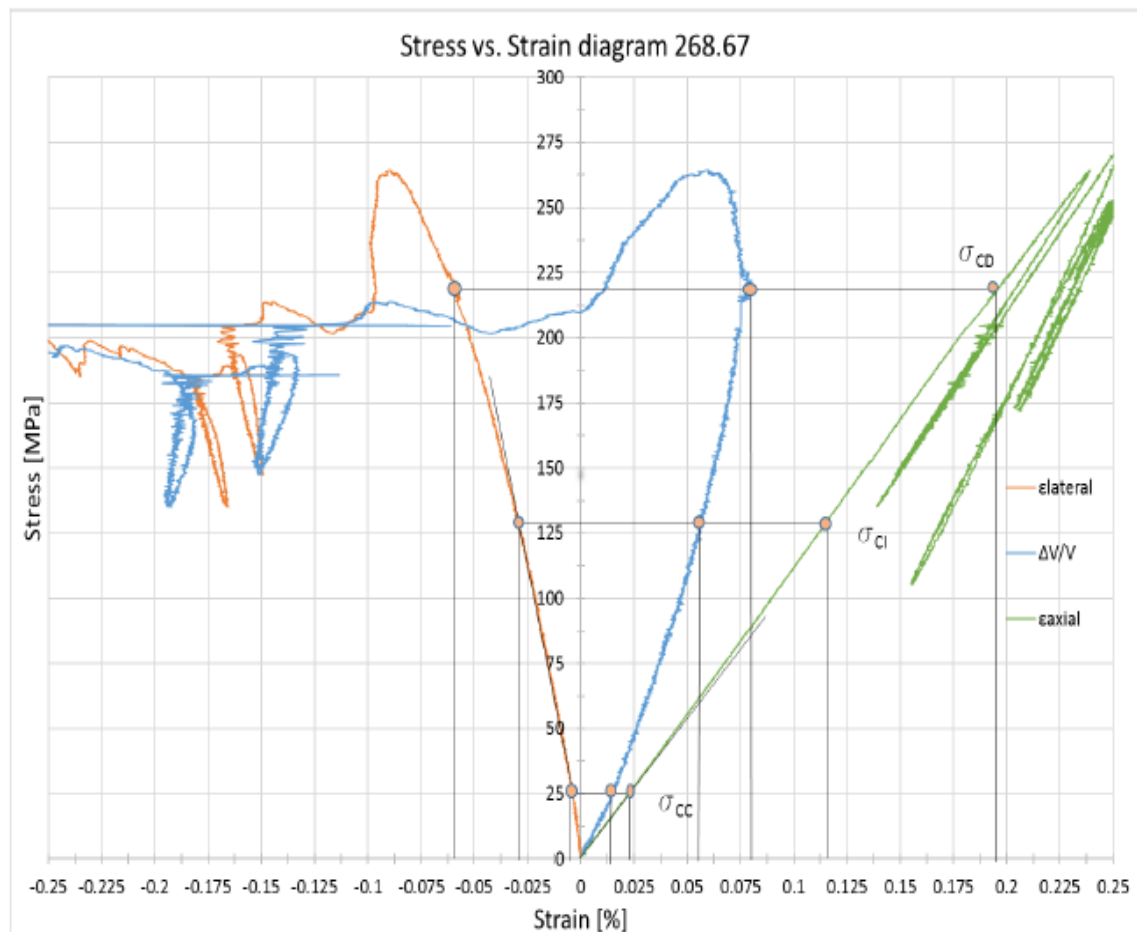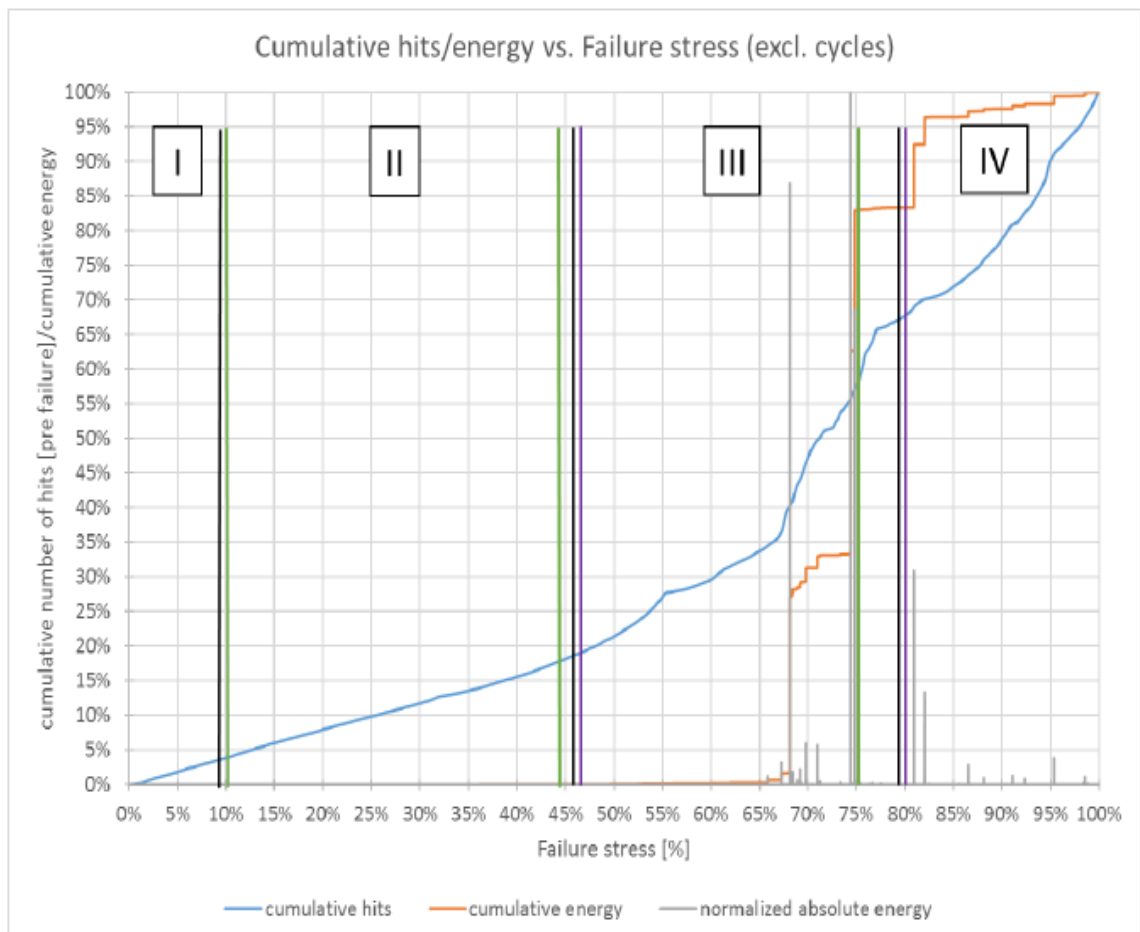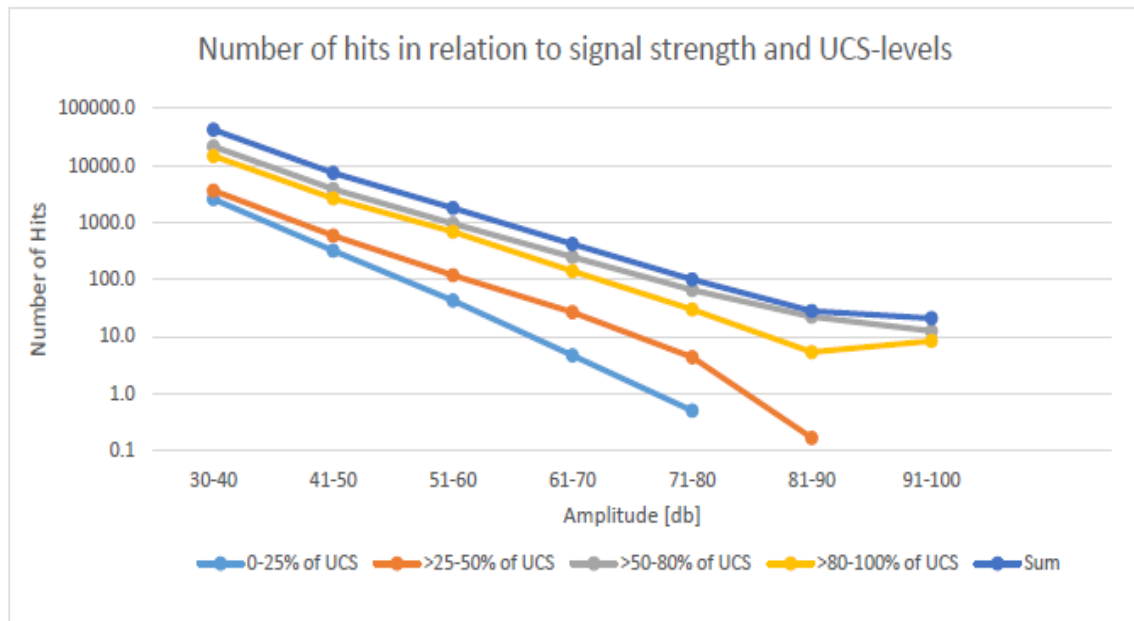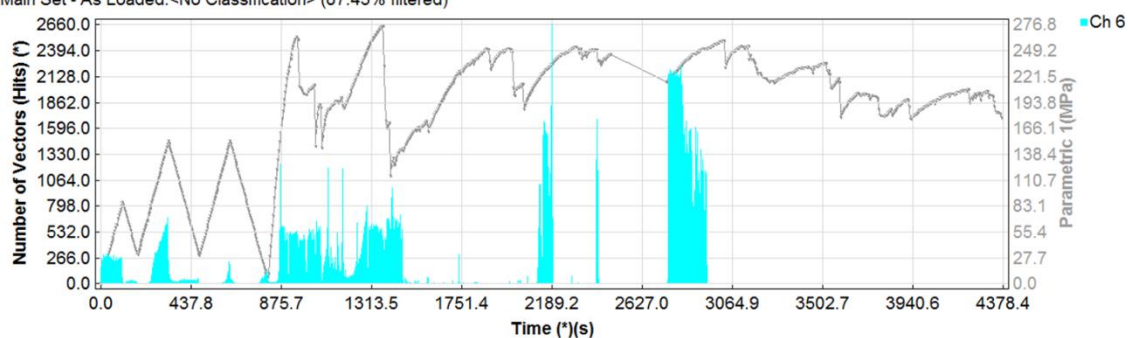
Hits vs. time (incl. Post-failure) 268.67

(Color: CHANNELS) , Ch (1-6), Class (ALL)
Main Set - As Loaded:<No Classification>
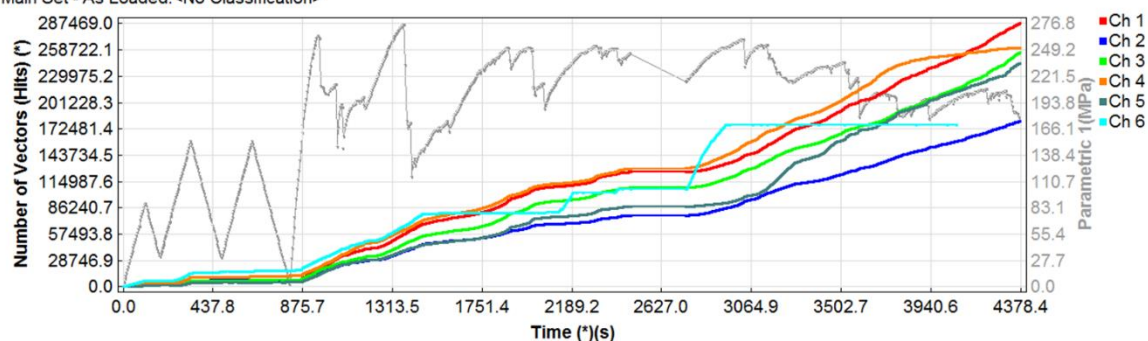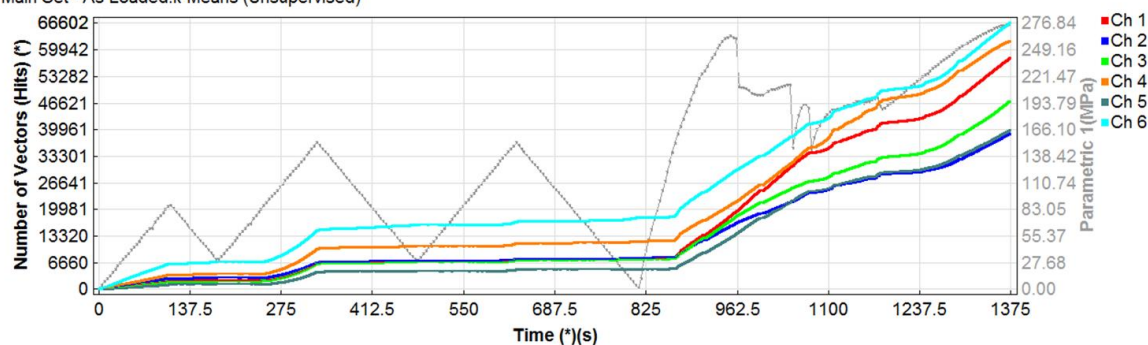

(Color: CHANNELS) , Ch (6), Class (ALL)
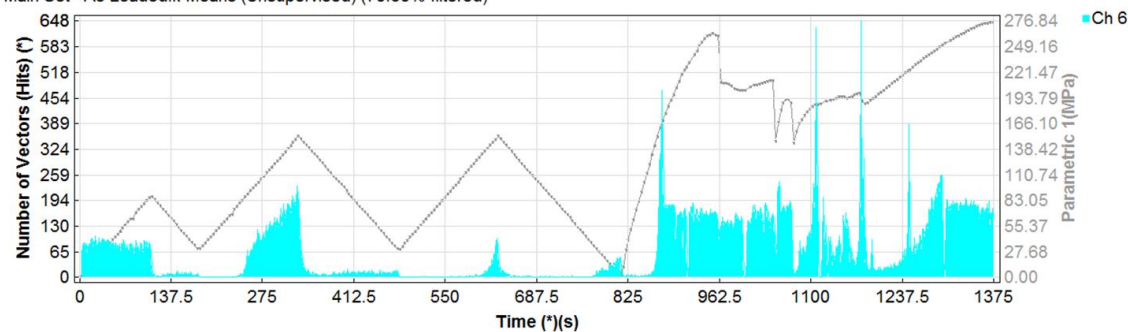Main Set - As Loaded:<No Classification> (87.43% filtered)

Hits vs. time (pre-failure) 268.67

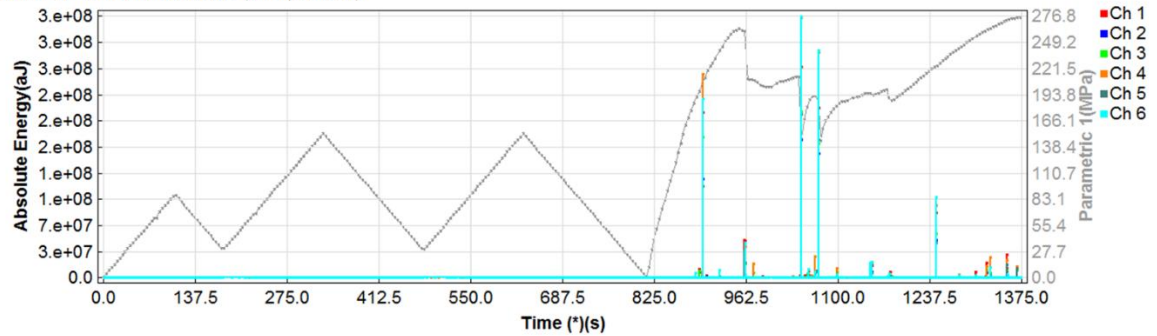(Color: CHANNELS) , Ch (ALL), Class (ALL)
Main Set - As Loaded:k-Means (Unsupervised)

(Color: CHANNELS) , Ch (6), Class (ALL)
Main Set - As Loaded:k-Means (Unsupervised) (78.68% filtered)
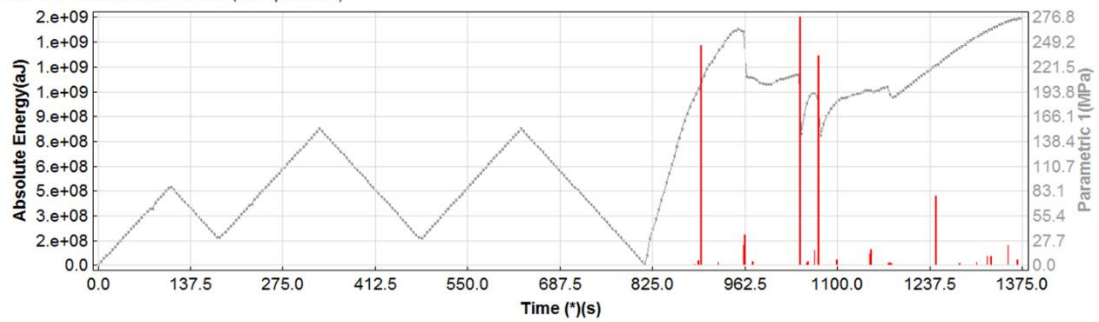
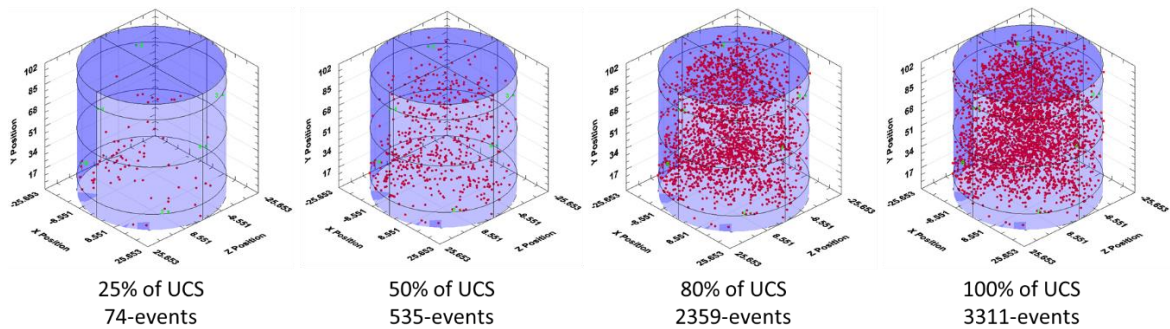## Energy vs. time (pre-failure) 268.67

(Color: CHANNELS) , Ch (1-6), Class (ALL)
Main Set - As Loaded:k-Means (Unsupervised)

(Color: NONE) , Ch (1-6), Class (ALL)
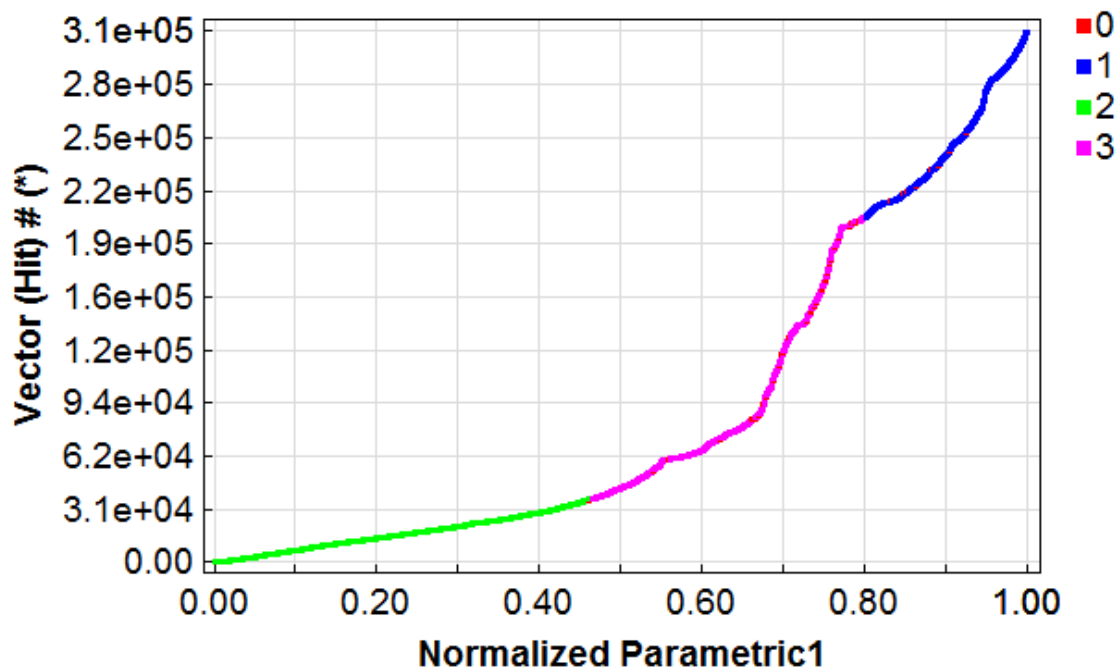Main Set - As Loaded:k-Means (Unsupervised)

Events vs. time visualization 268.67

25% of UCS
74-events

50% of UCS
535-events

80% of UCS
2359-events

100% of UCS
3311-events

Pattern recognition plot 268.67

Destruction energy from the sample 268.67